Electrical imaging of light-induced signals across and within retinal layers

Dissertation

zur Erlangung des Grades eines
Doktors der Naturwissenschaften

der Mathematisch-Naturwissenschaftlichen Fakultät
und
der Medizinischen Faktultät
der Eberhard Karls Universität Tübingen

vorgelegt von

Meng-Jung Lee

Aus Kaohsiung, Taiwan

Oktober, 2020

Tag der mündlichen Prüfung: ....

Stellv. Dekan der Math.-Nat. Fakultät: Prof. Dr. József Fortágh

Dekan der Medizinischen Fakultät: Prof. Dr. B. Pichler

1. Berichterstatter: Dr. Günther Zeck

2. Berichterstatter: Prof. Dr. Thomas Euler

Prüfungskommission: Dr. Günther Zeck

Prof. Dr. Thomas Euler

Prof. Dr. Alexandra Koschak

Prof. Dr. Frank Schäffel

Erklärung / Declaration:

Ich erkläre, dass ich die zur Promotion eingereichte Arbeit mit dem Titel:

„Electrical imaging of light-induced signals across and within retinal layers "

selbständig verfasst, nur die angegebenen Quellen und Hilfsmittel benutzt und wörtlich oder inhaltlich übernommene Stellen als solche gekennzeichnet habe. Ich versichere an Eides statt, dass diese Angaben wahr sind und dass ich nichts verschwiegen habe. Mir ist be-kannt, dass die falsche Abgabe einer Versicherung an Eides statt mit Freiheitsstrafe bis zu drei Jahren oder mit Geldstrafe bestraft wird.

I hereby declare that I have produced the work entitled "Electrical imaging of light-induced signals across and within retinal layers", submitted for the award of a doctorate, on my own (without external help), have used only the sources and aids indicated and have marked passages included from other works, whether verbatim or in content, as such. I swear upon oath that these statements are true and that I have not concealed anything. I am aware that making a false declaration under oath is punishable by a term of imprisonment of up to three years or by a fine.

Tübingen,

den ....
          Datum / Date   Unterschrift /Signature

Summary

The mammalian retina processes sensory signals through two major pathways: a vertical excitatory pathway, which involves photoreceptors, bipolar cells and ganglion cells, and a horizontal inhibitory pathway, which involves horizontal cells and amacrine cells. This concept explains the generation of excitatory center – inhibitory surround sensory receptive fields but fails to explain modulation of the retinal output by stimuli outside the receptive field. Electrical imaging of the light-induced signal propagation at high spatial and temporal resolution across and within different retinal layers might reveal mechanisms and circuits involved in the remote modulation of the retinal output.

Here I took advantage of a high-density complementary metal-oxide semiconductor -based microelectrode array and investigated light-induced propagation of local field potentials in vertical mouse retina slices. I found that the local field potentials propagation within the different retinal layers depends on stimulus duration and stimulus background. Application of the same spatially restricted light stimuli to flat-mount retina induced ganglion cell activity at remote distances from stimulus center. This effect disappeared if a global background was provided or if gap junctions were blocked. I hereby presented a neurotechnological approach and demonstrated its application, in which electrical imaging evaluates stimulus-dependent signal processing across different neural layers.

Abbreviations

CMOS	complementary metal-oxide semiconductor
MEA	micro-electrode array
PR	photoreceptor
BC	bipolar cell
AC	amacrine cell
HC	horizontal cell
RGC	retinal ganglion cell
ONL	outer nuclear layer
OPL	outer plexiform layer
INL	inner nuclear layer
IPL	inner plexiform layer
GCL	retinal ganglion cell layer
Cx	connexins
WT	wildtype
DNQX	6,7-Dinitroquinoxaline-2,3-dione
DL-AP5	DL-2-Amino-5-phosphonopentanoic acid sodium salt
L-AP4	L-2-amino-4-phosphonobutyric acid
TPMPA	((1,2,5,6-Tetrahydropyridin-4-yl) methylphosphinic acid
SR95531	6-Imino-3-(4-methoxyphenyl)-1(6H)-pyridazinebutanoic acid hydrobromide
MFA	meclofenamic acid
LFP	local field potential
cGMP	cyclic guanosine monophosphate

Abbreviations

PDE   phosphodiesterase

T   transducin

GABA   gamma-Aminobutyric acid

mGluR   metabotropic glutamate receptor

iGluR   ionotropic glutamate receptor

AMPA α-amino-3-hydroxy-5-methyl-4-isoxazolepropionic acid

NMDA   N-methyl-D-aspartate

KO   knock-out

PLL   poly-L-lysine hydrobromide

PI   propidium iodide

Contents

Contents

Chapter

1. Introduction

1.1. **The mammalian eye**

Humans rely intensively on vision as the source to sense our environment. Evolution gives each animal, based on their survival strategy, unique eyes for the fitness. Mammalians are equipped with simple eyes (in contrast to compound eyes). The structure of the eye is to optimize the goal of projecting the scene in the front to the back of the eye and send the visual signals to the brain. The most outer layer of the eye is formed by sclera and cornea. Sclera, the apparent white part of the eye, serves as a protection to the inner parts and maintain the shape of the eye. Cornea on the other hand, is completely transparent so that the light can enter our eyes. The circular muscles, iris, which also gives us the color of our eyes, control the size of pupil and further adjust the amount of light that enters by contraction. Behind the iris lies the transparent lens. The curvature of the cornea and lens together function as converging lens to focus the images right onto the retina. Outside the retina are the retinal pigment epithelium and the choroid layer, this is where the blood vessels are located and nourish the highly metabolized retina. In the back of the eye, the axons from retinal ganglion cells form a bundle called optic nerve. The optic nerve works as the electrical wire and send the visual signals to the brain. Human eye and the mouse eye are in principle very similar, but there is one major difference between the retinas in the two species- the human eye has an additional structure on the retina called fovea (Figure 1.1). Fovea is a small area that is highly specialized for high spatial resolution vision. It contains only photosensitive cell cones with a much higher density

than other region to make the images sharp. For human, this 2 degree area is the only clear vision we can have to fine detailed images for activity like reading. In the mouse retina however, this structure does not exist. The density of cone cells is much more even across the retina. In the coming sections, further details will be addressed on the topic of this study, the retina.
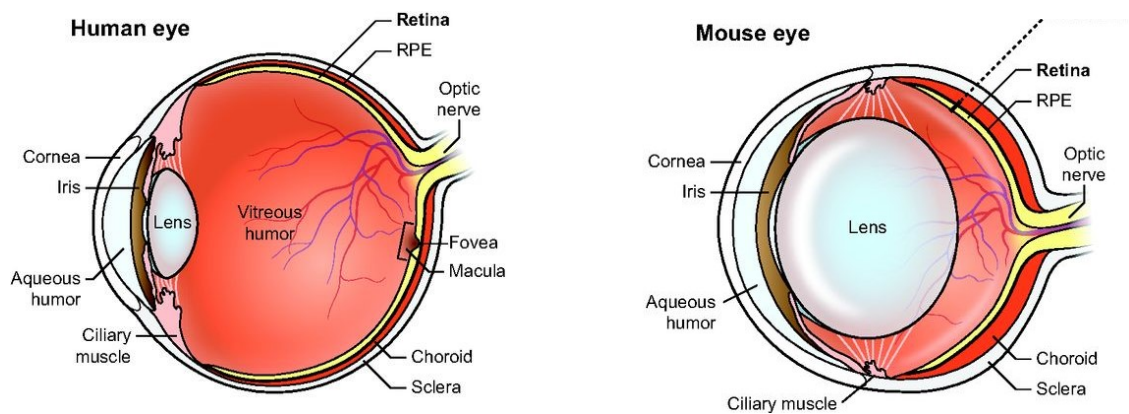

Figure 1.1: Schematic of human eye and mouse eye. Left: schematic human eye. Right: schematic mouse eye. The anatomy of human and mouse eyes are very similar except the size of the lens and the fovea structure. While the lens in mouse retina occupies a much bigger proportion than the human retina, the fovea structure does not exist in the mouse retina. Source: (Veleri et al., 2015)

1.2.   **Anatomy of the Retina**

Retina is the first stop to transmit light into the meaningful visual signals to the brain. Here, retinal cells turn the light into the neuronal language, spiking activity, for further processing. Almost hundred retinal cell types breakdown the images into different visual cues with their individual property of unique filter effect. The well-structured nuclear and plexiform layers make retina an ideal sample to study neural information processing. Three nuclear layers follow the path of signal transduction include the 1. outer nuclear layer (OPL), formed by rod and cone photoreceptors (PRs), 2. inner nuclear layer (INL), which include horizontal cells (HCs), bipolar cells (BCs) and amacrine cells (ACs) and 3. ganglion cell layer (RGL), as the name implies, mainly made by retinal ganglion cells (RGCs) and displaced ACs (Figure 1.2). Two plexiform layers are the areas where the dendrites and the axons from retinal neurons form connections. The signals from PRs are sent to the dendrites of BCs and HCs at the outer plexiform layer (OPL), while inner plexiform layer (IPL) is where RGCs receive inputs from BCs and ACs. The IPL can be further divided into 5 strata, the strata 1 and 2 belong to sublaminar a and strata 3,4 and 5 are assigned to sublaminar b for different visual pathways (see section 1.4). In the mouse retina, at least 14 types of BCs (Behrens et al., 2016; Tsukamoto and Omi, 2017), more than 40 types of ACs (Diamond, 2017) and more than 30 types of RGCs (Baden et al., 2016) form a delicate visual network to process different visual features. The further details of how the light signal is processed in each level will be introduced in the coming sections.
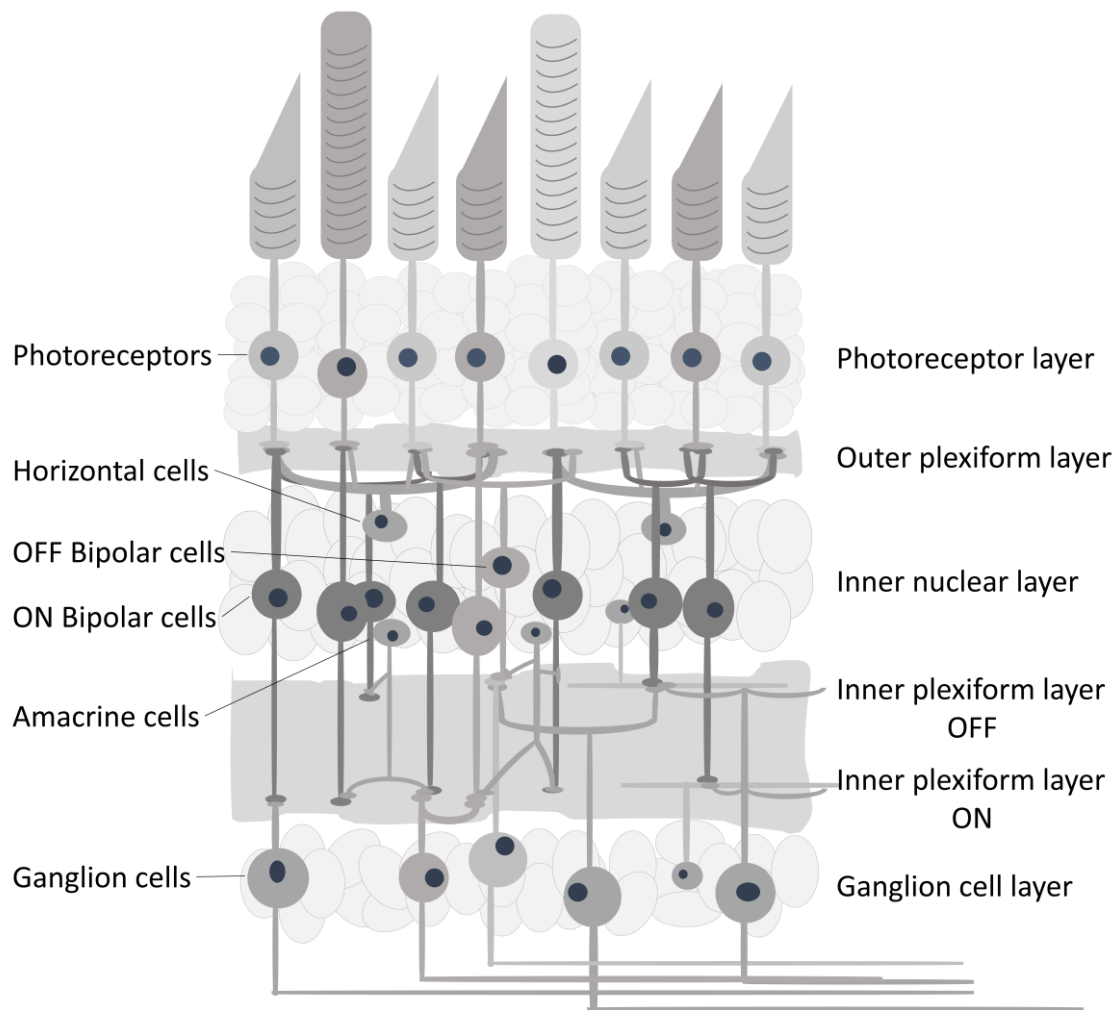
Figure 1.2: Schematic of retina anatomy. The retina can be mainly divided into nuclear layers and plexiform layers. While the three nuclear layers are where the cell somata locate, plexiform layers are made by dendrites and axons of the retinal neurons and is therefore also the layers for synaptic connections. The photoreceptor layer contains the inner segments of the rods and cones and function as a light receiver. The inner nuclear layer, where the bipolar cells, horizontal cells and amacrine cells can be found, serves as a switchboard and filter the incoming visual signals. The ganglion cell layer is made of ganglion cells and amacrine cells. The ganglion cells in this layer converges visual signals and send out the action potential output to the brain.

1.3.   **The initiation of sensing the light**

In the absence of light, cyclic guanosine monophosphate (cGMP) - gated sodium channels located at the membrane of outer segments from PRs remain open, resulting in a sustained inflow of extracellular positive charged sodium ions to the PRs. This constant inward current of PRs in the dark is called the dark current (Hagins et al., 1970; Klapper et al., 2016). The dark current maintains the constant depolarization of PRs, which leads to a constant release of the glutamates at their axon terminals when unstimulated by light.

When light enters to the back of the eye, it first travels through all the retinal layers to the discs inside the outer segments of PRs and activates the phototransduction cascade. At the membrane of the discs, the light sensitive protein rhodopsin (in rods) or cone opsin (in cones) absorbs the light, the molecule inside the rhodopsin called retinal change the conformation from 11-cis to all trans form. This conformation change leads to the alpha unit of the G-protein transducin (T) to bind and activate the protein phosphodiesterase (PDE), which will turn cGMP into GMP. With lower intracellular concentration of cGMP, the cGMP-gated sodium channels cannot be opened and thus hyperpolarizes the PRs. By stopping the release of glutamates from their ribbon synapse at the axon terminals, PRs signal the post synaptic cells of the incoming light.

Once the rhodopsin is activated by light and change the form of retinal from 11-cis to all trans, this rhodopsin is no longer sensitive to light and need to be transported to the retinal pigment epithelium to reverse the structure back to 11-cis form. That is, for all the PR discs, there is a pool of photosensitive rhodopsin. Once this pool is empty, the PR will no longer be light sensitive anymore. During the performance of mouse retina dissection, we remove the retinal pigment epithelium from the retina, which will potentially lead to run out of light sensitive rhodopsin. However, different from human retina, mouse retina only has two types on cones. L/M cones that are sensitive to green light and S cones that are sensitive to blue light. The mouse retina is not sensitive to red light; therefore, we can perform our experiments under dim red light to avoid bleaching the light sensitivity of the retina.
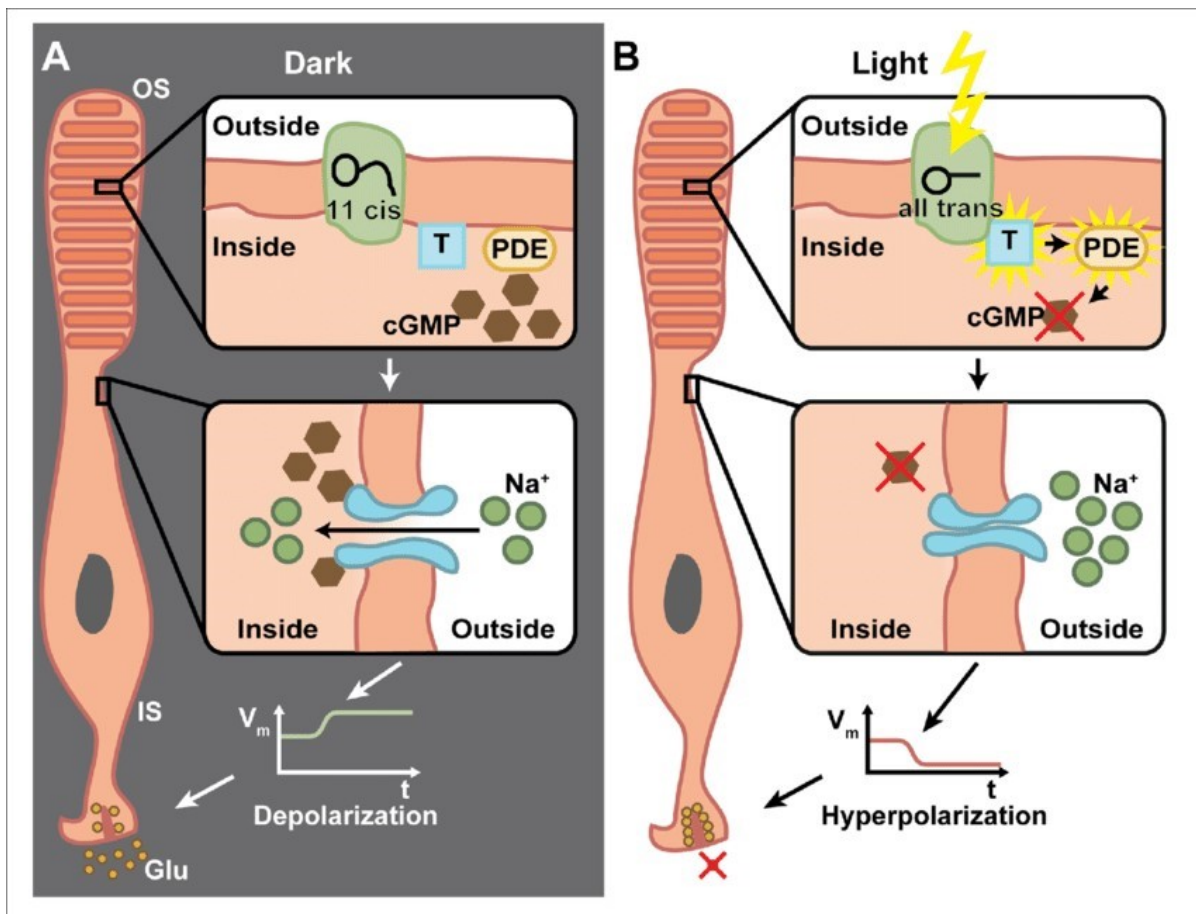
Figure 1.3: Dark current and phototransduciton. Source: (Klapper et al., 2016)

(A) Schematic of a photoreceptor in the dark. Retinal stays as the form of 11-cis. The transducin (T) and the phosphodiesterase (PDE) remain inactivated. cGMPs bind to cGMP-gated sodium channels and the channels open. The photoreceptor is therefore depolarized and release glutamates at its axon terminal.

(B) Schematic of a photoreceptor in the light. Retinal changes into all trans form and activate the transducin (T) and the phosphodiesterase (PDE). The PDE turns cGMPs into GMP. There is not enough cGMP binding to cGMP-gated sodium channels. The channels close, leading the photoreceptor to hyperpolarize and stop releasing glutamates at the axon terminal.

1.4.   **Excitatory and inhibitory pathways**

The process of the visual signal in the retina involves both excitatory and inhibitory pathways, while the excitatory pathways are in charge of sending the light signals and activate the post synaptic neurons, the inhibitory pathways are important for shaping the signals and creating the diversity of cell responses (Franke et al., 2017). Glutamate is the most essential excitatory neurotransmitter in the retina, as it mediates the signal transductions from PRs to BCs and from BCs to RGCs in the up to down, one-way vertical direction. The inhibitory neurotransmitters like gamma-Aminobutyric acid (GABA) and glycine released from HCs or ACs not only modulate the excitatory pathway, but also show lateral interactions and inhibition among each other, resulting a disinhibition effect.

1.4.1. *Excitatory pathway*

The excitatory pathways, or as vertical pathways in the following context, are referred to the signals that are sent via the release of the excitatory neurotransmitter glutamate from the PRs to BCs and to RGCs. Responses from retinal neurons can be grouped into ON and OFF responses. When a cell is activated by the increase of light, we say the cell has an ON response, otherwise if a cell is more active when the light intensity is decreased, it has an OFF response. Some cells are sensitive to the changes of light intensity and respond to both increase and decrease of light, in this case they would be called ON-OFF cells. The mechanisms to separate the same input from PRs into ON and OFF responses are via the expression of receptors at the postsynaptic membrane. After PRs receive the light, they send the signals to either ON or OFF BCs. The dendrites of ON BCs express metabotropic glutamate receptors (mGluRs). These receptors are G-protein-coupled receptors that would activate a series of indirect metabotropic process and close the cation channels on the membrane when bind to glutamates, eventually lead to hyperpolarization of the cell. That is, the ON BCs reverse the sign of PRs. When PRs receive the light and stop releasing glutamates, the ON BCs are activated (Figure 1.4 A). In contrast, OFF BCs express ionotropic glutamate receptors (iGluRs) on their dendrites. The iGluRs are ligand-gated ion channels, which means they open and activate the neuron when bound to their ligand glutamate. This makes the OFF BC response sign conserving, the OFF BCs are depolarized whenever the PRs are also depolarized (Figure 1.4 B).

The iGluRs express in the mouse retina are α-amino-3-hydroxy-5-methyl-4-isoxazolepropionic acid (AMPA) receptors, N-methyl-D-aspartate (NMDA) receptors and kainate receptors. These iGluRs are also expressed on the dendrites of RGCs, the postsynaptic neurons of BCs. As the visual signals continue to be passed on through the excitatory neurotransmitter glutamates, RGCs keep the same polarity as their input BCs. The ON and OFF signal pathways are segregated in the IPL by different stratifications, with sublaminar a for OFF channel and sublaminar b for ON channel. RGCs then send the visual signals through their axons to the brain in the form of spiking activity.
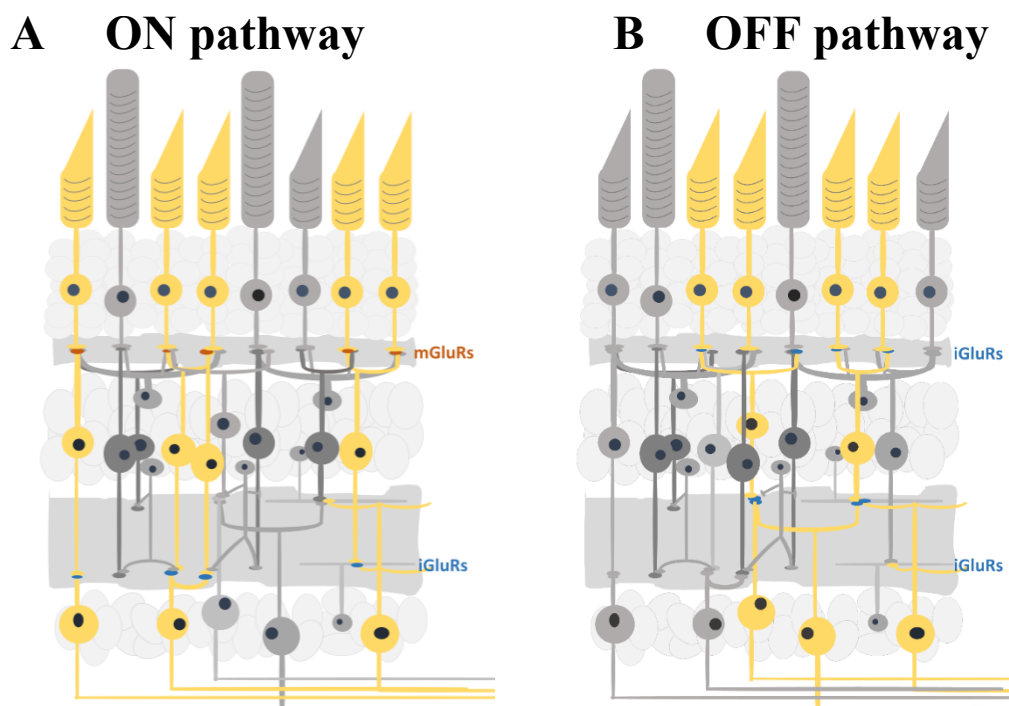
Figure 1.4: Schematic of excitatory ON and OFF cone pathways in the retina.

(A) Schematic ON cone pathway. PRs absorb light and hyperpolarize. The metabotropic glutamate receptors (mGluRs) at dendrites of ON BCs don't receive glutamate and therefore open the cation channels and depolarize. The depolarized BCs release glutamates at axon terminals and activate the connected RGCs via the ionotropic glutamate receptors (iGluRs). The ON BCs and ON RGCs form synaptic connections at the sublaminar b in the IPL.

(B) Schematic OFF cone pathway. When PRs absorb light and hyperpolarize. The iGluRs at OFF BCs dendrites close the cation channels and hyperpolarize, so as their downstream OFF RGCs. In the dark when PRs are depolarized, the glutamates bind to

the iGluRs and depolarize the OFF BCs. The same mechanism happens at the level of OFF BC - OFF RGC connection. The OFF BCs and OFF RGCs form synaptic connections at the sublaminar a in the IPL.

Except the functional criteria, another common way to distinguish the ON and OFF from BCs and RGCs is to check their stratifications. The IPL can be equally divided into 5 strata, it is generally agreed that strata 1 and 2 (sublamina a) are the OFF layers where the OFF BCs make connections to dendrites of OFF RGCs, while the strata 3,4 and 5 (sublamina b) are the ON layers and that ON BCs make synaptic contacts with ON RGCs here. The stratification of a cell's dendrites and axons are important in a sense that only those cells who are physically close to another have the chance to form synaptic connections. When a cell has stratification across multiple layers, it very often carries the communication between ON and OFF responses or it has both ON and OFF responses at the same time. For example, the ON - OFF RGCs are bi- or tri-stratified in both ON and OFF strata of IPL, therefore have the property of both ON and OFF light responses (Weng et al., 2005; Puller et al., 2015).

1.4.2. *Inhibitory pathways*

Within each synaptic layer of the excitatory pathways, there are the lateral inhibitory pathways modulating the PRs-BCs-RGCs excitatory pathway, mainly the HCs in the OPL and the ACs in the IPL. These neurons may use either GABA or glycine as their inhibitory neurotransmitters.

In the OPL of mouse retina, the single-type HCs receive inputs from many PRs with their dendritic arbors cover around 5000 μm^2 (Raven et al., 2007) and provide long range interactions and inhibitory feedback to the PRs. The GABAergic HCs express iGluRs and therefore preserve the sign of PRs after receiving glutamate (Chapot et al., 2017). The depolarized HCs release GABAs to inhibit their connected PRs and BCs and form a feedback loop with PRs. The more depolarized PRs are, the more depolarized the HCs are as well. As a result, HCs give more inhibition input back to the PRs. This feedback loop helps modulating the glutamate release at the PR axon terminals. Another important function of HCs is that it initiates the center-surround opponency of color and ON- OFF- responses by lateral inhibition.

The mechanism of center-surround opponency will be explained in further detail in the next chapter.

In the IPL, inhibitory ACs serve as the second level of lateral modulation to the BCs and RGCs. There are more than 40 types of ACs in the mouse retina, implying the potential variety of functions they have. Most of them are inhibitory neurons, but some release the excitatory neurotransmitters glutamate or acetylcholine. ACs can be divided into two major groups: the small-field and the wide-field ACs. The small-field ACs have dendrites that are small but vertically cross a broad range of sublaminae in the IPL. They modulate the relatively small region of visual field by releasing glycine as their neurotransmitters. The dendrites of wide-field ACs are usually monostratified and can extent to far distance laterally in the IPL. They shape the information from much broader area through the inhibitory neurotransmitters GABAs. ACs not only connect to the axon terminals of BCs and dendrites from RGCs, they also form connection among each other. When an inhibitory AC is inhibited by another inhibitory ACs, it leads to a disinhibition effect and further strengthens the excitatory pathways.

1.5.   **Center-surround receptive field**

In the mammalian retina, different morphological and functional types of RGCs cover the visual space with their receptive field in a mosaic organization to encode different features of the visual scenes uniformly (Wassle, 2004; Field et al., 2007; Anishchenko et al., 2010). This mosaic-like structural and functional organization is guaranteed by the classical receptive field. A cell's receptive field is defined as the region in visual space driving neuronal activity. What is special about the receptive fields of BCs and RGCs is that they have the opponent characteristic. Because of this ON- OFF- opponency, we are able to see the edges and contrast very well. When a light stimulus is within the central area of an ON- center OFF- surround cell, the activity of the cell increases as the size of the stimulus increases. However, when the size of the stimulus increases and reaches the surround area, the activity will start to decrease. As the size of the stimulus further increase, the inhibitory input is further strengthened and the activity decrease to a mild level. On the contrary, when a light hits the center of an OFF-center cell, the cell activity would decrease until the size of the stimulus increases and reaches the surround again (Figure 1.5).
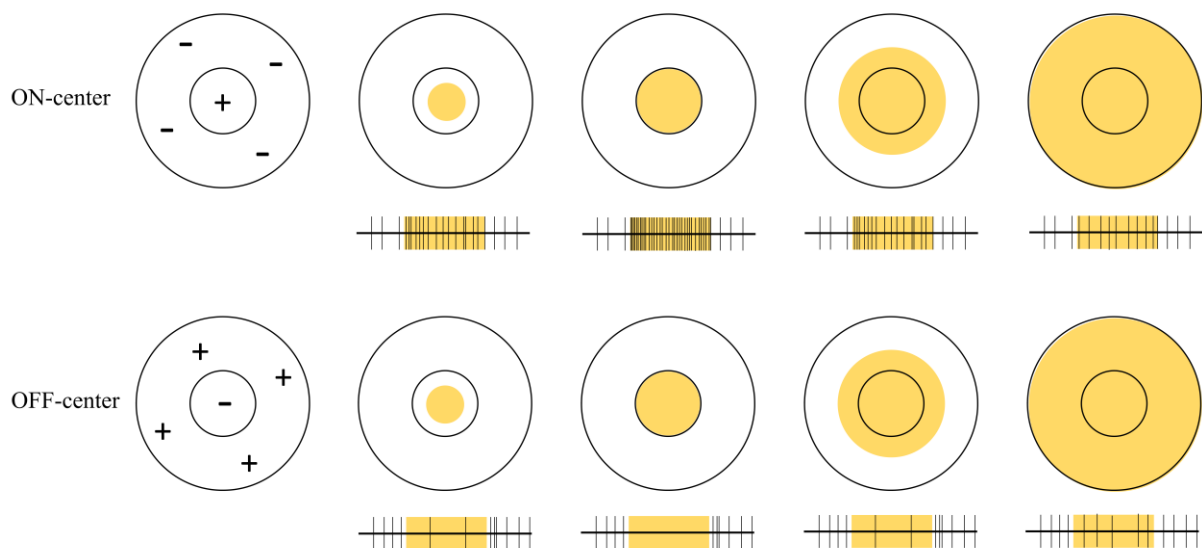

Figure 1.5: Illustration of center-surround receptive field for RGCs.

Top: receptive field of a ON-center OFF- surround RGC. When the light is located and restricted to the center of receptive field, the spiking activity increases as the size of stimulus

increases. When the stimulus increases and enters the surrounding area, the activity decreases until the stimulus reaches the broader of the receptive field. Down: receptive field of an Off-center ON- surround RGC. Similar as the ON- center cell, only that the cell is less active when it is illuminated at the center of receptive field. When the size of the stimulus is large enough to cover the surround area, the activity would increase again. Figure adapted from (Kandel et al., 2000).

The center-surround antagonism results from the lateral inhibition of the retina. Here the ON-center OFF-surround cell is used to address the mechanism of center-surround effect. When the receptive field center is stimulated, center cones reduce the release of glutamates and further depolarized the downstream ON BCs (mechanism explained in early chapter: 1.4.1 Excitatory pathway). The HC, whose receptive field covers both center (stimulated) and surround area (unstimulated), is stimulated by the release of glutamate from the surround area (note that PRs only release glutamate when unstimulated). The activated HCs release GABAs and inhibit the center cones and cause less glutamate to release, which means the BCs are even more active. When the size of the stimulus increases and covers the surround area, the HCs receive less glutamates than when only center is stimulated and therefore the strength of inhibition to cone terminals is less. Less inhibition at PR axon terminals from HCs make them release more glutamates, therefore the less active ON BCs (Figure 1.6). Since the connections between BCs and RGCs are sign-conserving, hence the less active RGCs at the end.
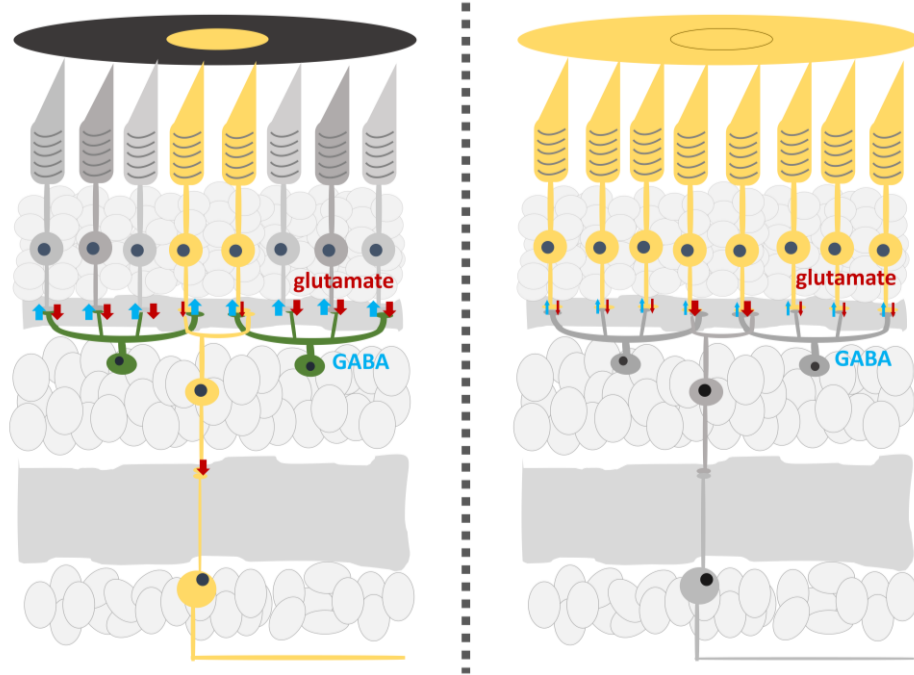
Figure 1.6: Schematic of lateral inhibition in the retina.

Left: When only the receptive field center is stimulated, the PRs at the center stop releasing glutamate, causing the ON BCs to depolarize. The HCs receive glutamates from the surrounding PRs and are thus activated. The activated HCs release GABAs to further inhibit the central PR terminals to release glutamate, leading ON BCs to further depolarize.

Right: When the stimulus covers the surround area, HCs receives much less glutamates from the dendritic field from PRs and are therefore less active. The less active HCs release less GABAs as negative feedback to PR terminals. The less inhibited PRs release more glutamates to BC dendrites, making them more hyperpolarized. Figure modified from (Baker, 2016).

1.6.   **Rod pathway**

The two types of PRs, cones and rods, are in charge at different times of a day with their special characteristics. In the daytime while the light is sufficient, the cones that absorb different wavelengths are dominating and provide color vision. When the night comes and the level of illuminance is low, the extremely light-sensitive rods take place. Since there is only one type of rods, there is no color vision under scotopic environment. Unlike cone pathways, rod BCs are not directly connected to the RGCs, instead, the visual signals need to bypass cone pathways via a particular type of ACs, the AII amacrine cells, to reach RGCs.

AII ACs are narrow-field, multistratified glycinergic neurons. They are postsynaptic to ON type rod BCs and make connections to both ON and OFF cone BCs at the dendrites in sublaminar b and sumlaminar a respectively. In the sublaminar a of IPL, AII ACs conduct to OFF cone BCs via the release of neurotransmitter glycine. At the same time, AII ACs pass rod signals to ON cone BCs by making gap junctions with them at sublaminar b. With different outputs from AII ACs, the single polarity rod-driven information can be distinguished into ON and OFF responses and passes to the corresponding RGCs.
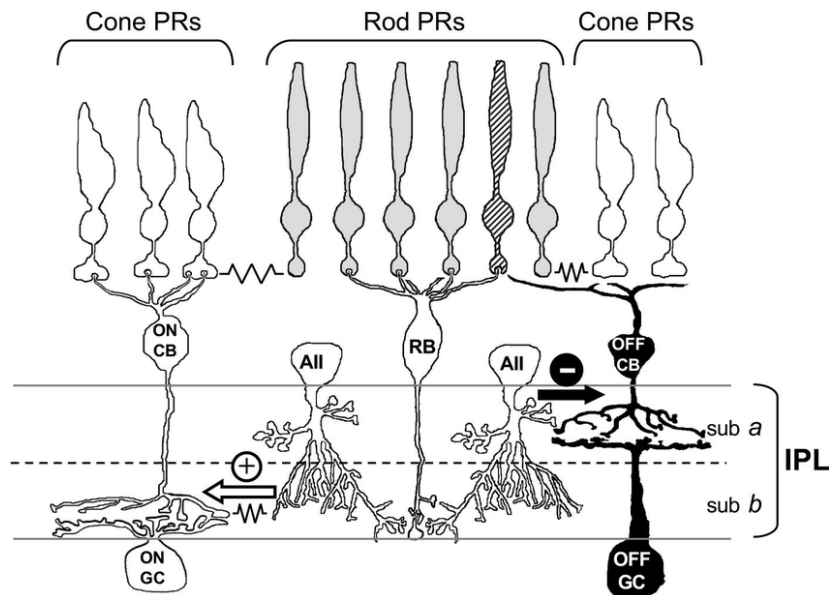

Figure 1.7: Rod signal pathway. As rod BCs don't have direct connection with RGCs, the rod signals use AII ACs to pass the signals to cone BCs and RGCs. By making gap junctions to ON cone BCs in sublaminar b and releasing glycine to OFF cone BCs in sublaminar a, the multistratified AII ACs divide the single ON input from rod BCs into ON and OFF channels. Souce: (Protti et al., 2005)

1.7.   **Gap junctions**

Besides neurotransmitters, neurons can also use electrical synaptic transmission to communicate. These channels are gap junctions, instead of synaptic connections, gap junctions directly connected the membrane between two neurons and allow the direct exchange of ions and small molecules. Gaps junctions are commonly seen in the brain and retina, as they offer a much faster signal transduction than neurotransmitters.

Each gap junction is formed by two hemichannels from the opposed cells, and each hemichannel is comprised of 6 connexin protein subunits. The combination of two hemichannels can be either homotypic or heteromeric. Among the many types of connexins (Cx), the coupling between Cx-36, -45, -50 and -57 are known to express in mouse retina between PR-PR, HC-HC, BC-BC, AII AC- AII AC, RGC-RGC, RGC-AC and AII AC- cone BC. HC-HC are connected by Cx50 (Dorgau et al., 2015) or Cx57 (Hombach et al., 2004), Cx45 is expressed in RGC and AII AC connection, while the majority of the electrical couplings involve Cx36.

Gap junctions are important in mediating the properties of retina from many levels. PRs use gap junctions to pool up signals at night and extend the functional range for both rods and cones (Trenholm and Awatramani, 2015). Gap junctions between ACs and BCs pass the rod-driven signal to the cone pathway. Neurons connected with gap junctions can easily form a synchronized network activity since they are physically connected together. The HC-HC network greatly increase the receptive field of a HC and thus can regulated much broader range of PRs (Xin and Bloomfield, 1999a; Shelley et al., 2006). The AII-AII network was found very likely to be the source of oscillation activity in the photoreceptor degenerative retina (Choi et al., 2014b; Margolis et al., 2014; Trenholm and Awatramani, 2015; Zeck, 2016). The coupled ON direction-selective RGCs show synchronous activity and are able to detect the direction of moving objects (Ackert et al., 2006)

The coupling strength between gap junctions is mediated by many different factors, such as circadian rhythm (Jin et al., 2015), background illumination (Bloomfield and Volgyi, 2004, 2009), dopamine level (Lasater, 1987; Kothmann et al., 2009) or nitric oxide (Patel et al., 2006). For example, the couplings between AII ACs are the strongest at twilight and decrease when the level of light either increase or decrease. Thus, the coupling strength is dynamic and always adapt to the environment at the moment.
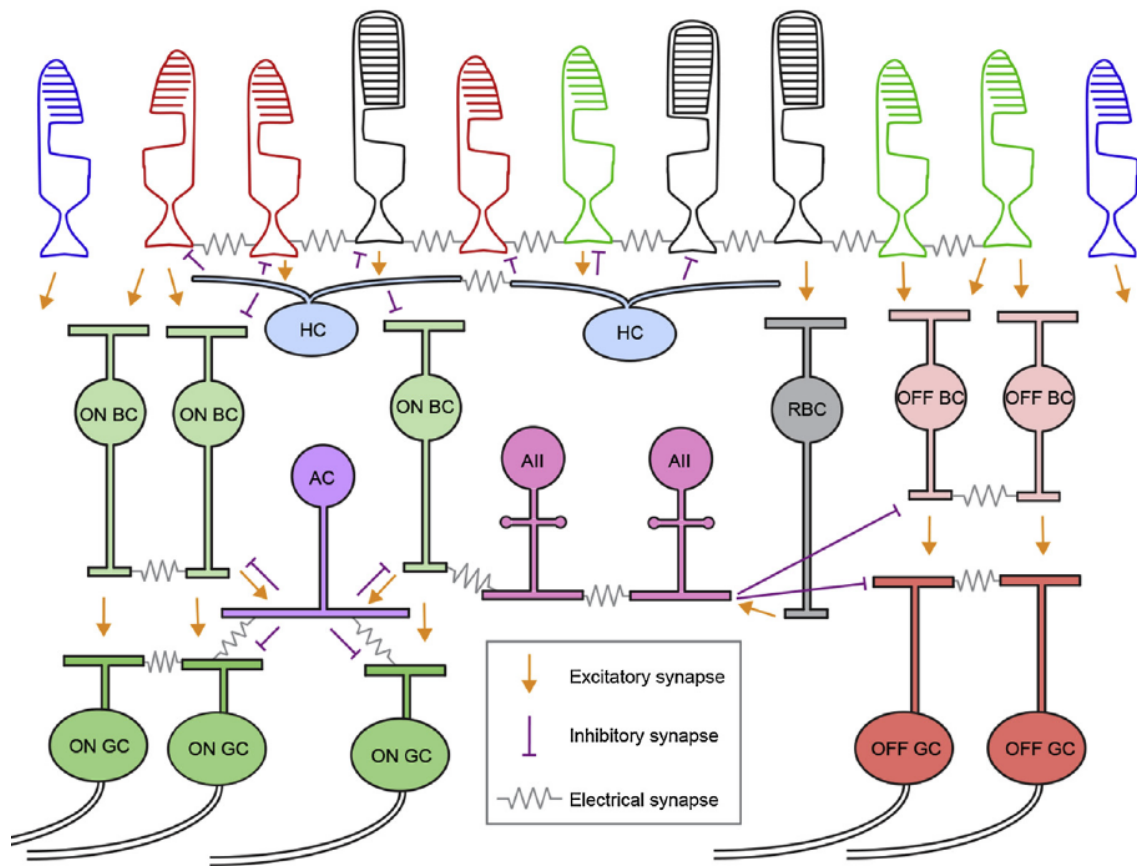
Figure 1.8: Gap junction network in the mammalian retina. The diagram represents an overview of the gap junctions between retinal neurons. Springs in the figure mark gap junctions. Electrical coupling can be found in between the same cell type like PR-PR (rod-rod, cone-cone, rod-cone), HC-HC, AII-AII, BC-BC and RGC-RGC. AII ACs connect to ON BCs via gap junctions to pass the rod signals. RGCs connect to their neighbor ACs to make indirect couplings with other RGCs and results in synchronous spiking activity. More details in the text. Source: (Trenholm and Awatramani, 2017)

1.8.   **Dynamic receptive field of RGCs**

Though the excitatory center- inhibitory surround has been the rule of thumb for receptive field for retinal neurons, reviewed in Wienbar and Schwartz, 2018 has shown that retinal neurons can be activated by stimulus outside classical receptive field as well (Wienbar and Schwartz, 2018).

For instance, Mani and Schwartz found one type of RGC in mouse retina called ON delayed RGC responded to stimulus far outside their dendrites and respond earlier when they were stimulated with a bigger diameter spot, opposite to the expectation of inhibitory surround effect (Figure 1.9A). They found further that the distant activation was due to the disinhibition effect, which means the AC that inhibits the BC was inhibited by other long range ACs (Mani and Schwartz, 2017). Other examples like J-RGCs, found by Kim et al., showed polarity change when the size of the stimulus change (Kim et al., 2008). The polarity change was also observed in other RGC types (Sw1-, Sw2-, and Sw3-RGCs), who switch polarity preference in a luminance dependent manner (Pearson and Kerschensteiner, 2015).

When stimulated with dynamic stimuli, RGCs show two different computations co-existed within the same population for central (inside receptive field) and distal (outside receptive field) stimuli. Deny et al. discovered that RGCs could be activated by distal stimulus, but the response was suppressed when a stimulus appears inside the receptive field of the cell (Figure 1.9C). They further found out that the distal activation was by the disinhibition of glycinergic ACs by distant wide-range GABAergic ACs (Deny et al., 2017).

Remote modulation of RGCs was not only observed in mice, but also in cats (Passaglia et al., 2001; Passaglia et al., 2009), salamander (Olveczky et al., 2003) and rabbit (Chiao and Masland, 2003) retinas. Studies have found that it is important for the RGCs to detect global image motion moving in a different trajectory to the center receptive field in order to identify the moving objects in a stationary scene. Grating patterns moved outside the classical receptive field suppressed the activity of RGCs when it was coherent with the stimulus within the receptive field. The antagonistic effect was diminished with the blockage of glycine receptors by applying strychnine and was most likely driven by ACs.

These studies provided strong evidences for the importance and complexity of non-classical activations, which involve the sophisticated modulations of the lateral inhibition or disinhibition.
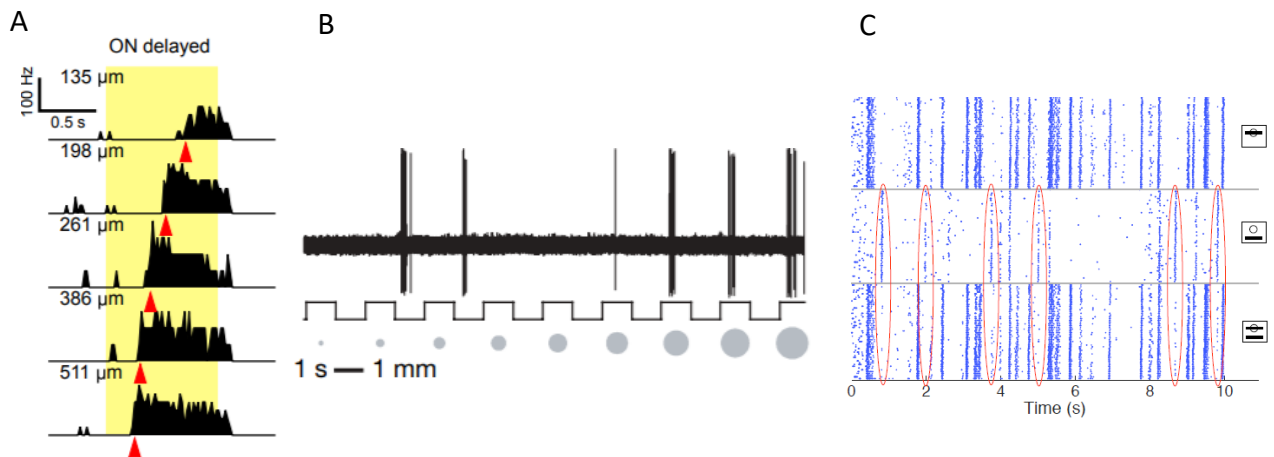
Figure 1.9: Non-classical receptive field of RGCs. Several studies showed the atypical receptive field responses of RGCs. (A) The latency of ON delayed RGC response decreased as the stimulus size increased. (B) J-RGCs showed different polarities at different stimulus sizes. (C) RGCs respond to distal stimulus, but when the central and distal stimuli were presented together, the distal response was suppressed. Figures adopted from A: Mani and Schwartz, 2017, B: Kim et al., 2008, C: Deny et al. ,2017.

1.9.   **Aim of the thesis**

To investigate the non-classical remote activation of retinal neurons, mainly in BCs and RGCs discussed in the previous section, I proposed a methodological approach by adapting retinal vertical slice onto the high-density Complementary Metal-Oxide-Semiconductor-based microelectrode array (CMOS MEA) (Bertotti et al., 2014) to study signal processing across different layers using electrical imaging (Zeck et al., 2017) over large areas (1 mm^2) at high temporal (milliseconds) and spatial resolution (micrometer).

By imagining the propagation of local field potentials (LFP) in vertical retinal slices upon well-defined local light stimuli with different background conditions and comparing them to ganglion cell recordings in flat-mount configuration, the light conditions that would stimulate remote RGCs could be identified and potential mechanisms could be investigated.

Instead of focusing on the stimulus-induced activity change in one or few very specific cell types to reveal the microscopic circuitry and the underlying signal processing mechanisms, the addressed approach would offer the macroscopic understanding of how the different retinal layers contribute to signal processing on a global scale.

Chapter

2. Materials and Methods

2.1. Animals

The mouse has been a very promising animal model for retina or brain researches, as it is close to human compare to other non-mammalian models like flies or zebrafish. The well-developed genetic tools offer many possibilities to study disease models as well as functions of certain gene or protein that the other mammalian models don't have. In this study, healthy and Cx36 knock-out adult mice from one of the most common model C57BL/6J background at aged between 1-7 months of either sex were used. Cx36 knock-out mice were kindly offered by lab of Prof. Dr. Karin Dedek (Meyer et al., 2014; Tetenborg et al., 2019). All of the animals were housed in a 12 h day-night rhythm. Mice were dark adapted for at least 1 hr prior to experiments, anesthetized with CO_2 and euthanized by cervical dislocation.

All procedures were approved by the animal use committee of the Natural and Medical Science Institute at the University Tübingen and performed in compliance with the ARVO statement for the use of animals in Ophthalmic and Visual Research. Protocols compliant with § 4 paragraph 3 of the German law on animal protection were reviewed and approved by the Regierungspräsidium Tübingen (AZ 35/9185.82-7). All efforts were made to minimize the number of animals.

2.2.   **Retina Dissection**

Eyes were removed and immediately transferred to carboxygenated (95 % O_2 and 5 % CO_2) Ames' medium (23 mM NaHCO3, A1420, Merck KGaA (Sigma Aldrich)) after cervical dislocation. Isolated eyes were both hemisected in glass petri-dish with surgical scissor under a dissecting microscope illuminated with dim red light (long-pass filter > 640 nm). The hemisected eye cup was further cut into half or 1/3 with blade in slice or flatmount preparation respectively. The remaining eye was kept in the carboxygenated Ames' medium in room temperature until used. The retina was carefully detached from the retinal pigment epithelium layer and the vitreous body was removed thoroughly with fine tweezers. To this step, the retina was ready for further preparation. The whole procedure was performed at room temperature in carboxygenated Ames' medium under dim red light.

2.3.   **Retinal slice preparation**

A 35 mm petri dish with half filled, solidified 4 % low-melting agarose gel (6351.5, Carl Roth, Germany) was prepared before retinal dissection. The isolated retina was transferred onto the top of the solidified low-melting agarose gel with RGCs side up, then the excess Ames' medium was removed to flatten the retina. 37 °C, 4 % low-melting agarose gel was gently poured into the petri dish to embed the retina. The petri dish with retina was immediately transferred on ice for 1 min for the newly added gel to solidify (Figure 2.1 A). Afterwards, the agarose gel block with retina was trimmed into a proper size and glued onto the vibratome specimen disc with histoacryl (1050052, B. Braun, Germany). A similar size of 5 % broad range agarose gel block (T846.2, Carl Roth) was glued on the same specimen disc right against the gel block with retina (Figure 2.1 B). The additional gel block offered a support to the embedded retina and the gel so it did not detach easily from the specimen disc from the force from slicing. The specimen disc was placed into the buffer tray and filled with cooled (around 10 °C), carboxygenated Ames' medium. The buffer tray was placed into the vibratome (VT1200 S vibrating blade microtome, Leica) with the retina facing the blade (Figure 2.1 C). The flatmount retina was sliced into 500 μm thick of slices with razor blade (Extra Double Edge Safety Razor Blades, Derby) vibrating in 0.01 mm/s speed and 0.25 mm amplitude (Figure 2.1 D). The cut slices were collected from the buffer tray and kept in Ames' medium on 37 °C water bath with continuous carboxygenation until used.
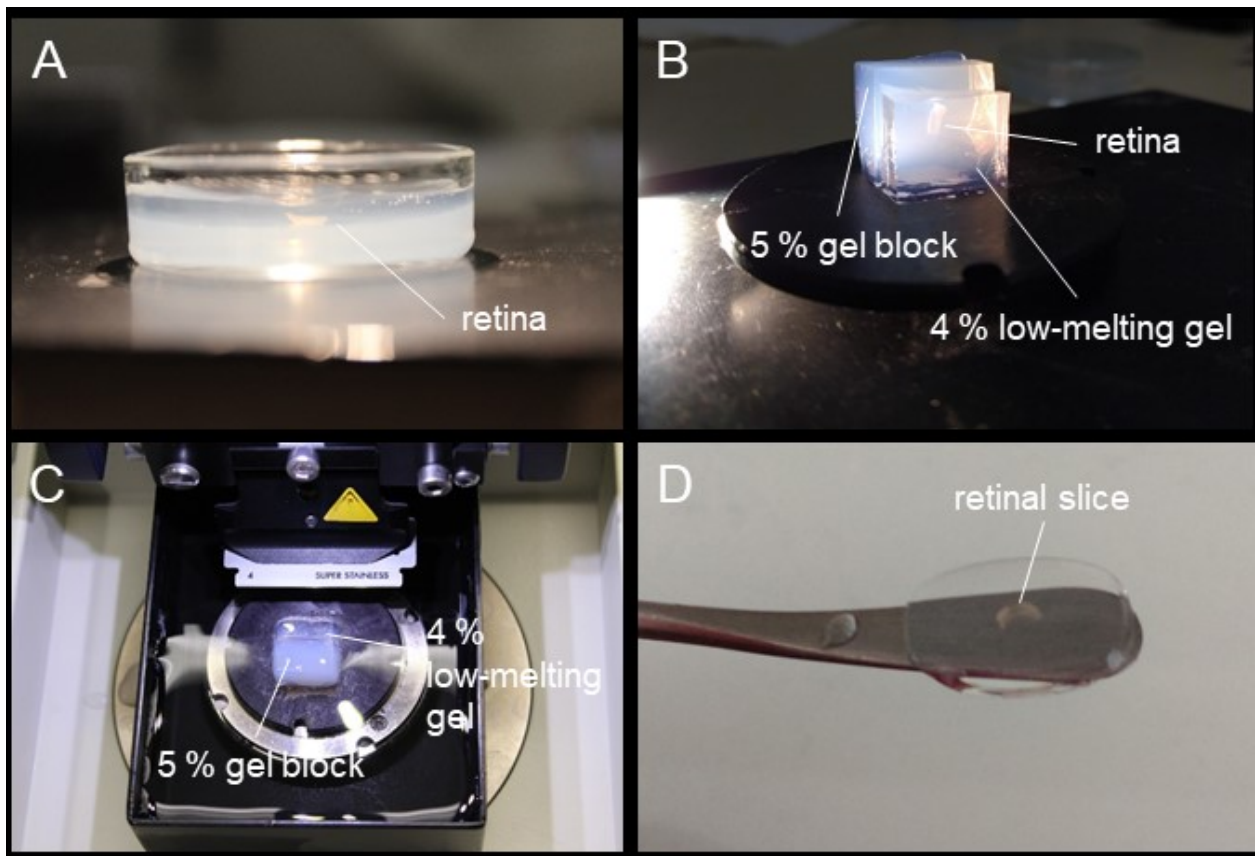
Figure 2.1: Pictures of slice preparation. (A) Side view of dissected retina embedded in the 4% low-melting agarose gel. (B) A 5 % broad range agarose gel block glued right next to the gel block with retina on the specimen disc. (C) Flat-mount retina with gel blocks in buffer tray filled with Ames' medium on vibratome. (D) Sliced retinal slice (500 µm thick).

2.4.   **The CMOS MEA 5000 system**

Both RGC spiking activity as well as LFPs from retinal neurons were recorded from the high-density Complementary Metal-Oxide-Semiconductor-based microelectrode array (CMOS MEA) (CMOS-MEA5000-System, Multi Channel Systems MCS GmbH, Reutlingen, Germany)(Bertotti et al., 2014). The system allowed recording from 4225 (65 x 65) electrodes in 1 mm^2 along with 1024 (32 x 32) stimulation sites at the sampling rate up to 25 kHz. Each electrode is 8 µm in diameter with 16 µm distance between the center of each electrode. The electrodes are made of TiN and the whole surface of the chip is covered with a thin layer of Zr/TiO$_2$ as a protection to the underlying circuitry. The interface-board connected the recording computer and the headstage. The gold pins on headstage made contacts to the chip and send the recorded data through the interface board to the recording computer (Figure 2.2). The headstage is equipped with a temperature control, which was set to 36 °C during the whole recording.

Figure 2.2: Components of CMOS 5000 system. Top: Interface-board, middle: Headstage with a mounted chip bottom: CMOS-MEA chip. Source: Multi Channel Systems MCS GmbH

2.5. **Interfacing retinal tissues to the CMOS MEA**

2.5.1. *Preparation of right-angle (45 degree) mirror*

To prevent the light from directly stimulating the light-sensitive CMOS MEA and to be able to stimulate on the PR side of the vertical slice, a 3 mm mirror (#49-405, Edmund Optics, Germany) was adapted onto the CMOS MEA outside the recording area (Figure 2.3) to reflect the light stimulus from the objective to the vertical slice. The mirror needed to be preprocessed first to ensure the fix position during the whole experiment. To make a removable yet stable mirror, a 20 µm thick silicone sticker (SILPURAN ® Film 2030, Wacker Chemie AG, Germany) was attached to the bottom of the mirror with the following procedure. The surfaces of the mirror and silicone sticker were cleaned with isopropanol and dried with N_2 gas. The mirror and the silicone sticker were carefully placed into a plasma cleaner for 1 min at medium level. Afterwards, the mirror was immediately attached onto the silicone sticker. Note that there should not be any dust or air bubble in between. The mirror with silicone sticker were kept in a clean container overnight for the covalent bonds to form. The sticker is later trimmed to the same size as the bottom of the mirror with a surgical blade.
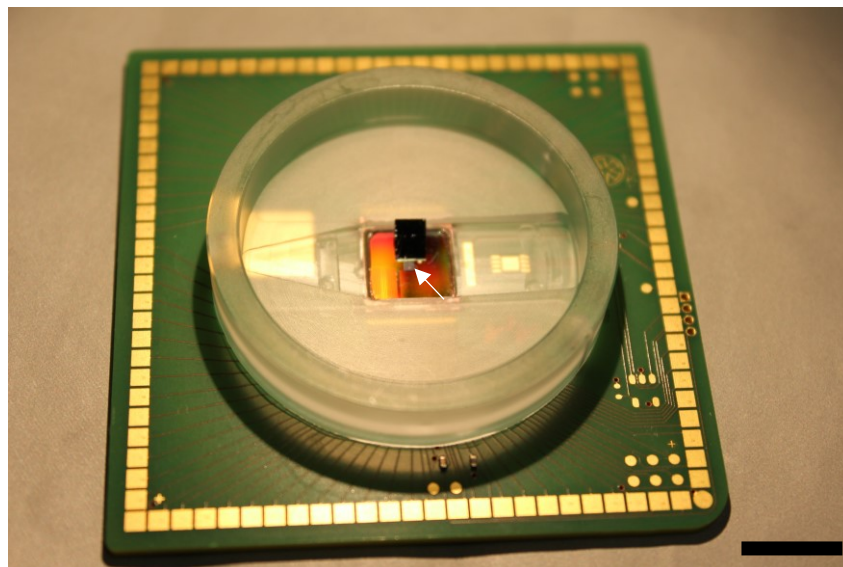

Figure 2.3: A CMOS MEA with a right-angle mirror adapted on top. The mirror was preprocessed with a thin 20 µm silicone layer at the bottom and placed right next to the sensor array (white arrow). Scale bar: 1 cm.

2.5.2. *Interfacing vertical slices to the CMOS MEA*

The CMOS MEAs were first cleaned with 5%, 80 °C Tickopur R60 (Dr. H. Stamm GmbH, Germany). After rinsing with bidistilled water, the right-angle mirror which was preprocessed a silicone layer was attached to the surface of CMOS MEA outside the recording area. The CMOS MEA surface was then coated with poly-L-lysine hydrobromide (PLL) solution until used (1 mg/ml in bidistilled water, 150 kDa molecular weight; Sigma Aldrich, Germany). Prior to retinal interfacing, the CMOS MEA was rinsed with Ames' medium to remove the unbounded PLL. The gel embedded retinal slice was trimmed into proper size (remove additional gel, note that the slice should not be cut) and placed onto the coated CMOS MEA with the cutting side. The PR side was faced to the mirror (Figure 2.4A). A small amount (30-50 µL) of 37 °C, 4 % low-melting agarose gel was dropped on top of the positioned retinal slice and let solidified to ensure the position of retinal slice during the whole recording. The CMOS MEA chamber was filled up with Ames's medium and placed into the headstage (Figure 2.4B).
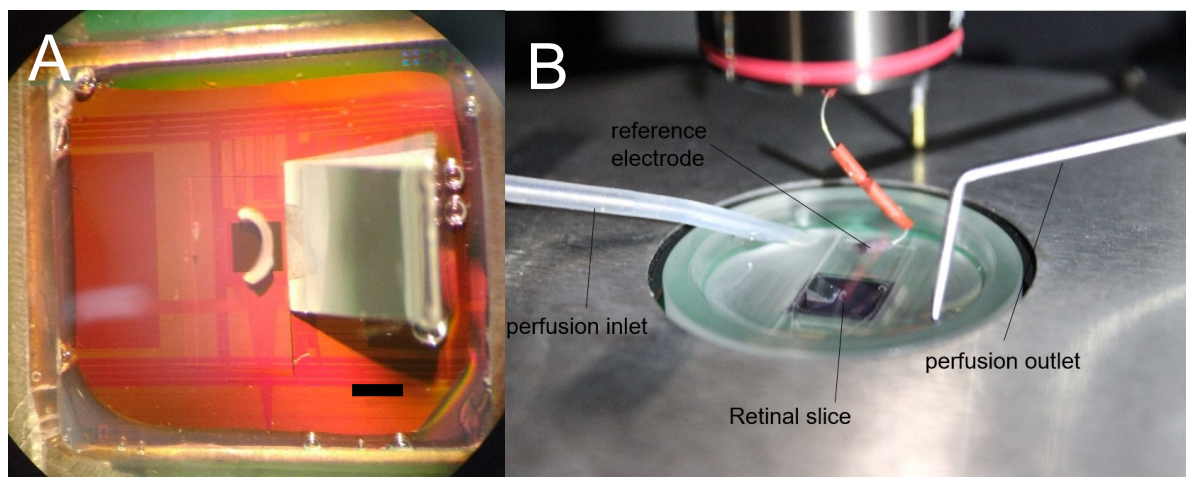
Figure 2.4: Retinal slice interfaced to CMOS MEA. (A) Top view of a vertical slice adapting to CMOS MEA with a positioned right-angle mirror. The black area at the center is the 1 mm^2 recording area. Scale bar: 1 mm. (B) Picture of adapted retinal slice on CMOS MEA in the headstage ready for recording. The perfusion inlet and outlet make sure the slice was constantly perfused with fresh carboxygenated Ames' medium. Note that the Ag/ AgCl reference electrode must be immersed in the medium the whole time.

2.5.3. *Interfacing flat-mount retina to the CMOS MEA*

Generally, for flatmount recordings, the CMOS MEAs were cleaned and coated as mentioned above. After removal of vitreous body, the retina was placed carefully onto the CMOS MEA sensory area with RGC side down (Figure 2.5). However, if there was too much curvature of the retina, flatten the retina properly on the CMOS MEA could be very difficult. In this case, the following method would be applied. The sensory area of CMOS MEA was cleaned as mentioned above, then coated with 1 µL of Cell-Tak (354240, Corning BV Life Sciences) and let air-dry. After removal of vitreous body, the retina was placed PR side and flatten on a membrane filter (Merke, Millipore, HABP02500). The membrane and retina were transferred together carefully RGC side down (Chiao et al., 2020) onto the CMOS MEA. The membrane filter was removed and Ames' medium was added immediately to the MEA chamber. Note that with the second method, any adjustment of the position of the retina after placement should be avoided. The retinas were constantly perfused with carboxygenated Ames' medium at 33-35 °C. Both retinal slice and flatmount were kept in the recording chamber for at least 30 min before the beginning of recording to ensure stable neural activity. The retinal activities were recorded with 20 kHz sampling rate.
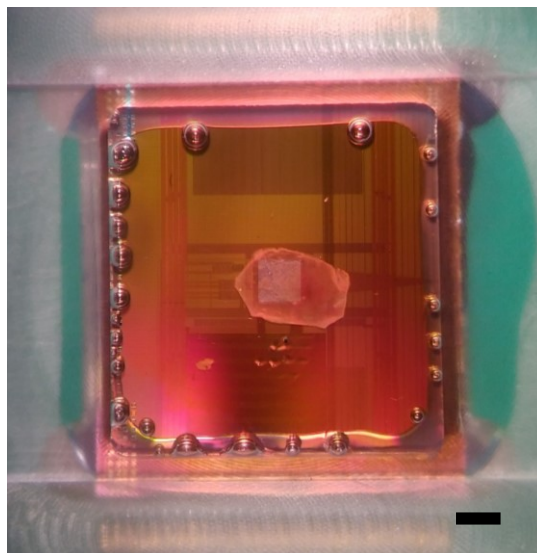

Figure 2.5: A flat-mount retina on recording area of CMOS MEA. Picture of a flat-mount retina adapting to the CMOS MEA. The gray area at the center is the 1 mm^2 recording area. Scale bar: 1 mm.

2.6.   **Optical Stimulation**

2.6.1. *Stimulation hardware*

The CoolLED pE-4000 system (CoolLED Ltd., Andover, UK) was the light-source in this study. The system provides light at 16 different wavelengths in the range from 365 nm to 770 nm (wavelength spectrum shown in Figure 2.7). In this study, 490 nm wavelength (full-width half maximum= 28 nm) was used for light stimulation and 740 nm wavelength (full-width half maximum= 35 nm) was used to illuminate the retinal slice and the sensor array of the CMOS MEA for positioning (Figure 2.7).

The CoolLED pE-4000 system composition with the μ-Matrix DMD (Rapp OptoElectronic GmbH, Germany) were used to provide light stimuli to the retinal tissues (Figure 2.8). The μ-Matrix DMD together with its own software allow users to customize the given stimuli. More detail in the coming section.
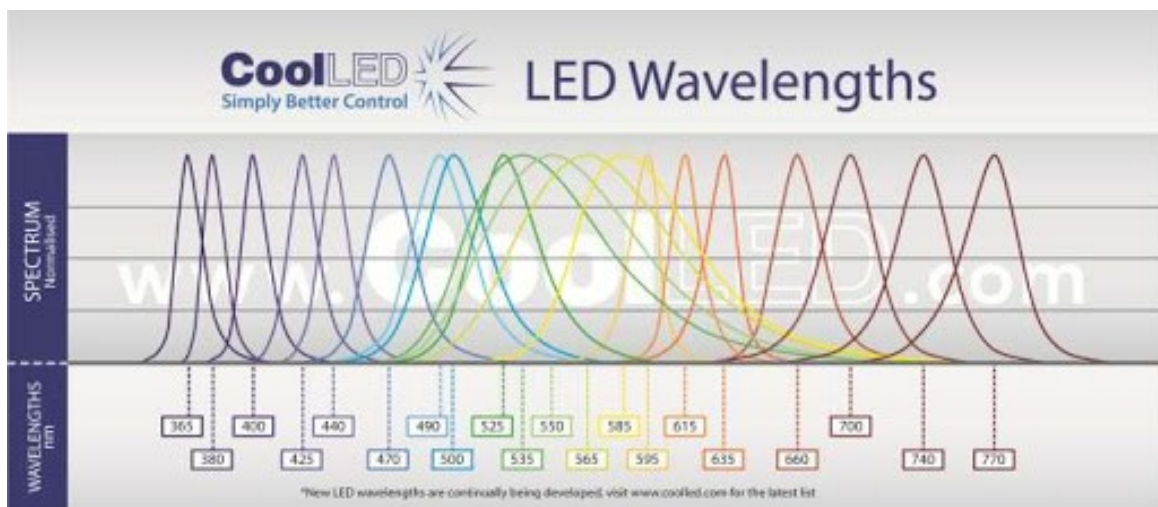
Figure 2.6: Wavelength spectrums of CoolLED system. Source: CoolLED Ltd.

The CoolLED system provided 16 different wavelengths in 4 channels, with 4 choices of wavelengths within each channel. In this study, only the 490 nm and 740 nm were used.
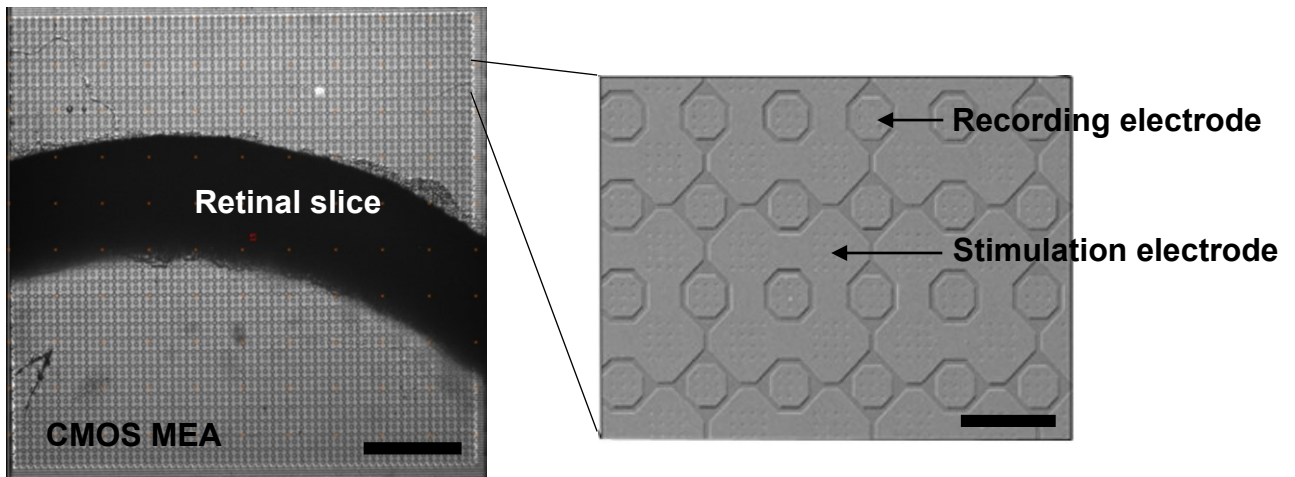
Figure 2.7: Vertical slice on CMOS MEA illuminated with 740 nm red light.

Left: Top view of the retinal slice of a CMOS MEA illuminated with 740 nm. The 740 nm was used to make sure of the position and focus of the given stimulus without bleaching the retina. Scale bar: 200 µm. Right: Zoom in view of the sensory area of a CMOS MEA. Scale bar: 20 µm.
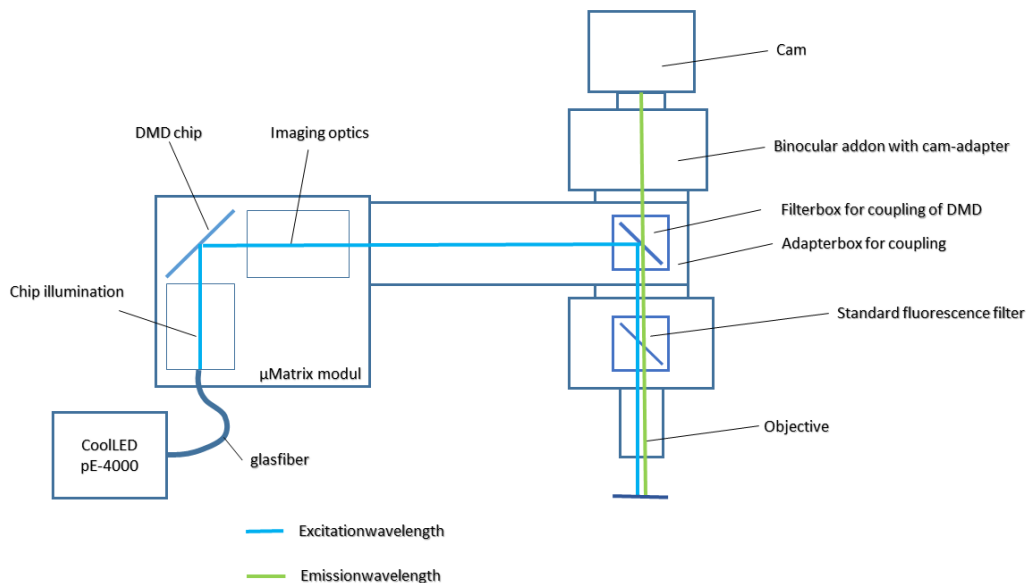
 Figure 2.8: Illustration of the beam-path for the µ-Matrix DMD. The light-source for the µ-Matrix system is provided from CoolLED pE- 4000 systems. The light was transmitted to the µ-Matrix module via glass-fiber and illuminates the DMD-chip. Reflected light then passed the imaging optics and exited to µ-Matrix module and entered the microscope's beam-path by mirrors placed in the adapter box. The light was then focused by an objective onto the sample. Reflected light was collected by a CCD-camera mounted on top of the microscope.

After confirming the position of the retinal sample, the µ-Matrix DMD was used in composition to provide spatially confined stimuli to the retina. Stimuli can be configured directly on the image acquired with red light (as in Figure 2.7) or with customized implemented images in the corresponding software tool. Source: Adapted from Rapp OptoElectronic GmbH.

2.6.2. *Light stimulation of retinal slice via 45 degree right-angle mirror*

Figure 2.9A summarizes the experimental design of the light stimulation on to retinal slice via a right-angle mirror with a schematic figure. In the retinal slice preparation, the relative position of the slice and of the mirror was first located with 740 nm light source, then the focus was adjusted to acquire the image of the PR layer reflected from the mirror (Figure 2.9 B.C). The light stimulation areas were selected precisely with the software in µ-Matrix system and the light stimulus was projected onto the PRs via the mirror (Figure 2.9D).

The light stimulation protocol is schematically shown in Figure 2.9E. Combinations from two stimulus sizes (small field :100 x 30 µm^2 and global field: 1000 x 300 µm^2) and two light intensities (light stimulus :10^7 R* rod-1 s-1 and background :10^5 R* rod-1 s-1) form the three stimuli used for this study. (1) "local background": a small field light stimulus projected onto a same size local background (2) "global background": a small field light stimulus projected onto a global background (3) full field stimulus: global field stimulus projected onto a global field background. Short light pulses of 10 ms, 20 ms, 40 ms, 80 ms, 160 ms and 320 ms were given after 2 sec of the adaptation with 1 sec interval in between each pulse onto the PR layer. Each stimulus duration was repeated 12 times.

For flat-mount retina stimulation, the same three stimuli were applied directly without a mirror to the PRs through a 5X objective (LMPlanFl, 5X/0.13, Olympus) of an upright microscope (BX50WI, Olympus)
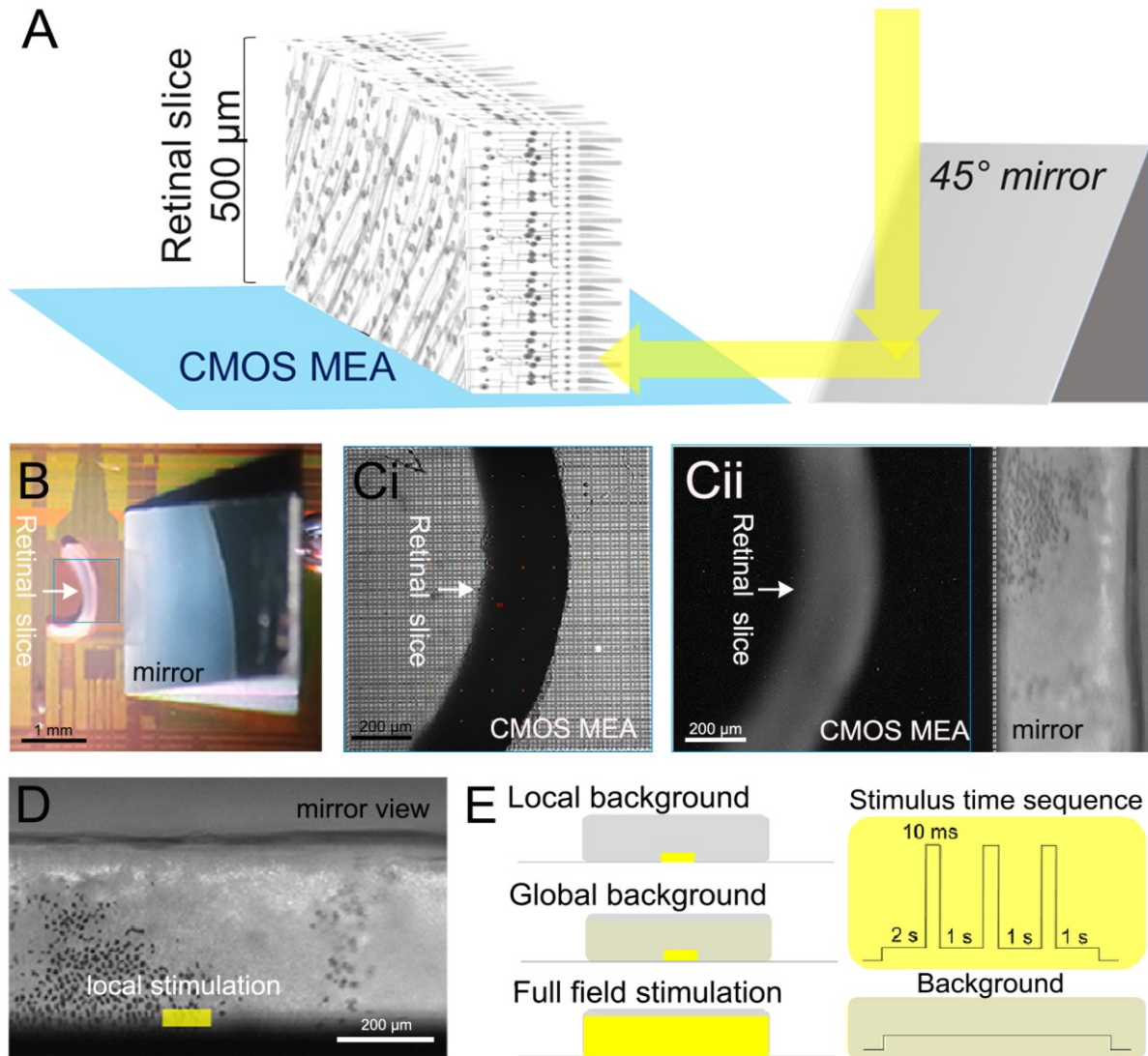
Figure 2.9: **Experimental setup and light stimulation protocol** (A) Schematic description of the experiments investigating signal propagation in retinal layers of a vertical slice. Light was projected through a microscope objective onto a 45° right angle mirror, which stimulated the photoreceptor layer. (B) Photograph showing the slice interfaced to the 1mm^2 sensor surface of a CMOS MEA (marked by blue square). The mirror was visible on the right. (Ci) Photograph taken through the microscope objective focused on the sensor surface. (Cii) Photograph taken through the microscope objective focused on the mirror. The photoreceptor layer with scattered black retinal pigment epithelial cells (black spots) was visible. (D) Zoomed image onto the micro-mirror with the light stimulus overlaid. The light stimulus area was 100 x 30 μm^2. (E) Description of the three light stimuli: Local background stimulus: 100 x 30 μm^2 light stimulus on a same size background (100 x 30 μm^2). Global background stimulation: 100 x 30 μm^2 light stimulus on a global background (1000 x 300 μm^2). Full field stimulus: 1000 x 300 μm^2 light stimulus on a same size background (1000 x 300 μm^2). Right hand side shows time

sequence of common to the three light stimuli with various durations (10 – 320 ms) interleaved by 1 second long background stimuli.

2.7.   **Pharmacological treatment**

All drugs were carboxygenated and bath applied through perfusion for at least fifteen minutes before recordings. The following drug concentrations were used (in µM): 50 DNQX (6,7-Dinitroquinoxaline-2,3-dione, 0189, Tocris Bioscience, Bristol, UK), 50 DL-AP5 (DL-2-Amino-5-phosphonopentanoic acid sodium salt, 3693, Tocris Bioscience), 20 L-AP4 (L-2-amino-4-phosphonobutyric acid, 0103, Tocris Bioscience), 50 TPMPA ((1,2,5,6-Tetrahydropyridin-4-yl) methylphosphinic acid, 1040, Tocris Bioscience), 50 SR95531 (6-Imino-3-(4-methoxyphenyl)-1(6H)-pyridazinebutanoic acid hydrobromide, 1262, Tocris Bioscience), 5 Strychnine (S8753, Sigma-Aldrich), 100 MFA (meclofenamic acid, M4531, Sigma-Aldrich).

2.8.   **Fluorescent dye staining and imaging**

The slices were stained with Hoechst 33258 (10 µg/ml, H3569, ThermoFisher) to visualize the retinal layers of vertical slices (Figure 3.1 and 3.2). The slices were stained in the CMOS MEA chamber with carboxygenated Ames' medium for 1 hr in room temperature. Propidium iodide (PI, Sigma (Merck) was used to confirm the damage caused by the slicing procedure (Figure 3.1). PI (200µg-ml) was applied to the Ames's medium for 30 min at room temperature.

Both stainings were imaged with confocal microscope (Cell Observer, Zeiss, Germany).

2.9.   **Data Analysis- Vertical retinal slices**

2.9.1. *Reconstruction of electrical images*

Each dataset was averaged using 12 repeats of the stimulus and afterwards smoothened by 3rd degree Savitzky-Golay filter. For each slice sample, the light response from 160 ms full filed stimulus (electrical image, i.e. Figure 2.10B and Figure 3.2C) was used as a standard image for fitting. Bresenham's line algorithm (Figure 2.10A) was applied for the reconstruction of the curved slices. More specifically, points at edge of the slices were manually selected from the standard image (Figure 2.10B). Then the coordinates from the selected points were fitted with a circle. The curved images were reconstructed into straight images by considering that electrodes pass by the same radius belong to the same column in the straightened image using Bresenham's line algorithm. Though there could be some missing electrodes due to the reconstruction, most of the electrodes covered by the slices were kept (Figure 2.10C). The straightened images were used for further analysis.
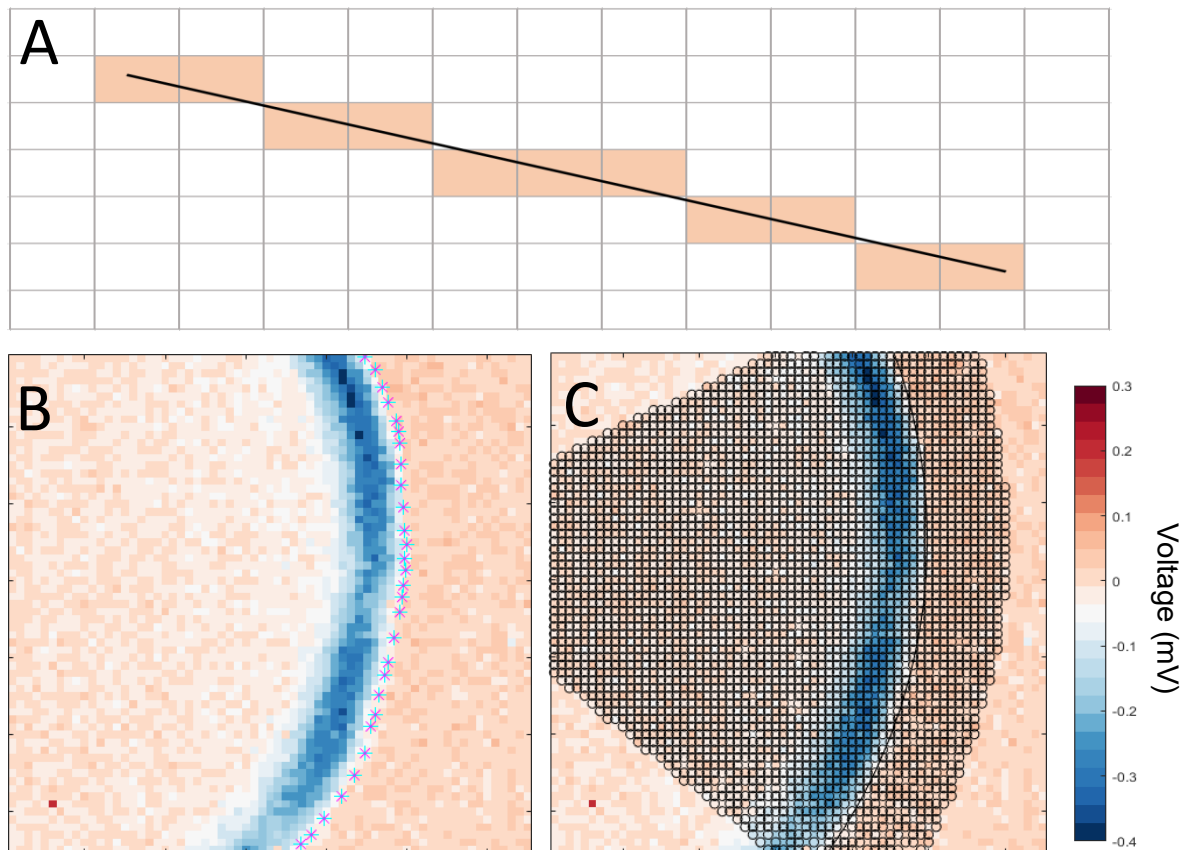

Figure 2.10: Reconstruction of curved slice electrical image with Bresenham's line algorithm. (A) Illustration of the Bresenham's line algorithm. Each grid corresponds to a certain coordination. The colored grids are those points to form the close approximation to

the black straight line. (B) The standard image from 160 ms full field stimulus was used for the determination of the individual slice curvature. Blue crosses represent the manually selected points along the edge of the depolarizing light response. This edge is considered having the same curvature of the slice. (C) The selected points in (B) were used to fit a circle (black line). Electrodes form the closest approximation to the same radius are then reconstructed into the same column. Black circles mark the electrodes that were selected in the reconstruction, showing that the reconstruction of the slice would not lead to serious loss of electrodes. See also Figure 3.2 for straightened slice image.

2.9.2. *Light responses detection*

Averaged voltage signals 200 ms before light onset were considered as baseline. An electrode was considered as detecting a light response if the maximum depolarizing voltage is greater than 15 standard deviations from the baseline signal. If an electrode recorded light response with the mentioned standard, the electrode was considered here as an active electrode (Figure 3.2A). For measuring signal propagation distance, the furthest two active electrodes along x-axis in a straightened image were first measured. Assuming that the signals always propagated symmetrically to both sides, the measured value was divided by two to represent the distance to the stimulus center. The amplitude of the light response was defined as the maximum recorded voltage amplitude. Peak latency was defined as the latency to reach the 80 percent of the maximum voltage amplitude. The offset latency was defined as when the recorded voltage reached the half of the maximum amplitude at the repolarization phase (Figure 3.2A, B, timepoints 2,3,4).

2.9.3. *Linear function fitting*

The peak latency and offset latency were fitted with linear functions to obtain the kinetic of the light response. Since the signal collected in INL seemed to be the key to answer the hypothesis (see result section 3.7), only the peak latency and offset latency from INL were kept (Figure 2.11 top). Then the latencies from the same column (3-4 electrodes) were averaged (take the INL as one thin layer). From each slice under each stimulus background and duration, the data of either peak latency or offset latency to distance (from the center of

stimulus) were calculated. Then a generalized Gaussian distribution as below was fitted to the traces. An optimal beta value was used for different conditions.

$$G(x; \beta) = \frac{\exp\left(-|x|^{\beta}\right)}{2\Gamma(1 + {}^{1}/_{\beta})}$$

β =3.6 for peak latency of control and MFA group, β =2.5 for peak latency of Cx36 knock-out group, β =6.7 for offset latency of control, MFA and Cx36 knock-out groups. After confirming β for the different conditions, only the linear functions to the group of 160 ms duration was used because of best fitting results. Only the samples that showed a high fit quality (r-square > 0.65) were included into the results. After fitting, the mean ± 1.5 standard deviation distance was taken as the proximal (central) area, where there was an obvious turning point for the latency. The electrodes located further as distal area for each individual slice (Figure 2.11). Linear functions are then fitted to the proximal and distal points separately.
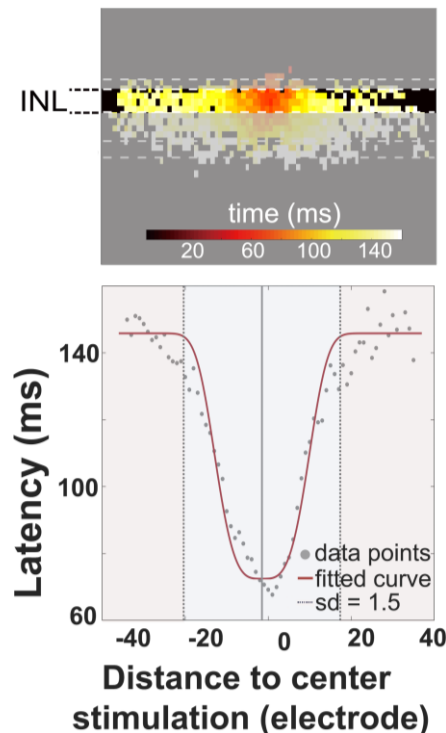

Figure 2.11: Exemplary scatter plot overlayed with the fitted curve. Top: Heatmaps of active electrodes color code with peak latency in different retinal layers with 160 ms light stimulus. Only the active electrodes from INL were used for the fitting (the gray area covers the excluded active electrodes). Bottom: Each point from scatter plot represents the averaged

peak latency to distance from electrodes in the same column. Peak latencies to distance collected from INL in single slice can be fitted with a normalized Gaussian distribution. The same Gaussian distribution was fitting to all slices, the area from stimulus center to distance of 1.5 standard deviation was considered as proximal area (blue), the further area was considered as distal area (red) for each individual slice.

2.9.4. *Statistical Analysis*

Significance tests were performed with Wilcoxon rank-sum test.
The analysis of vertical slices including statistical analysis (Wilcoxon rank-sum test) was performed using custom-written Matlab code (MathWorks Inc., Natick, MA).

2.10. **Data Analysis- Flat-mount retina**

2.10.1. *Spike sorting*

All the recordings were first processed using a 100 Hz high pass filter and a 3k Hz low pass filter, then spike sorted using the default setting of CMOS-MEA-Tool software (Multichannel Systems MCS GmbH, Reutlingen, Germany). The sorting software first assigned connected electrodes whose signal to noise ratio passes certain threshold into different regions of interest (ROI). Second step is to identify different units within the same ROI. Because of the high density of the CMOS MEA electrodes, single RGC usually occupy multiple electrodes, likewise, one single electrode could also record multiple RGCs because of the cell density. The software then extracted signals based on a convoluted independent component analysis algorithm. Afterwards, redundancy removal would be performed to exclude the highly similar units within 33 µm radius (Leibig et al., 2016). After spike sorting, all the units were manually confirmed again in case there is any high noise electrodes mistaken as a spiking RGC included into the results. Timestamps of the spiking activity was saved for further analysis.

2.10.2. *Light response detection in RGCs*

The 12 light stimulation repeats were saved in 12 individual recordings and went through spike sorting independently to avoid generating one single long recording that would overload the spike sorting process. Due to the sorting algorithm, the same cell might be detected in

slightly different positions. In order to make sure the units from each individual file were from the same RGC, the positions of the units as well as the waveforms of the action potentials (Figure 2.12) were compared. The process sequence is presented in the flow chart below (Figure 2.13). In brief, the RGC that located on the same electrode in different files was considered as the same RGC. If the RGC jittered in between different recordings, then the averaged waveform of the action potentials would be used to clarify the identity of a RGC. Then the RGCs were ordered by the distance to the center of light stimulus. The spiking of RGCs was displayed as raster plot. For robust light response detection, spike number 200 ms before and after light onset for 12 repeats were compared and a paired student t test was performed to decide the significance of the change. When the spiking activities were significantly different ($p<0.05$), either increase or decrease, the RGC was considered to have a robust light response. The latency of the first spike was considered as the latency of a RGC's light response.
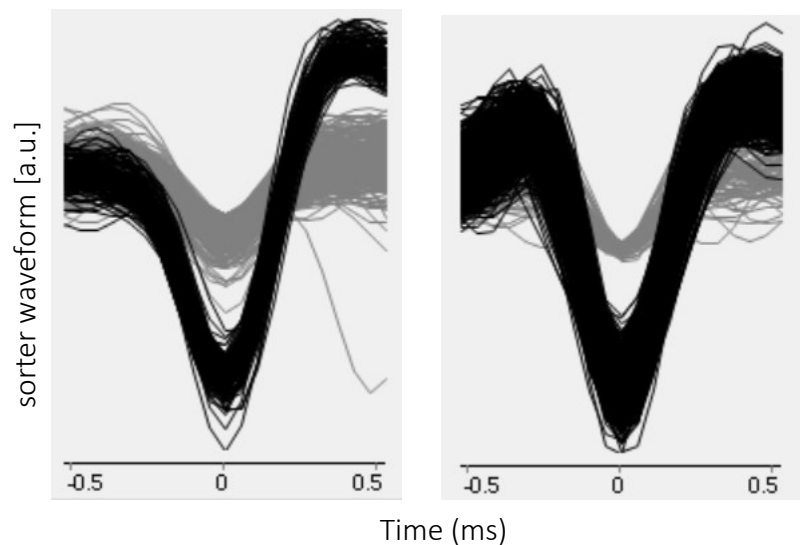
Figure 2.12: Waveforms of action potentials from different RGCs. Examples of identified action potentials from two RGCs (black lines) from the noise (gray lines). The waveforms of the RGCs could be used to differentiate closely located RGCs.
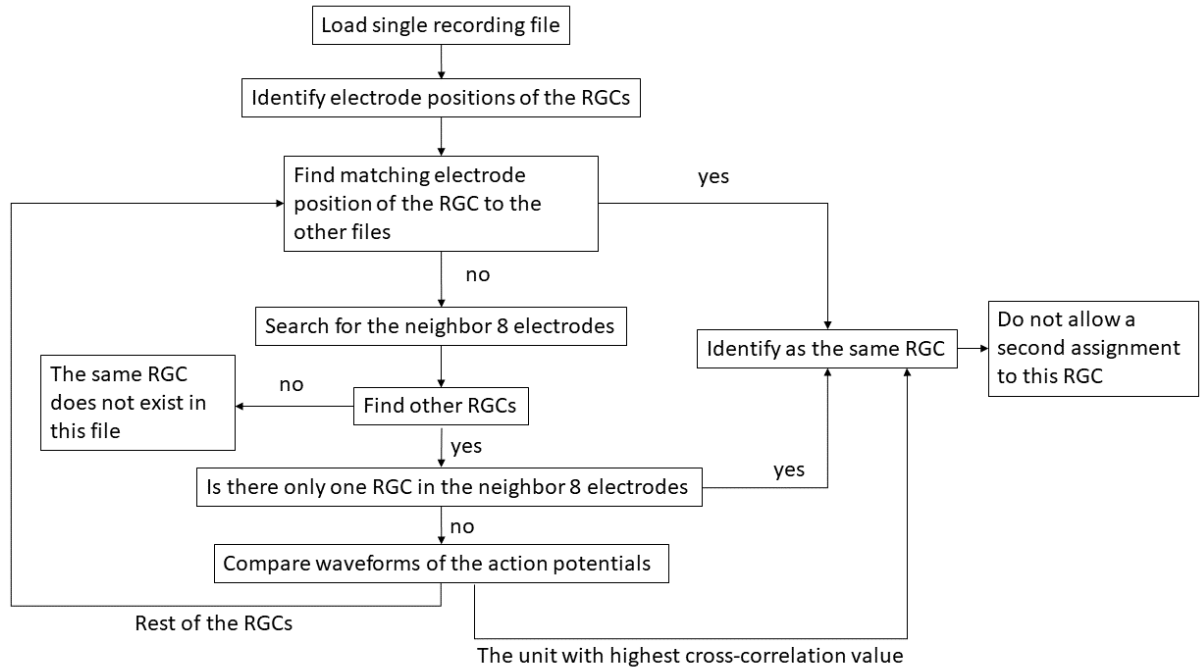
Figure 2.13: Flow chart of identifying the same RGC in different recording files. Detected spiking units from different recording files were assigned to the same RGC based on the location and waveform of a unit.

Chapter

3. Results

The results of this chapter largely correspond to a manuscript accepted for publication at "Frontiers in Neuroscience"

3.1. **Viability of retinal slices**

One important concern from this experimental method was that the contact surface of the retinal slice to the CMOS MEA might be extensively damaged by the cutting procedure. To confirm the viability of the retinal slices, the cell impermeable fluorescent nuclear dye propidium iodide (PI) was used to stain the damaged cells. Since PI is not permeant to live cells, it can only bind to the nucleic acid when a cell membrane is perforated or dead. The retinal slice was double stained with PI and Hoechst 33258 for 30 min in Ames' medium in room temperature right after slicing, then immediately imaged with confocal microscopy (Figure 3.1). Some cells from INL and GCL could be stained with PI, while very few of the PRs were damaged from the cutting. This difference might be that the missing dendritic tree in PRs make them easier to fell off when they are damaged compare to the retinal neurons in INL and GCL, which have broad dendrites and form tight connections with the remaining intact cells.

Although there was certain level of cell damage, the majority of the cells remained unstained and light responses (local field potential) from the remaining cells could still be recorded.
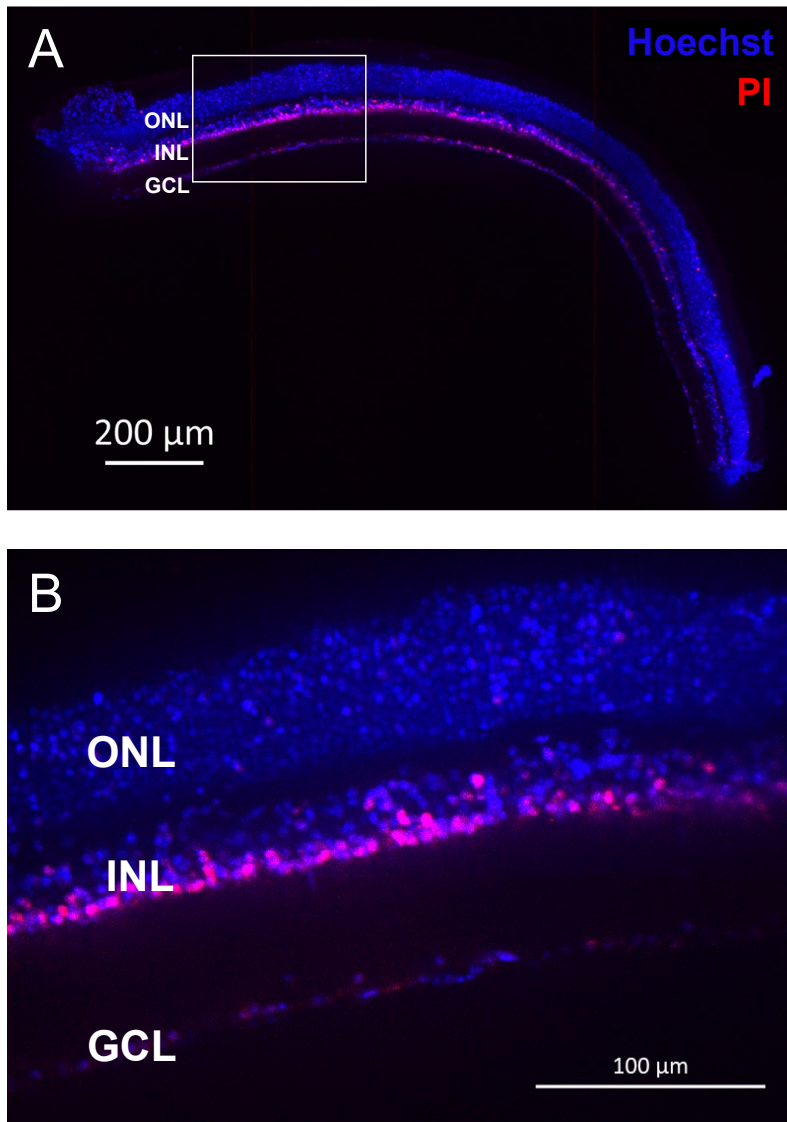
Figure 3.1: Cell damage of the slicing procedure. (A) Double staining of PI (red) and Hoechst 33258 (blue). Red fluorescence shows the damage cells after cutting. The image shows that some cells at the cutting surface were damaged, however a larger portion of the cells stayed unstained by PI. (B) Zoom in view from the white box in (A).

3.2.   **Electrical imaging the signal propagation in vertical slices**

To investigate light-induced signal propagation across and within different retinal layers, the sliced retina was placed onto the CMOS MEA in a vertical fashion (Figure 2.9). After light stimulation was projected onto the PR layer via a mirror, the light induced LFP from the slices was recorded (Figure 3.2A). Electrical recording by all electrodes is visualized in a color code. Here, positive extracellular voltages, which indicate cell hyperpolarization, are coded in red, while negative extracellular voltages that indicate cell depolarization are coded in blue. This process of visualizing signal propagation via voltage changes over time is called electrical imaging (Figure 3.2B, (Zeck et al., 2017)). In figure 3.2B, five instances in time as demonstration were selected: light onset (1), depolarizing phase (2), peak of depolarization (3), repolarizing (4) and finishing (5). Among the five instances, the voltage at time points (2), (3) and (4) were used for quantifying the recorded signals and their dynamics (definition given in the Method section – 2.9.2 Light responses detection).

It is important for this study to confirm that the recorded LFPs induced by light stimulation match the slice dimension. The slice was therefore stained using Hoechst nuclear staining and overlaid with the color-coded voltage signal induced by light (Figure 3.2C). The three major retinal layers are clearly visible and allow matching the recorded voltages. To quantify signal propagation, electrical images from the curved slices were reconstructed and straightened (Figure 3.2D, see section 2.9.1 for reconstruction method). After straightening, each column of electrodes represents a functional unit including all cell layers from PRs to RGCs. The vertical signal transduction pathway within one column was revealed after a stimulus was given (Figure 3.2E). Notably, signals underneath the photoreceptor layer showed a positive polarity, while below the other layers negative extracellular voltages were detected.

This result was expected, considering that light onset hyperpolarizes PRs and horizontal cells and depolarizes the majority of all other retinal cells. It also proved that the light induced voltage changes can be assigned broadly to the photoreceptor layer or the inner retinal layers. The positive extracellular potentials could also be from the return currents from bipolar cell dendrites, nevertheless, it did not affect the following analysis. In the following, the negative voltage deflections (depolarizing signal) were focused to study the signal propagation in lateral direction in the retinal slice. A threshold for the recorded LFP on each individual electrode was introduced. An electrode was only evaluated if exceeded the threshold (Figure 3.2A, see Method section for definition). Electrodes recording supra-threshold signals are referred to as an active electrode in the following.

Using the presented methodology, the signal propagation for different light stimuli was analyzed and presented in the following sections.
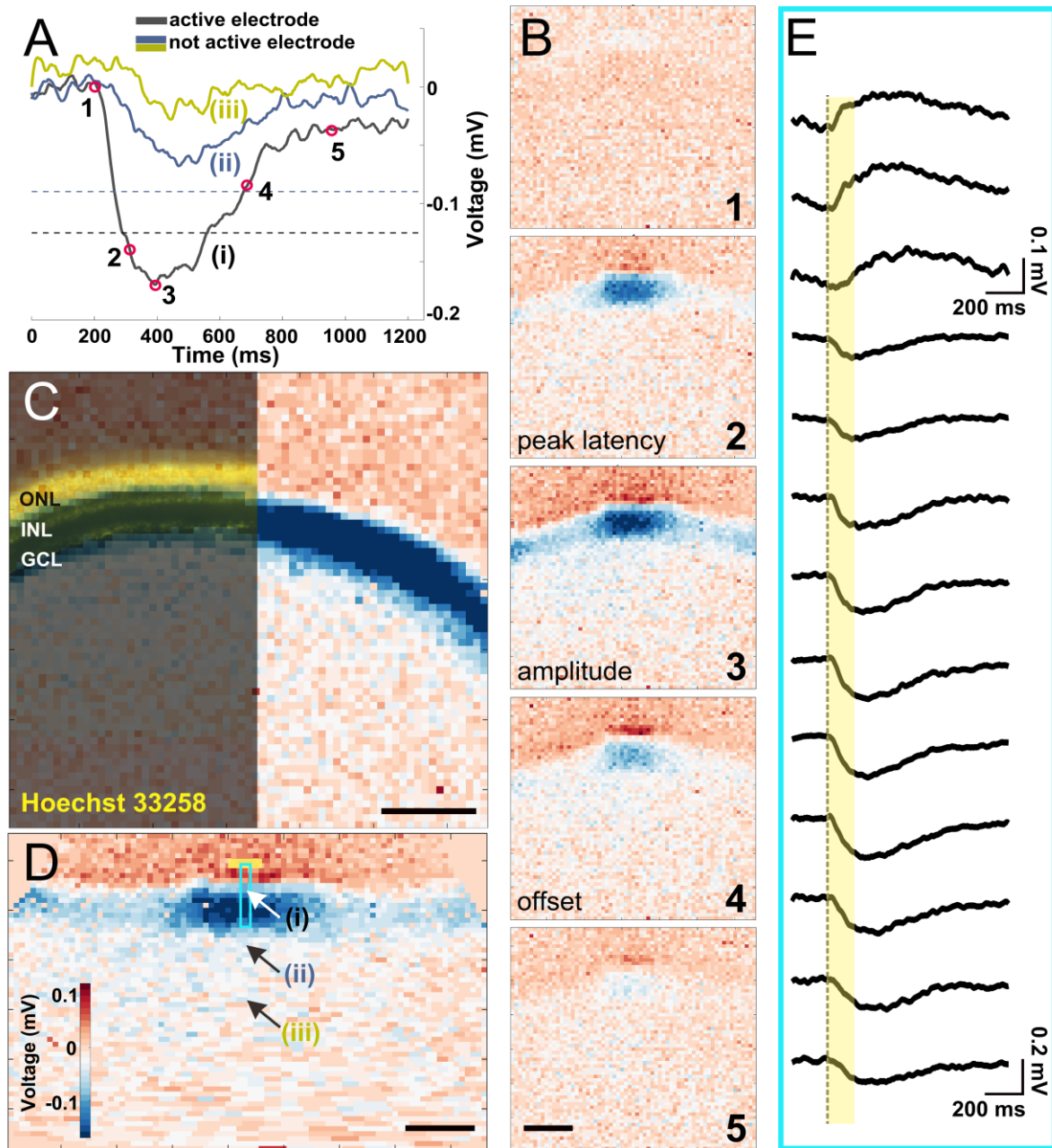
Figure 3.2: Electrical imaging the light-induced activity in a vertical slice. (A) Voltage traces of light-induced activity from 160 ms on local background stimulation. Three recorded traces from electrodes represent (i) active electrode whose amplitude passes its threshold (black dash line) and (ii) not active electrode which though detects depolarizing signal, but the amplitude is not strong enough to pass the threshold (blue dash line) and (iii) an electrode ~ 250 µm from the slice, showing that light stimulus via mirror does not cause artifact on the CMOS MEA. The electrode positions (i)-(iii) are marked in panel (D). (B) Exemplary electrical

images at five timepoints marked in (A). Timepoints of 2,3 and 4 are used in further analysis for peak latency, amplitude and offset latency respectively. (C) Overlay of Hoechst 33258 nuclear dye staining and electrical image with 160 ms full field light stimulus. Nuclear dye staining revealed the three major cell layers (ONL, INL, GCL) that matched to physiological recording. (D) The reconstructed straightened vertical slice of an electrical image from timepoint 3 in (B). Three arrows point to the electrode recorded traces in (A). Yellow box stands for the light stimulus area. (E) Extracellular voltage recorded by 13 electrodes arranged along one column under the slice (marked with blue rectangle in (D)), covering a distance of ~ 200 µm. The yellow bar indicates light stimulus. Scale bars in (B − D): 200 µm.

3.2.1. *Light artifact on CMOS MEA*

Study has shown that CMOS MEAs are light sensitive for blue light (Bertotti et al., 2014), therefore one might concern that the recorded LFP is simply light artifact instead of cell response. As a matter of fact, the 45 degree mirror was specifically applied for this study to prevent the light from falling on to the CMOS sensor array and therefore avoided the contamination of the artifact signal. Some evidences are provided in this section to clarify that no light artefacts were being recorded under the experimental conditions used here.

First, if the light stimulus was directly given from top of the slice without the 45 degree mirror, artifact from light could be detected with the same polarity of depolarizing cells, but only at the area with no retinal tissue (Figure 3.3). Note that the light intensity used here was about 6-7 times higher than in this study, therefore the artifact caused by the stimulus from this study could not have been so strong as shown in Figure 3.3. The area which is roughly at the PR layer remained hyperpolarized even a strong light stimulus was given.

Second, the depolarizing signal propagation area (Figure 3.3 middle) matches the area of the retinal slice (Figure 3.3 left). If it would have been light artifact, it would not be restricted to the retinal slice but a much broader area.

Third, after applying metabotropic glutamate receptor agonist L-AP4, the light response at the slice area was abolished, yet the negative extracellular voltages caused by light artifact remained, suggesting that the abolished signal was originated from the cellular responses. When the light stimulus was given via the mirror, the light artifact shown in figure 3.3 could not be observed on the electrical image (Figure 3.2). The electrode away from the slice showed no light response as well (Figure 3.2 A and D). These evidences support that the LFPs recorded in this study were from the retinal neurons instead of light artifact.
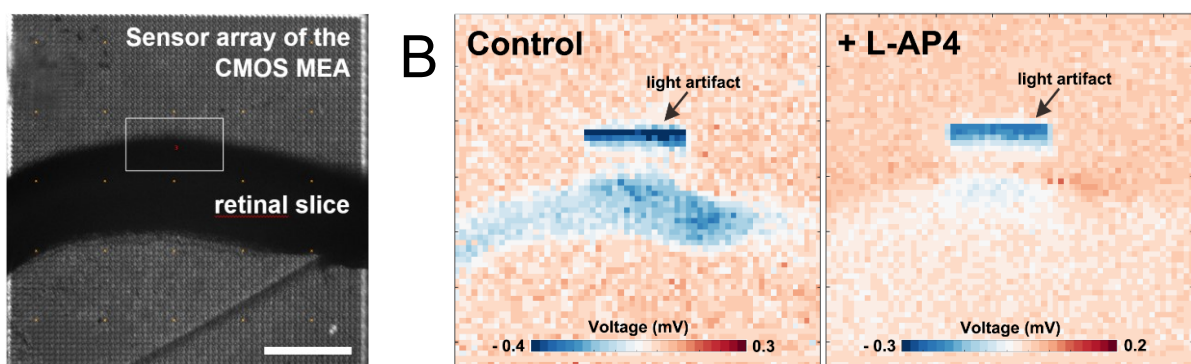
Figure 3.3: Examples of electrical imaging with light artifact. (A) A top view of the retinal slice on a CMOS MEA. The white rectangle marks the area where the 10 ms, 490 nm light stimulus

with intensity of ~ 10^7 R* rod^{-1} s^{-1} was directly given from top without a mirror. Scale bar: 200 μm. (B) Electrical images of the peak latency instances of light-induced retinal activity in the slice together with light artifact on the MEA. In addition to the LFP from the slice, a negative voltage fluctuation evoked by the light artifact (indicated by the arrow) could be recorded at the area that was not covered by the retinal slice. L-AP4 was applied to further distinguish neural activity from light artifact. When stimulated in the control condition (left), the depolarization from the retinal neurons and light artifact both could be clearly seen. After applying L-AP4 (right), the depolarization from the slice could barely be recorded, leaving the negative voltage fluctuation from the artifact. This result proved that the LFP from the slice was not affected by the light artifact.

3.3. **Signal propagation in a retinal slice depends on duration and background of the activating light stimulus**

Next, the signal propagation using the active electrodes was evaluated under three different light stimulus conditions: (1) stimulus presented on a local background, (2) stimulus presented on a global background that activates the inhibitory surround to the small field stimulus and (3) a full field stimulus served as control to confirm homogenous attachment and extracellular recording of the slice on the electrode array (Figure 2.9E).

In the first experiment, the signal propagation upon presentation of local light stimuli of six different durations were investigated. Interestingly, not only the signals propagated much further in lateral direction than the size of the stimulus, the propagation distance was also stimulus duration dependent (Figure 3.4A, D). As the stimulus duration increased from 10 ms to 320 ms, the mean propagation distance increased from 233 to 607 μm (n=13 slices) and saturated after a certain distance (around 600 μm). The saturation most likely occurred because the signal had reached the border of the electrodes array (~ 500 μm from stimulus center). Note that the slice curvature allows for measurement of maximal propagation distance larger than 500 μm. However, for longer stimuli like 160 and 320 ms, the size of the sensor array could lead to an underestimation of the real propagation distance.

To further investigate if the wide lateral signal propagation would be suppressed by surround inhibition, a global, low intensity background stimulus was provided onto the small field stimulation. Indeed, the light-induced extracellular signal was restricted to smaller areas, with mean distances of 85 μm when stimulated with 10 ms light pulse and 460 μm when stimulated with 320 ms light pulse (Figure 3.4B, D, n=9 slices). The propagation distance was significantly smaller under global background illumination compared to local background illumination, irrespective of the stimulus duration (Wilcoxon rank-sum test). Two effects shall be distinguished here: (1) the propagation distance reduced significantly compared to the local background condition, however (2) the trend of increasing propagation distance with increasing stimulus duration remained. The last result indicates that the duration dependent effect of lateral signal propagation is independent of the stimulus background.

To confirm whether the observed effect of stimulus duration dependent propagation was caused by different signal amplitudes, the raw traces from one active electrode right at the downstream of the stimulus area from different stimulus durations were examined (Figure 3.4E). The light evoked similar voltages except for 10 ms, showing that the duration doesn't

affect the voltage intensity of the light-induced responses. This result fits the patch-clamp recording of light response in BCs in the previous literature (Euler and Masland, 2000).

When the entire slice was stimulated with the full field stimulation, the signal was detected over a distance of between 605 to 620 μm (n=13 slices) regardless of the stimulus duration, which corresponds to the maximum distance of the electrodes covered by slices (Figure 3.4C, D).

The reduced propagation distance in global background condition as compared to local background condition may also be explained by a reduced signal amplitude. The signals recorded from three electrodes underneath the stimulus from three different stimulus conditions (all from 160 ms stimulus duration) show different signal amplitudes (Figure 3.4F). The fact that the signal has highest amplitude when stimulated by local background and lowest when stimulated with global background suggests that the central amplitude was inhibited by activation of inhibitory surround. When a full-field stimulus was applied, the reduced amplitude as compared to local stimulus on local background strengthens the hypothesis of recruitment of the inhibitors surround. However, full-field stimulus also activated more cells than local stimulus because of a bigger stimulus size, the signal amplitude was therefore higher than in the global background condition.

These results suggest that global background stimuli not only reduced the amplitude of stimulated activity, but also reduced the distance signal propagated laterally. Lateral signal propagation distance was duration dependent regardless of background stimulus. This may imply that the further the depolarizing retinal cells are located from the stimulus, the longer stimulus durations are required to activate these cells. Both findings may have implications on the spiking activity of RGCs.
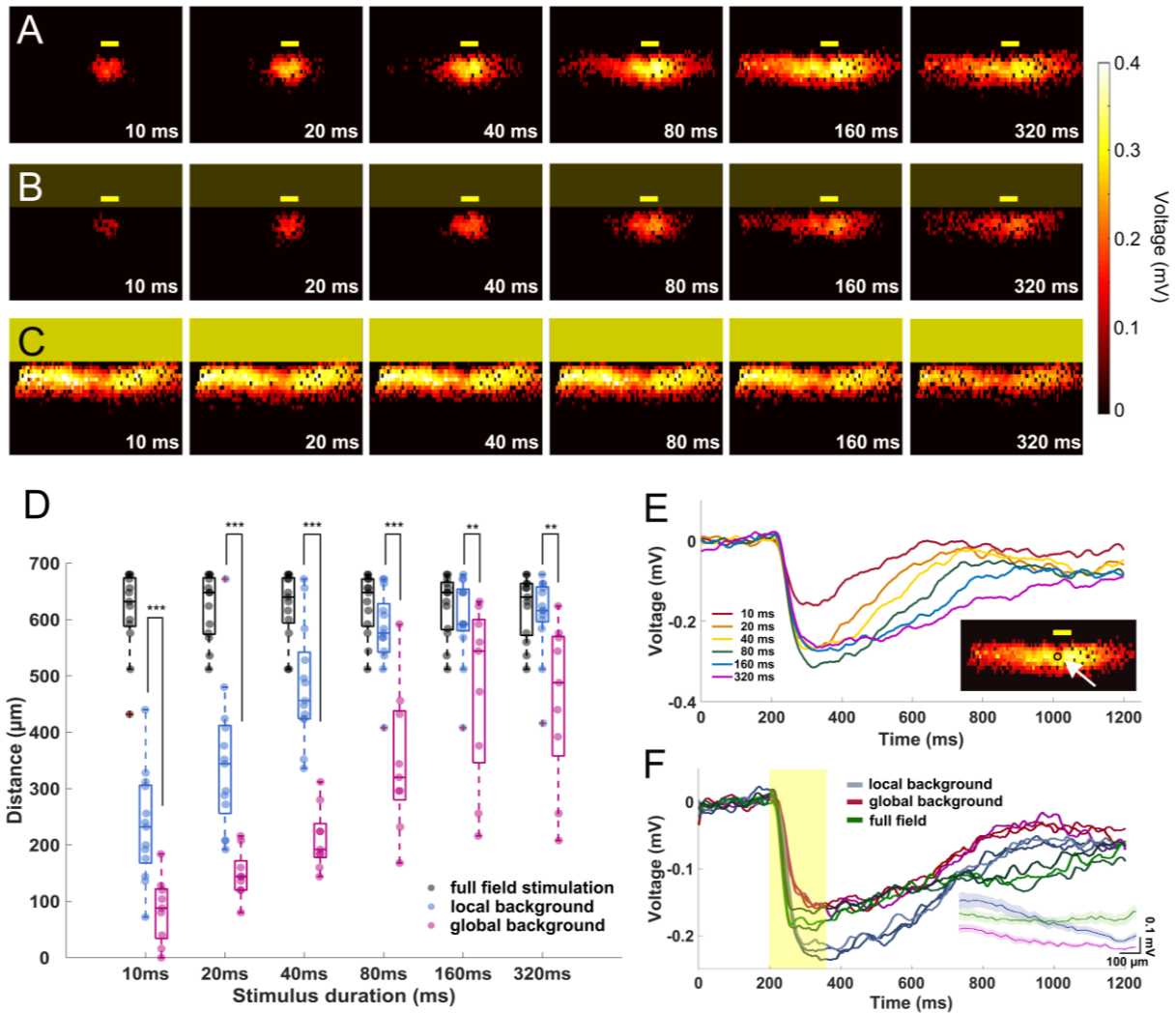
Figure 3.4: The signal propagation distance increases with stimulation duration. (A-C)
Heatmaps show active electrodes for different stimulus durations. Stimulus durations range
between 10 ms (left) to 320 ms (right). The heatmap color represents the amplitude of the
extracellular peak voltage. Yellow boxes mark the light stimulus. Size of the light stimulus: 100
μm wide / 30 μm high. (A) local background stimulus (B) global background stimulus (C) full
field stimulus. (D) The signal propagation distance for different light stimulus conditions. The
distance increases with stimulation duration for both local (n=13 slices) and global
background stimuli (n=9 slices). For all stimulus durations, signal propagated significantly
further under lobal background (no surround inhibition) than for global background (with
surround inhibition). Significance test were performed with Wilcoxon rank-sum test. **:
P<0.01; ***: P<0.001. Under full field stimulation (n =13 slices, black symbols) there was no
difference between stimulus durations. (E) Extracellular voltages recoded from an electrode
locates downstream of the local stimulus with local background from different stimulus

durations. Stimulation duration did not affect the voltage amplitude but only the duration of the responses except for 10 ms. The arrow in the insert points to the electrode for which the signals are shown. (F) Overlaid extracellular voltages recoded from three electrodes right downstream of stimulus area with local background (blue lines), global background (red lines) and full field stimuli (green). Yellow box represents the 160 ms light pulse. The voltage decreased when stimulated with global background or with full field stimulus, suggesting the recruitment of inhibitory input. The insert shows the average peak amplitude over distance from stimulus center for local background stimulus, global background and full field stimulus.

3.4. **Remote modulation of light-induced RGC activity depends on stimulus duration and background**

The results obtained in the vertical slice raised the question if increasing the duration of a spatially localized light stimulus affects the spiking activity from more distal RGCs in both local and global background stimulus conditions. To answer the question, the same light stimuli (Figure 2.9E) were repeated using flat-mount retinas. A representative raster plot showing the spiking activity of 153 identified RGCs from a single flat-mount retina to twelve repeats of each stimulus duration is shown in Figure 3.5A. In the local background condition, more than half of the RGCs located within 400 μm from the stimulus were light responsive regardless of the stimulus duration. A 10 ms stimulus failed to evoke light responses in more than half of the RGCs located further than 400 μm from the stimulus. At a distance larger than 600 μm, only the stimuli longer than 160 ms were able to evoke light responses in the majority of RGCs (Figure 3.5A, B).

This result showed that for a local stimulus without a global background, the further the RGC was located from the light stimulus, the longer stimuli were required to evoke light responses. This fits qualitatively with the previous finding on the vertical slice and suggests that the LFP propagation distance translated into spiking activity of RGCs at remote stimulus locations. (The increase in light response ratio for long stimuli at distances further 1000 μm from stimulus center (Figure 3.5B) is caused by the low number of detected cells and may not have any mechanistic basis.)

When an additional global background stimulus was presented, only nearby RGCs were activated. The raster plot of the spiking activity from 126 RGCs spiking to twelve repeats identified in one retina exemplifies this finding (Figure 3.6A, same retina as in Figure 3.5A). Within 200 μm distance, more than half of all recorded RGCs showed a robust light response irrespective of the stimulus duration (Figure 3.6B). However, longer stimuli such as 160 ms or 320 ms failed to evoke robust light response in most of the RGCs located further than 200 μm away.

This result differs from the previous finding in vertical slice that the propagation distance increases with the stimulation duration regardless of the background illumination. I therefore hypothesize that the lateral propagation analyzed and presented in Figure 3.4 does not reach the RGC layer. To address this, the signal propagation of the vertical slice needed to be analyzed in more detail.
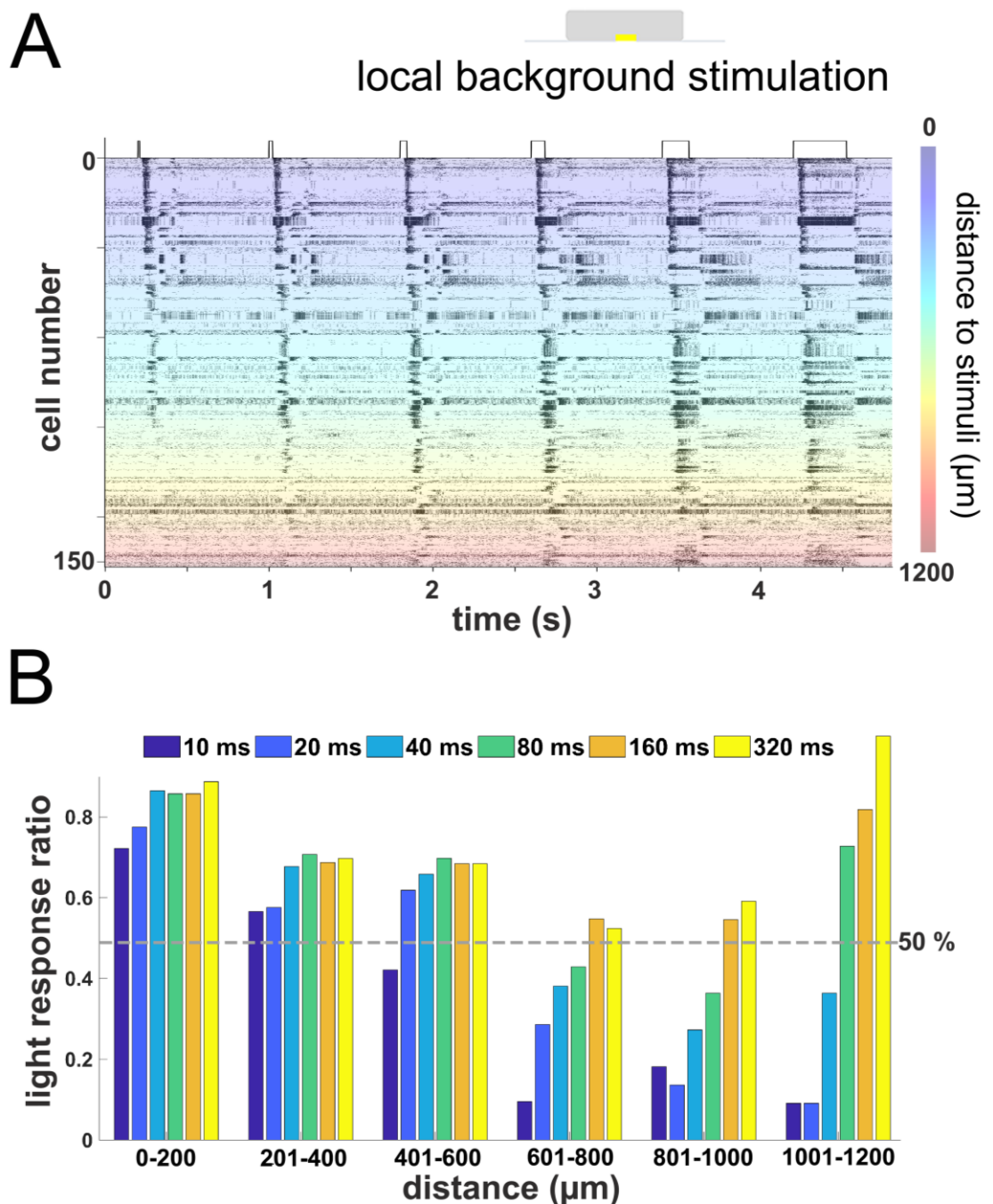
Figure 3.5: Duration dependent remote activation in RGCs from local light background stimulus. (A) Raster plot of RGCs from one flat-mount retina stimulated with local stimuli of different durations on a local background. Y-axis marks the number of cells in one retina, each cell was stimulated 12 times. The color codes for the distance of the RGC from the local stimulus. Most of the RGCs located close to the stimulus (blue-green area) were activated by all stimulus durations, while RGCs located at far distance (orange-red area) only responded to relatively longer stimuli. (B) Ratio of RGCs with robust light response for

different stimulus durations on local background versus distance to stimulus center (n = 385 RGCs from 3 retinas).
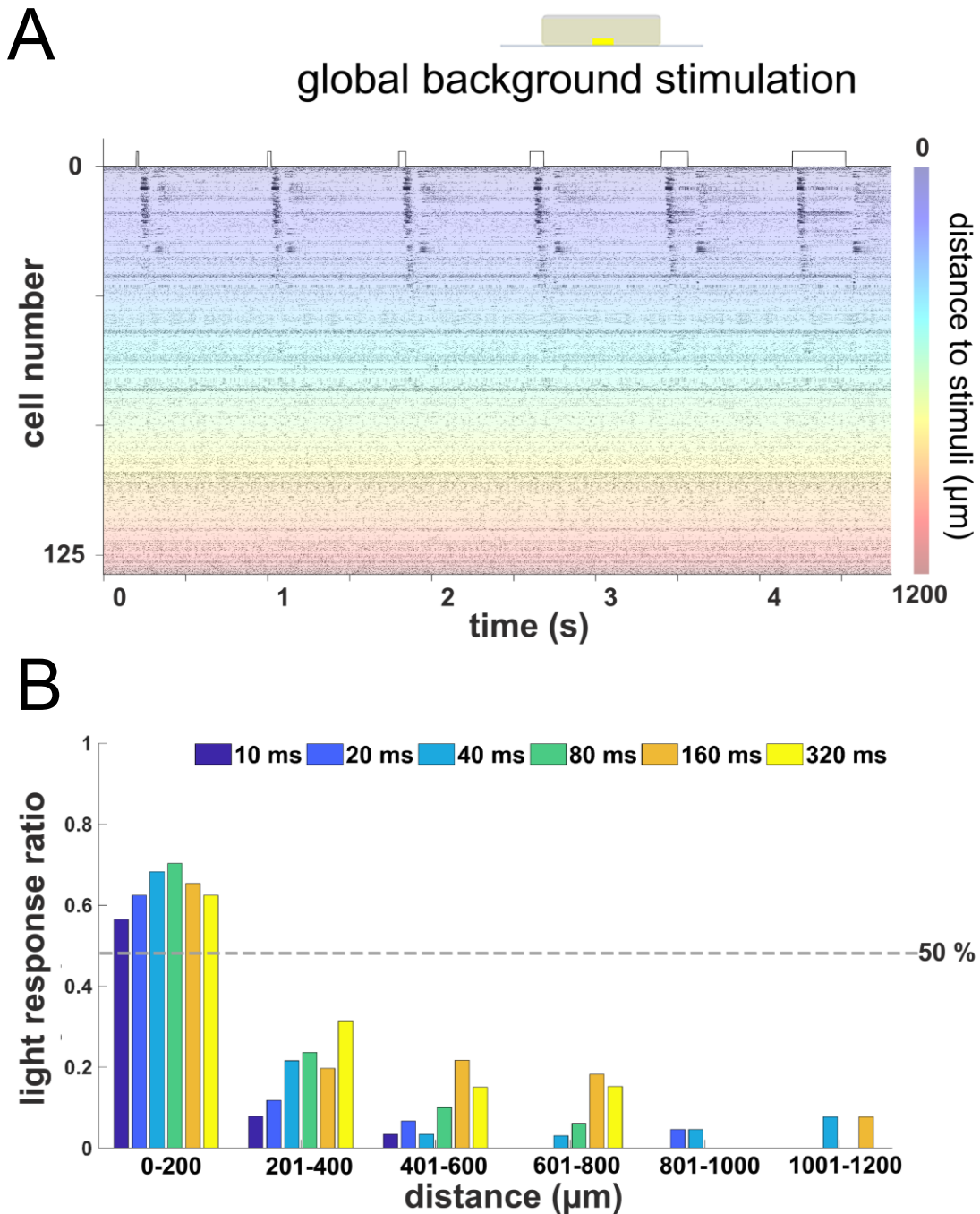
Figure 3.6: Remote activation in RGCs from local light stimulus is background and duration dependent. (A) Rasterplot of RGCs from the same flat-mount retina shown in (Figure 3.5A) with stimulation on a global background. Most RGCs located close to the light stimulus showed light responses, while those located distally were not activated. Color bar marks

the distance of the RGC from stimulus center. (B) Similar evaluation as in (Figure 3.5B) for stimulation on global background. Few RGCs located further than 200 µm away from stimulus showed robust light response (n = 281 RGCs from 3 retinas).

3.4.1. *Stimulus duration and background dependent spiking activity in the RGC layer remained after excluding the potential amacrine cells*

In the RGC layer, almost 60 % of the somata are occupied by more than 10 different types of displaced amacrine cell (Perez De Sevilla Muller et al., 2007). These ACs in the RGC layer also fire action potentials but do not have long axons to project to the brain. Therefore, there are always chances that the spiking activity recorded from RGC layer is from an amacrine cell instead of a RGC. To make sure ACs did not dominate the observed phenomenon above, spikes from each recorded cell were averaged to reveal the propagation of action potential. When the axon is close enough to the recording electrode, action potential propagation through the axon can easily be electrically imaged (Stutzki et al., 2014) (Figure 3.7A). Those cells that only show activity at the soma could be either an AC or a RGC whose axon is not detectable (Figure 3.7B). After keeping only the cells whose axon could be electrically imaged (62/153 cells), the raster plots (Figure 3.8) showed exactly the same trend as when all cells were considered (Figure 3.5 and 3.6), proving that the stimulus duration and background dependent light response persist in RGCs.
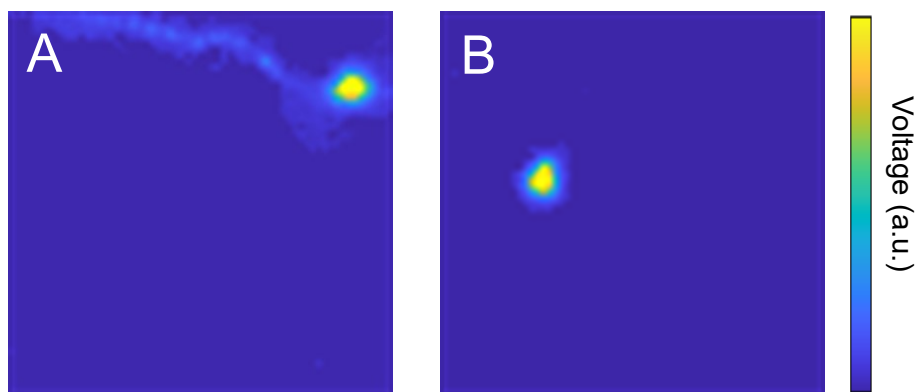
Figure 3.7 Amplitude color- coded footprints of neurons recorded at RGC layer. The square areas are the sensor arrays of the CMOS MEA. (A) Footprint of a cell with a visible axon. (B) Footprint of a cell without a visible axon.
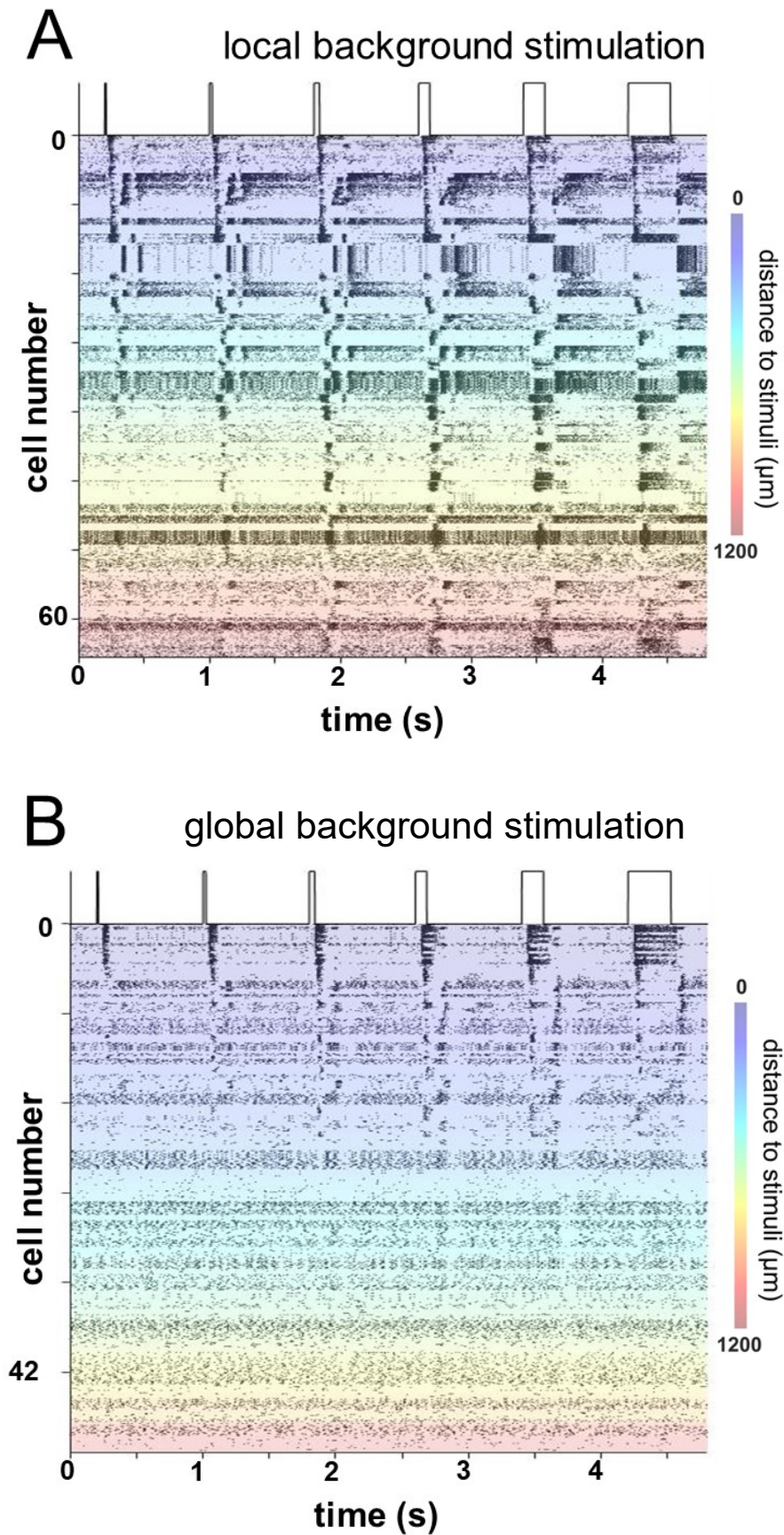
Figure 3.8: Background and duration dependent remote activation of spiking activity in the RGC layer remained when cells without axons were excluded. (A) Raster plot of RGCs from the

same retina as in figure 3.5A but exclude those whose axons cannot be electrically imaged (as in Figure 3.7B). The retina was stimulated by different durations of stimuli with local background. Y-axis stands for the number of cells and the color codes for the distance of the RGC from the local stimulus. The duration dependent activation tendency remained as in figure 3.5A. (B) Same flat-mount retina sample shown in A and in figure 3.6A with global background stimulus. Most of the RGCs locate relatively close to the light stimulus show light responses, but not from those who locate distal from light stimulus.

3.5. **Distance dependent light response latency in RGCs**

Last result showed the activation of distal RGCs was affected by the stimulus duration, what about the light response latency of RGCs? Was it also stimulus duration or distance dependent?

First, the histograms of latency from ON RGCs stimulated by different duration were examined (Figure 3.9). The latency was defined as the time of first spike after light on. The spike numbers were binned with 50 ms. Most of the RGCs have latencies between 20-100 ms with varieties. There are no obvious differences between different stimulus durations, with the mean latency between 55-63 ms for all six durations.
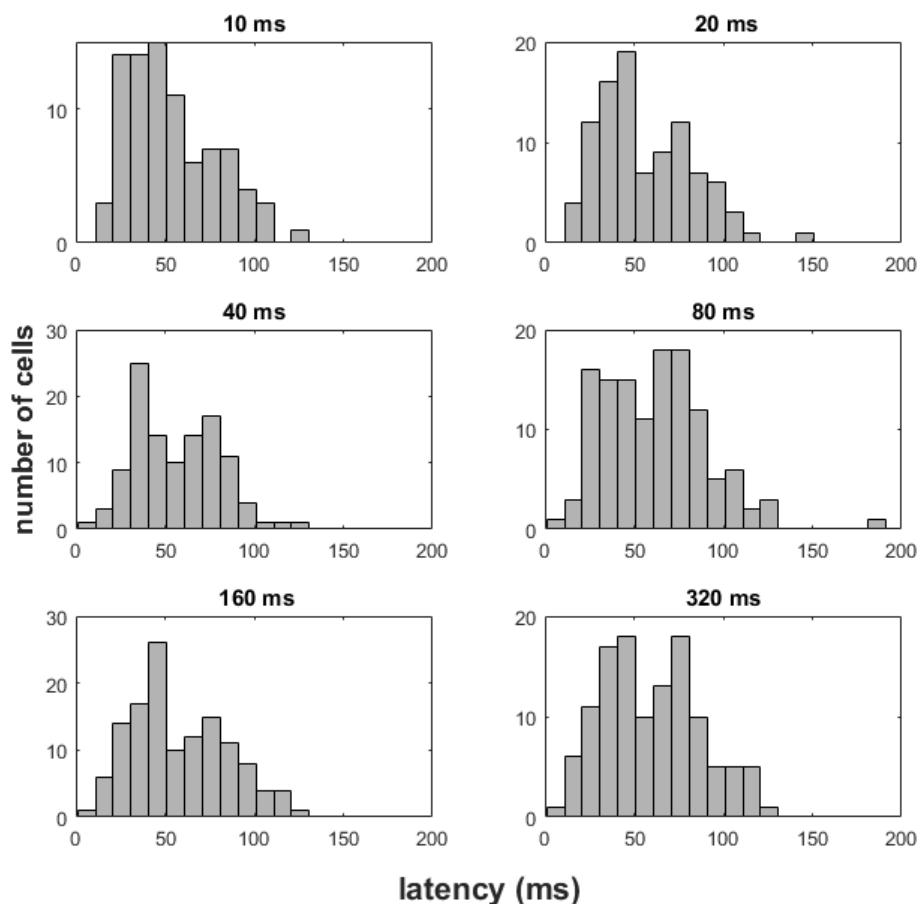
Figure 3.9: Mean latency of the ON RGCs in different stimulus durations for flat-mount recording. Histograms show light responsive ON RGCs latency vs distance distribution in different stimulus duration under local background stimulation. Most of the RGCs have the latencies between 20-100 ms. The average latency for each duration are 10 ms= 55.1 ± 26.7; 20 ms= 57.7 ± 28.9; 40 ms= 58.5 ± 26.5; 80 ms= 63.3 ± 31.8; 160 ms= 58.7 ± 27.9; 320 ms= 60.6 ± 28.5. unit= ms. Mean ± SD. n=158 cells from 3 retinas.

However, when the distance factor was included into consideration, tendency of increased latency by distance was revealed (Figure 3.10). For all stimulus durations, the ON response latency increase as the RGC located more distal from the center of stimulation.

This result shows that the further the cell was located from the center of stimulus, the longer it took to be activated, suggesting certain level of circuits modulation was involved.
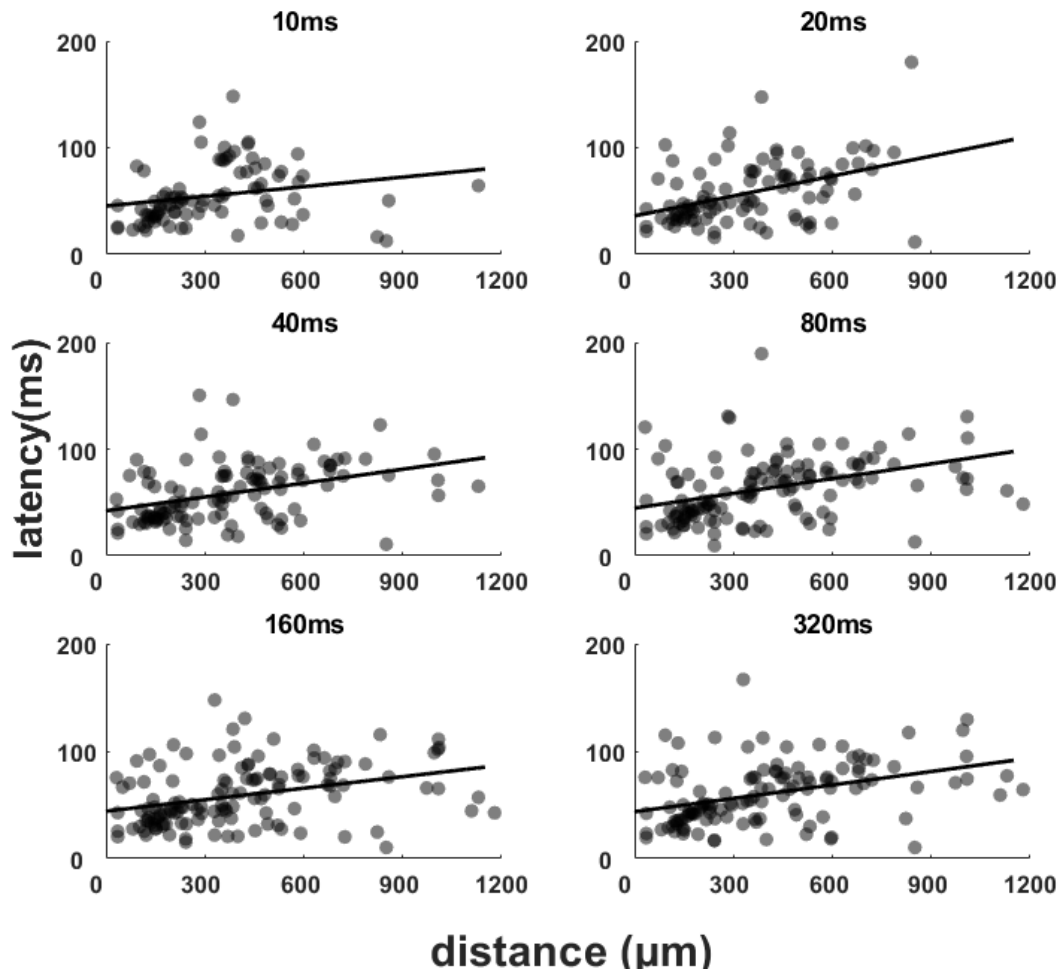
Figure 3.10: Scatter plots of first spike latency vs distance in ON RGCs in local background stimulation with different stimulus durations. The lines are the linear regression fittings of the scatter plots. The response latency increases with the distance from the stimulus center in all stimulus durations.

3.6. **Electrical imaging signal propagation in different retinal layers**

The lateral signal propagation over a long distance in the vertical slice was detected (Figure 3.4) but failed to confirm the result at the level of RGC spiking activity (Figure 3.5 and 3.6), one possibility would be that the propagated signal detect in slices did not travel to RGC layer, but stayed in INL or IPL instead.

To verify the assumption, the electrical imaging results from vertical slice recordings were re-analyzed by assigning the active electrodes to different retinal layers.

3.6.1. *Assignment of retinal layers to the electrical images of vertical slices*

Considering that each slice has a slightly different thickness, the layers were assigned by the relative position of the electrode to the corresponding depth of the slice. The layers were assingned based on the study of Ferguson, L.R., et al. (Ferguson et al., 2013) . The retinal layers were divided as follows: the OPL occupies 18 % of the slice; the inner nuclear layer (INL) 26 % and the rest of 56 % is assigned to IPL+GCL. The last three rows (48 µm) were further selected from IPL+GCL and assigned them to GCL only. This tentative separation may contain sublamina 5 of IPL, which cannot be resolved here.

There are few concernes why the Hoechst staining from this study was not used as the assignment of the layers directly. 1. The Hoechst staining only exist for a subset of experiments. 2. It was only possible to stain and image the very top surface of the slice (opposite of the recording side). Therefore, there might be misalignment from the imaging side and the recording side. 3. The top surface of the slices were not always in a good shape after long recording, making the confirmation of the layers very difficult. 4. The sample size is very limited.

To make sure the the results from the literature can be adapted to this study, the comparisons from both studies were down below.

Based on nuclear staining of the cell layers (Figure 3.11), a subset of slices (n =5) were evaluated and the thicknesses of OPL, INL and IPL+GCL were measured. The division was calculated by the mean value of 10 manually chosen thicknesses and measured using ImageJ software (NIH, Bethesda, MD, USA).
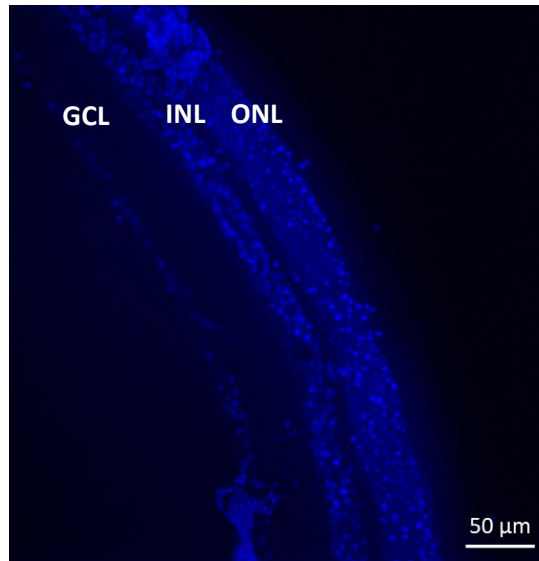
Figure 3.11: Hoechst staining of vertical slice to image the retinal layers. The thicknesses of the layers were further measured with imageJ.

The thicknesses from both studies are shown in the table below.

Thickness (μm±sd)	OPL	INL	IPL+GCL	Sample number
This study	10.17 ± 1.46	19.01 ± 4.44	52.43 ± 4.98	5
Ferguson et al.	19.22 ± 4.34	27.82 ± 4.04	59.62 ± 6.66	30

From this table, it is clear that the slice thickness from the measurement in this study is thinner than Ferguson et al. This may due to the differences of *in vivo* (Ferguson et al.) and *in vitro* (This study). The thicknesses can be translated into the percentages of occupancies as in the table below.

Thickness in %	OPL	INL	IPL+GCL
This study	0.13	0.23	0.64
Ferguson et al.	0.18	0.26	0.56

Although the occupancy percentages from images of staining (OPL: 13%, INL: 23%, IPL+GCL:64%) was slightly different from Ferguson et al., it would only be minor differences when translated into the numbers of electrodes. If considered that the majority of the slices cover between 10-12 electrode rows, there will be only ± 1 electrode difference for the assignment to each layer. To avoid evaluating layers covering only one electrode row (ex: the OPL for slices with 10 electrodes thickness), the Ferguson suggestion was therefore kept.

3.6.2. *Confirmation of the cell layer assignment with pharmacological treatments*

After assigning the layers to the slices, the accuracy must be confirmed. The most direct way is to check the activity changes in different layers after pharmacological treatments. By blocking glutamate receptors, signal transduction to certain layers would be blocked. By blocking inhibitory receptors, enhancement of the signal amplitude shall be observed.

BCs send signals to RGCs via iGluRs, therefore if the receptors were blocked, the signal would stay at INL and thus the signal intensity in the IPL should be strongly reduced. The electrical imaging showed indeed, the signal amplitude was reduced from 0.5 mV to 0.13mV (averaged amplitude of 10 active electrodes from IPL right underneath the stimulus center) after the application of DNQX and AP5 (Figure 3.12).

Inhibitory ACs release GABAs and glycine to inhibit BCs, RGCs and ACs. By adding GABA receptor antagonists TPMPA(GABA$_A$) and SR95531(GABA$_C$), the signal amplitude in the IPL should increase because of the removal of inhibition. The recording showed just as expected, the intensity of the signal in the IPL was increased from 0.5 mV to 0.63mV (averaged amplitude of 10 active electrodes from IPL right underneath the stimulus center) after blocking GABA$_A$ and GABA$_C$ receptors (Figure 3.12).

The above results confirmed that the assignment to the retinal layers can be trusted. The signal propagation in different layers were investigated in the following paragraphs.
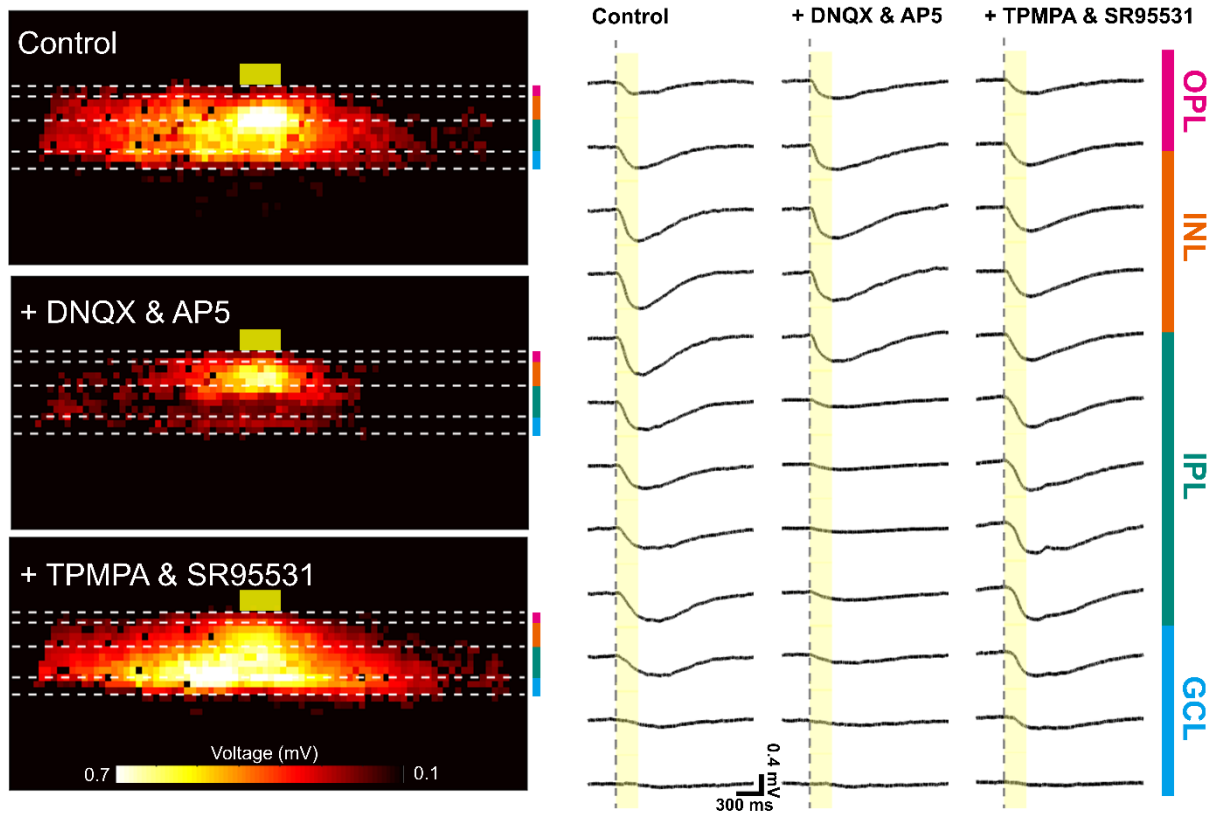
Figure 3.12: Light responses modified by pharmacological treatments in a retinal slice. Left: Heatmaps of light response signal amplitudes across different layers when stimulated with 160 ms light on local background in control condition (top), with DNQX and AP5 (middle) and with TPMPA and SR95531 (bottom). Color bars correspond to the same color bars at the right-hand side, which label their layers. Yellow boxes represent the given light stimulus (100 μm x 30 μm). Right: Signal traces averaged by 12 repeats from one column of electrodes right below the light stimulus.

3.6.3. *Stimulation on global background prevents signal propagation to the ganglion cell layer in the distal area*

When the layer separation following Ferguson et al. was applied to the electrical slice images, the distances signal propagated in different layers were revealed. The signals propagated from INL to GCL homogeneously with full field stimulus (Figure 3.13C) and was slightly decreased in the GCL for local background stimulation (Figure 3.13A). For a local light stimulus on a global background however, distal signals were mainly detected in the INL but not in the GCL (Figure 3.13B). Cumulative distribution diagrams were used here to present the homogeneity of signal propagation in different retinal layers (Figure 3.13D-F). If the signal propagated homogeneously through the lateral and vertical directions, then the number of active electrodes in INL and in GCL shall be similar; otherwise if signals were confined to INL and did not propagate to GCL, a clear difference can be expected. The example diagrams (Figure 3.13D-F) comprise the cumulative number of active electrodes in different retinal layers from all the recorded slices (13 from local background and full field, 9 from global background) stimulated with 160 ms light pulse. The signal traveled 86 % further in INL than in GCL under global background simulus (312 μm in INL and 168 μm in GCL, Figure 3.13E), as compared to only 12 % under local background stimulus (408 μm in INL and 364 μm in GCL, Figure 3.12D) and almost no change under full field stimulus (456 μm in INL and 470 μm in GCL, Figure 3.13F). The same conclusion can be obtained by examining the lateral signal propagation distances in different layers separately: the signal in INL propagated significantly further than in the GCL upon stimulation with a global background for all stimulus durations (n=9 slices). For local background or full field stimulus conditions, differences of propagation distances in INL and GCL showed no significance (Figure 3.13G-I, n=13 slices). These results explain why RGC activity at remote distance (> 200 μm) could not be recorded from the stimulus if a global background was presented (Figure 3.6).
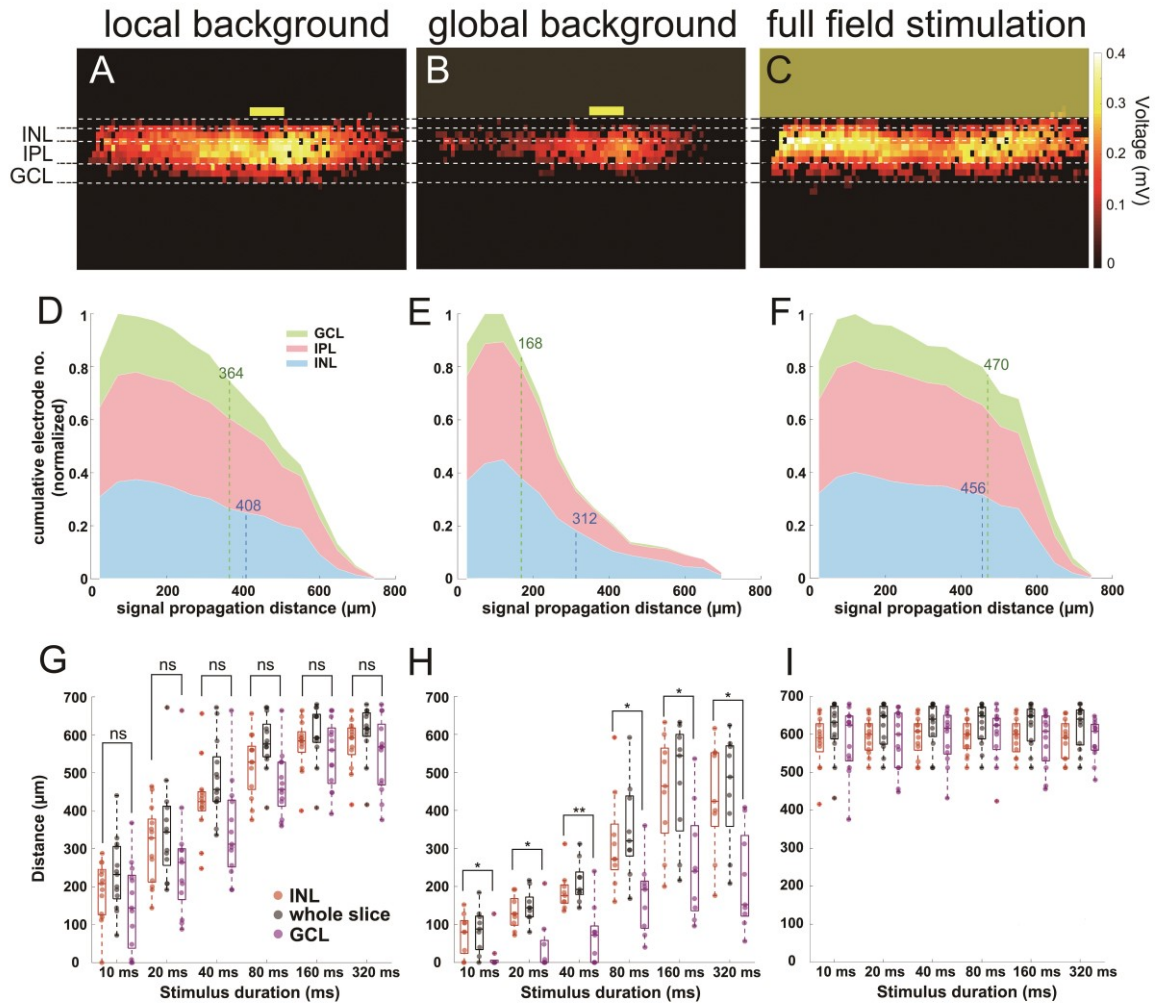
Figure 3.13: Signal propagation in INL and GCL in three light stimulus conditions. (A-C) Heatmaps show active electrodes from 160 ms light-induced field potential labeled with different retinal layers. Heatmap color codes for the maximum extracellular voltage. A: local background stimulation B: global background stimulation C: full field stimulation. Yellow boxes mark the stimulus position and size (100 μm x 30 μm in (A) and (B)). (D-F) Cumulative distribution diagrams from three different stimuli. Diagrams present the normalized active electrodes number to distance from stimulus in different retinal layers under 160 ms light stimulus D: local background stimulus E: global background stimulus F: full field stimulus. Numbers labeled at INL (blue dash lines) and GCL (green dash lines) mark the 80 % limit in the distribution as benchmark distances to avoid the misjudgment of the propagation by outlier electrodes. (G) Boxplot of signal propagation distance under local background stimulus measured in whole slice (black), INL (red) and GCL (purple). The signal propagation distances in INL and GCL show no significant difference in any of the stimulus duration. Each symbol in the box plots represents the result from one slice under the specified condition. (H) Same as

(G) for global background stimulus. The signal propagation distances are significantly larger in INL than in GCL. (I) Same as (G) for full field stimulus, signal propagation distances are similar regardless of measuring from whole slice, INL or GCL. Significance tests were performed with Wilcoxon rank-sum test. *: P<0.05; **: P<0.01.

The failure of LFP propagation to the RGC layer under global background condition may be explained by the low peak amplitudes in the INL. To understand if the signal amplitude in INL would affect the signal detection in the GCL, the average peak voltage amplitudes in INL under the two stimulus conditions (local background and global background) were compared. The peak amplitude decreased with distance for local background stimulus. The same trend was observed for the small field stimulus on global background albeit with a smaller starting amplitude (Figure 3.14).

Indeed, when relating the peak amplitude in the INL to the peak amplitude in the GCL from the same column under local and global background stimuli, a positive linear correlation was detected (average corr coeff = 0.81 and 0.79 for local and global background stimuli respectively, n = 9 slices), suggesting that signal amplitude in the GCL was highly correlated to the amplitude in the INL (Figure 3.15 A-B). On the other hand, there was little correlation under full field stimulation (average corr coeff = 0.4, n = 9 slices, Figure 3.15C).

By considering electrodes not covered by the slice (i.e. electrode (iii) in Figure 3.2A), the basic noise level with "amplitudes" below ~ 50 µV was obtained (Figure 3.15D). When comparing the signal amplitudes in INL under local background and global background stimuli, more electrodes covered by the slice detected signals below 50 µV in the global background stimulus condition and thus did not pass the threshold for being considered as an active electrode (Figure 3.16).

These evidences suggest that local background stimulation could evoke higher signal amplitude, therefore more electrodes would detect signals higher than ~ 50 µV as compared to the global background condition, resulting in a longer signal propagation distance.
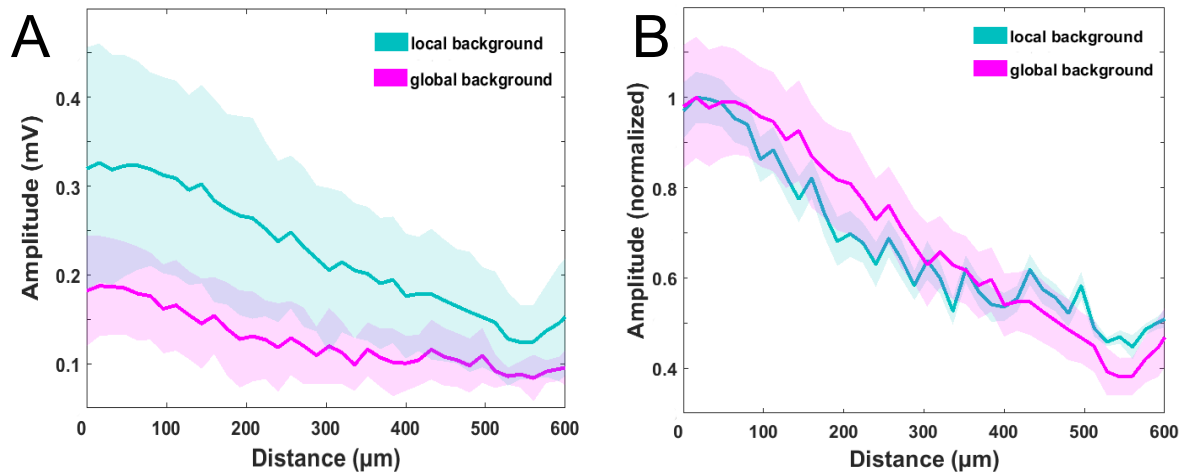
Figure 3.14: Stimulus background condition affects the peak amplitude of extracellular signals but not the decaying tendency. (A) Averaged peak amplitude versus distance recorded in INL under local and global background stimulus conditions. Local background stimulus evoked higher amplitude than global background stimulus. In both conditions the amplitude decreased with distance from stimulus center. (B) The normalized signal amplitudes show that the tendency for amplitude decrease by distance was irrelevant to background condition. This indicates that the diminished distal GCL activity in the global background condition was relevant to the evoked amplitude in INL.
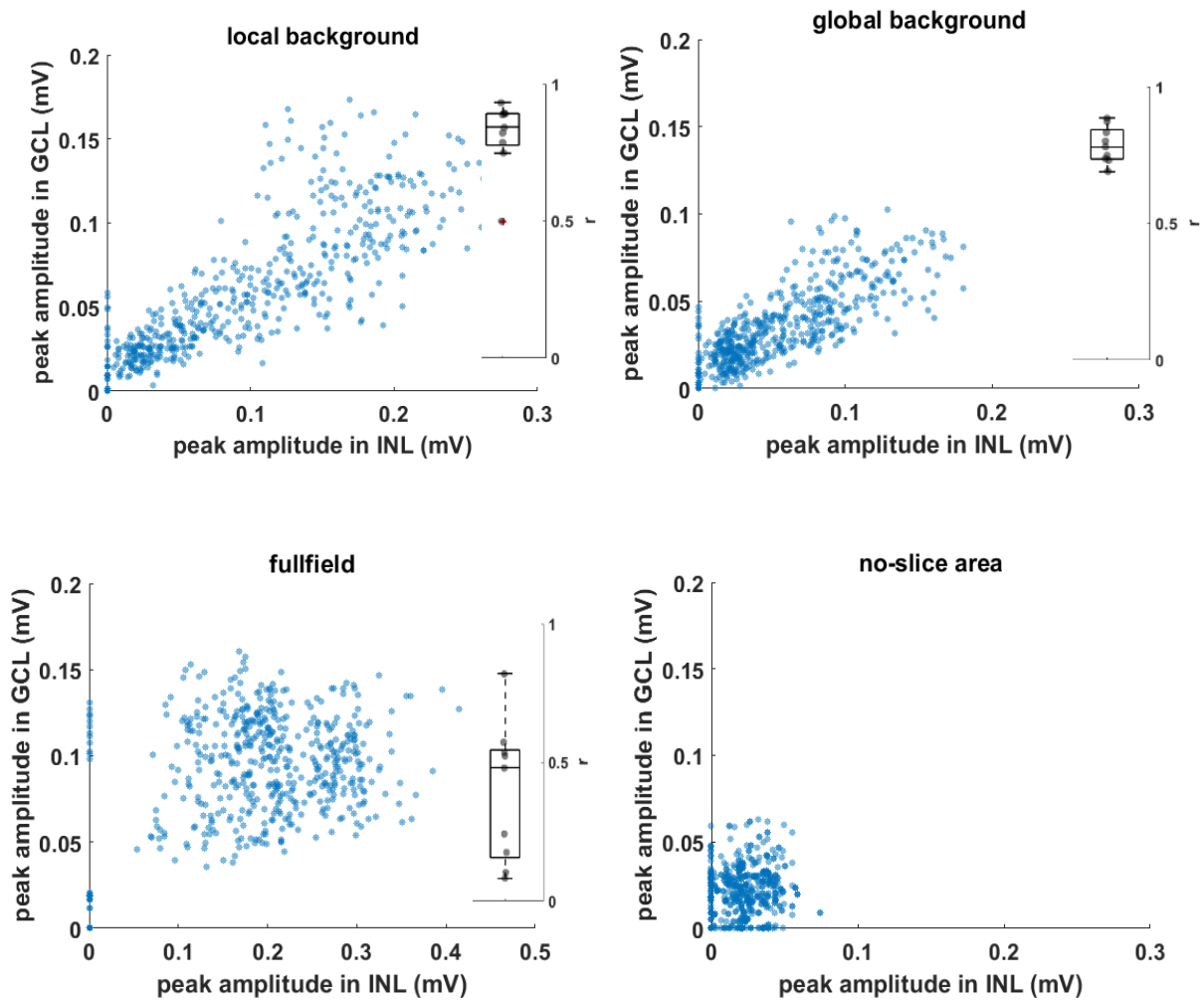
Figure 3.15: Scatter plots of averaged peak amplitudes in INL vs averaged peak amplitudes in GCL from the same column from one single slice. Box plots at the right bottom corner show the correlation coefficient values from 9 slices in different light stimulation conditions. In both local and global background stimuli (upper subplots), the signal amplitudes in GCL were positively correlated with the signal recorded in the INL (r = 0.81 ± 0.12 for local background; r = 0.79 ± 0.06 for global background, r= correlation coefficient). This indicates that upon stimulation with localized light the signal amplitude in the GCL was highly correlated with the signal amplitude from its upstream INL. When stimulated with full field stimulation, the correlation decreases to r= 0.4 ± 0.24. When two rows of electrode covered no retinal slice were selected, the correlation and signal amplitude were both very low (r =0.26).
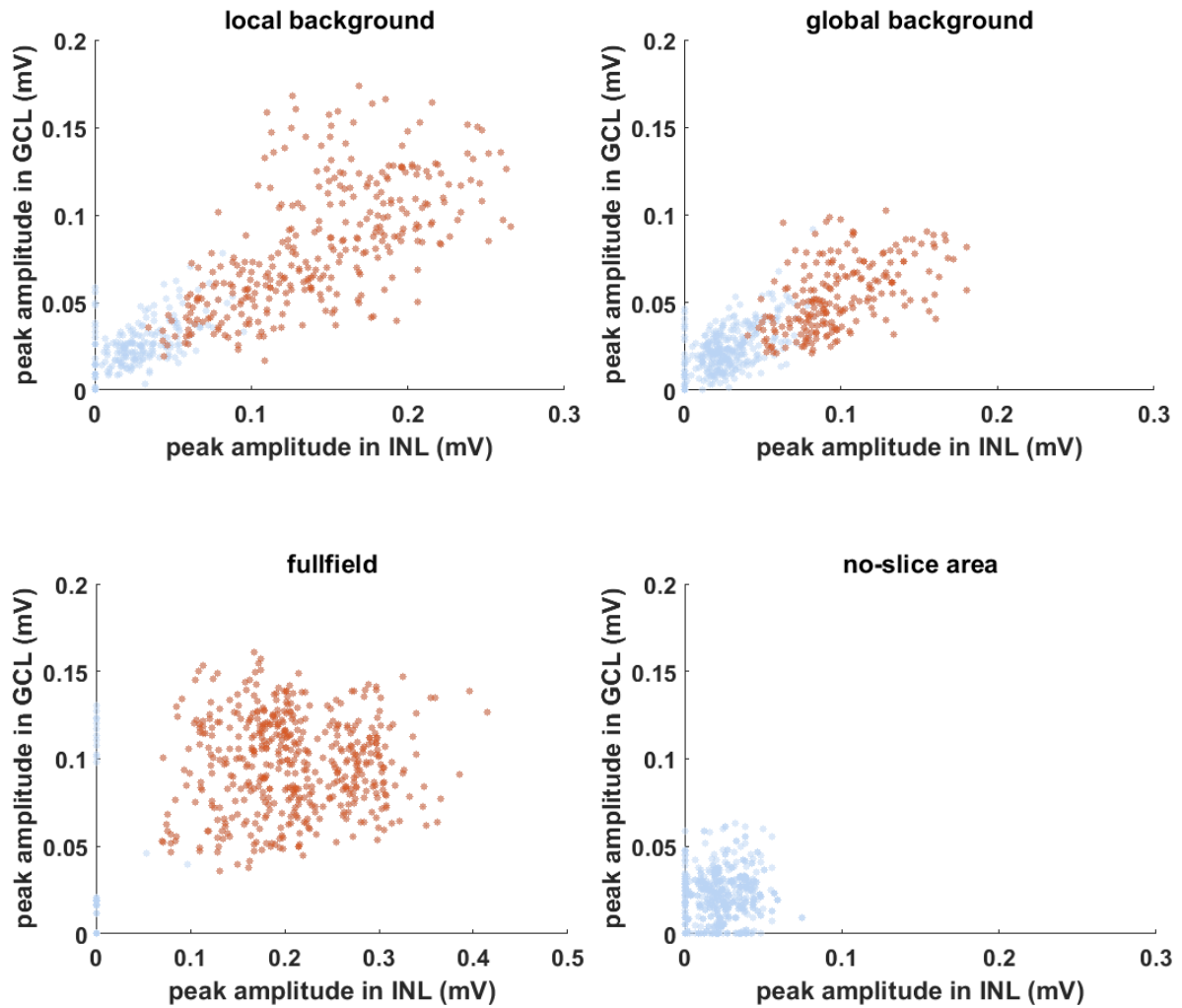
Figure 3.16: Scatter plots of averaged peak amplitudes in INL vs averaged peak amplitudes in GCL from active electrodes. Blue dots represent electrodes that were not considered as active electrodes, red dots stand for active electrodes. This figure shows that though the low amplitude signals might be missed by the "active electrode" threshold, however, the scatter plot patterns of non-active electrodes in local and global background stimulation conditions (blue dots) are very similar to the pattern recorded outside the retinal slice (" no-slice area"). This figure strongly suggests that the threshold used in this study was reasonable.

3.7.   **Kinetics in proximal and distal area**

Although the separation in individual layers (Figure 3.13) explained the finding in the flat-mount retina (Figure 3.5 and 3.6), it remained unclear which retinal circuitries might be involved for this effect. Therefore, the kinetics of the light responses were investigated by using the peak latencies and the offset latencies of the extracellular voltages from the recorded signals (Figure 3.2A, for definitions see section 2.9.2).

Heatmaps of peak latency and offset latency from local (Figure 3.17A-B) and global background (Figure 3.18A-B) stimuli both showed two very different kinetics from proximal and distal areas relatively to the light stimulus, with a short onset latency yet late offset latency at the proximal area and the opposite at the distal area.

To further define the proximal and distal area, the peak latency and offset latency from each electrode in only the INL were extracted. Latency versus distance was fitted using a normalized Gaussian distribution (see Method section 2.9.3) to the same slices analyzed in Figure 3.13. The division of proximal and distal area was set at the standard deviation = 1.5. The average proximal sizes were 255 µm and 299 µm measured from stimulus center for peak latency and offset latency in the local background stimulus (Figure 3.17, n=13 slices), and 221 µm and 283 µm for peak latency and offset latency respectively in the global background stimulus (Figure 3.18, n=9 slices).

After identifying proximal and distal areas, linear regressions were fitted to the data in the respective areas separately and obtained two distinct slopes that indicate the signal propagation velocities in both local (Figure 3.17C-D) and global background (Figure 3.18C-D) stimuli. The slopes showed two phases of the signal propagation: (1) a first phase with low propagation speed ("slow phase") confined to the proximal area and (2) a second phase with high propagation speed ("fast phase") which occured in the distal area.

For the peak latency, the slopes at the slow phases of local and global background stimuli are 0.21 and 0.23 respectively, translating to the signal propagation speed of 4.8 µm / ms and 4.3 µm / ms respectively. For the fast phase, slopes are 0.05 and 0.03 from local and global background stimuli respectively, translating to a propagation speed of 20 µm / ms and 33 µm / ms. The most likely candidate for the fast signal propagation may be gap junctions. In a flat-mount preparation, gap-junction mediated propagation of field potentials has been estimated to propagate with velocities between 5 - 20 µm / ms (Menzler and Zeck, 2011).

The separation of signal propagation in two phases was clearly seen in the offset latency as well: the slopes of -0.59 and -0.58 in the proximal area and 0.01 and -0.02 in the distal area under local and global background stimuli respectively suggested that there are two signal transduction mechanisms in the slices.

The analysis of signal kinetics showed that the INL received and processed signals from upstream even though the signals were not always transduced to the GCL, and that the light responses in proximal and distal areas were mediated by two different, slow and fast mechanisms. In the following the hypothesis that the fast signaling within the INL was mediated by gap junctions was investigated.
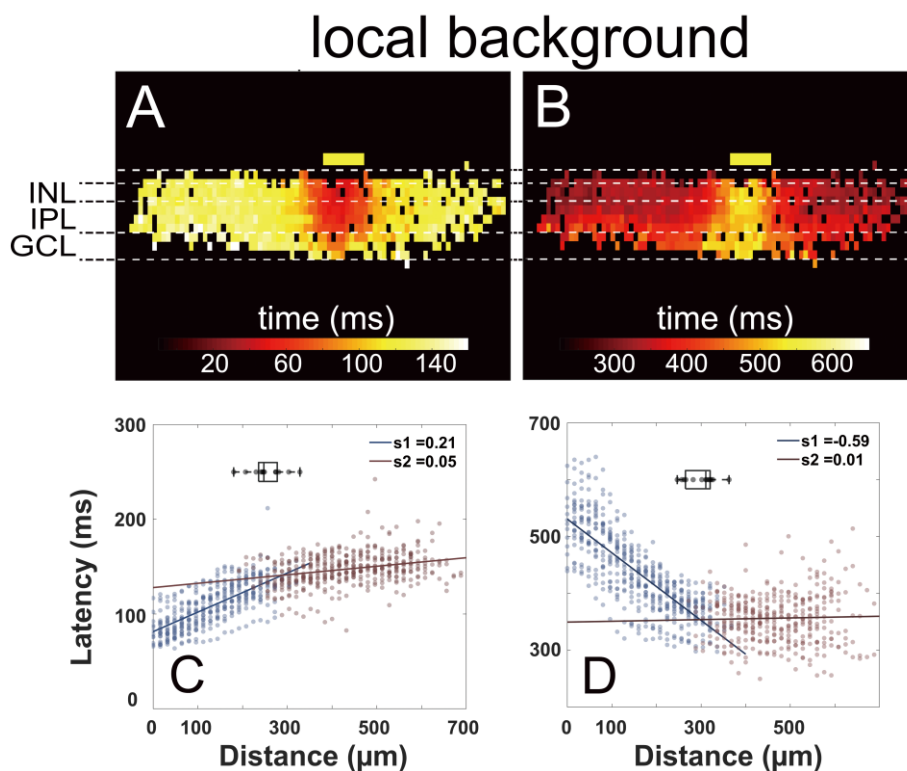
Figure 3.17: Proximal and distal areas show two different light response kinetics-local background stimulation. (A-B) Heatmaps of active electrodes color code with peak latency (A) and offset latency (B) in different retinal layers with 160 ms light stimulus. Yellow boxes mark the stimulus size (30 x 100 μm^2) and position. (C-D) Scatter plots show latency versus distance to stimulus of active electrodes in INL from multiple slices overlay with fitted linear regression. C: peak latency D: offset latency. Points in two areas were fitted with linear regressions separately. Boxplots in each subplot show the averaged distances for proximal areas. Average distances for individual plots are 255 μm (C), 299 μm (D).
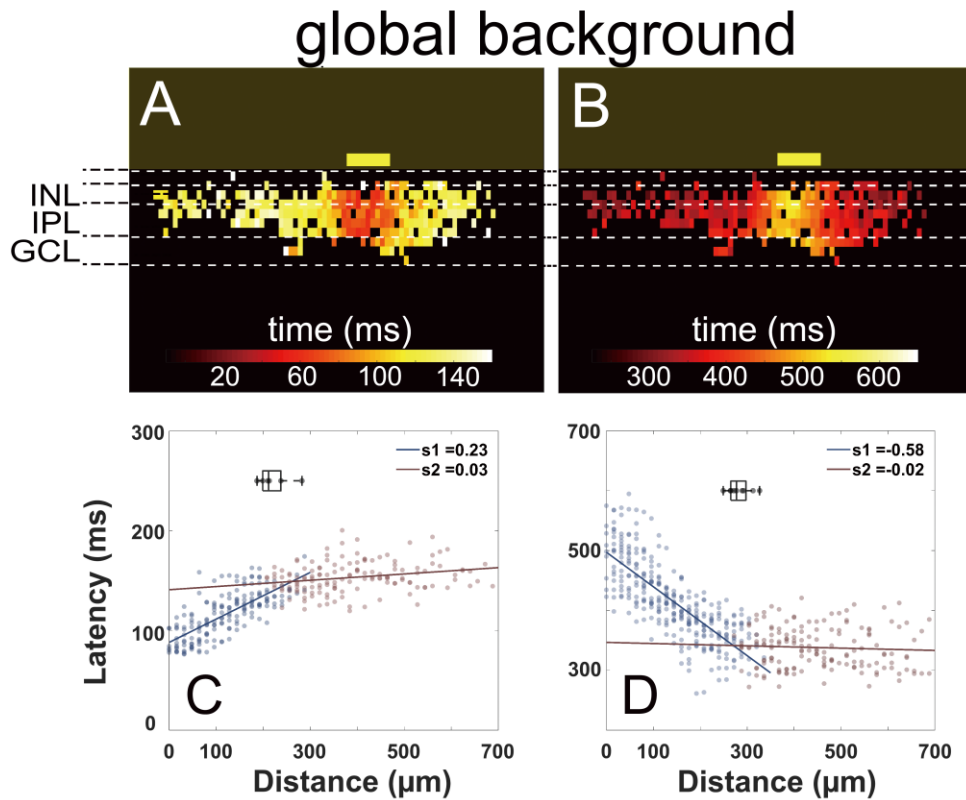
Figure 3.18: Proximal and distal areas show two different light response kinetics-global background stimulation. (A-B) Heatmaps of active electrodes color code with peak latency (A) and offset latency (B) in different retinal layers with 160 ms light stimulus. Yellow boxes mark the stimulus size (30 x 100 μm^2) and position. (C-D) Scatter plots of latency versus distance to stimulus from active electrodes in INL from multiple slices overlay with fitted linear regression. C: peak latency D: offset latency. Points in two areas were fitted with linear regression separately. Boxplots in each subplot show the averaged distances for proximal areas. Average distance for individual plots are 221 μm (C) and 283 μm (D).

3.8. The fast phase of signal propagation in the INL is mediated by gap junctions

The previous results showed that the light response recorded in slices could be divided into two different phases, with a fast phase potentially mediated by gap junctions. To test this hypothesis, MFA (100 µM) was applied to block gap junctions. After MFA application, the propagation distance in INL decreased in both local and global background stimulus conditions (n=7 slices from 7 animals). Color-coded peak latency heatmaps show the effect for a local background stimulus with reduced signal propagation distance (Figure 3.19A, B). The same effect was shown when the stimulus was provided on a global background (Figure 3.19E, F), indicating that gap junctions indeed mediated the recorded lateral signal propagation.

Among all gap junctions, Connexin 36 (Cx36) is the most commonly encountered one and plays an important role in the retina (Veruki et al., 2010; Trenholm and Awatramani, 2017). Therefore, it is important to know if and how Cx36 itself would already affect the lateral signal propagation. To answer this question, the same stimuli were applied to slices obtained from Cx36 knockout (Cx36 KO) mice (Meyer et al., 2014; Tetenborg et al., 2019) that were kindly offered by the lab of Prof. Dr. Karin Dedek. The signal propagation distances in the Cx36 KO slices for both local and global background stimuli for all durations significantly decreased in most cases (Figure 3.20C, G, L and M, n=5 slices from 3 animals). The full field stimulus on both MFA applied (n=7 slices) or Cx36 KO slices (n=5 slices) showed almost no difference to the propagation distance, proving that the decrease is not caused by any preparation artifact (Figure 3.20D, H and N). The cumulative distribution diagrams upon 160 ms light stimulus from Cx36 KO slices once again show the loss of active electrodes at the distal area after the loss function of Cx36 gap junctions (Figure 3.20I-K). These results suggested that when the retina is stimulated with light, the lateral signal transduction in the INL is strongly dependent on the gap junctions, predominately from Cx36.
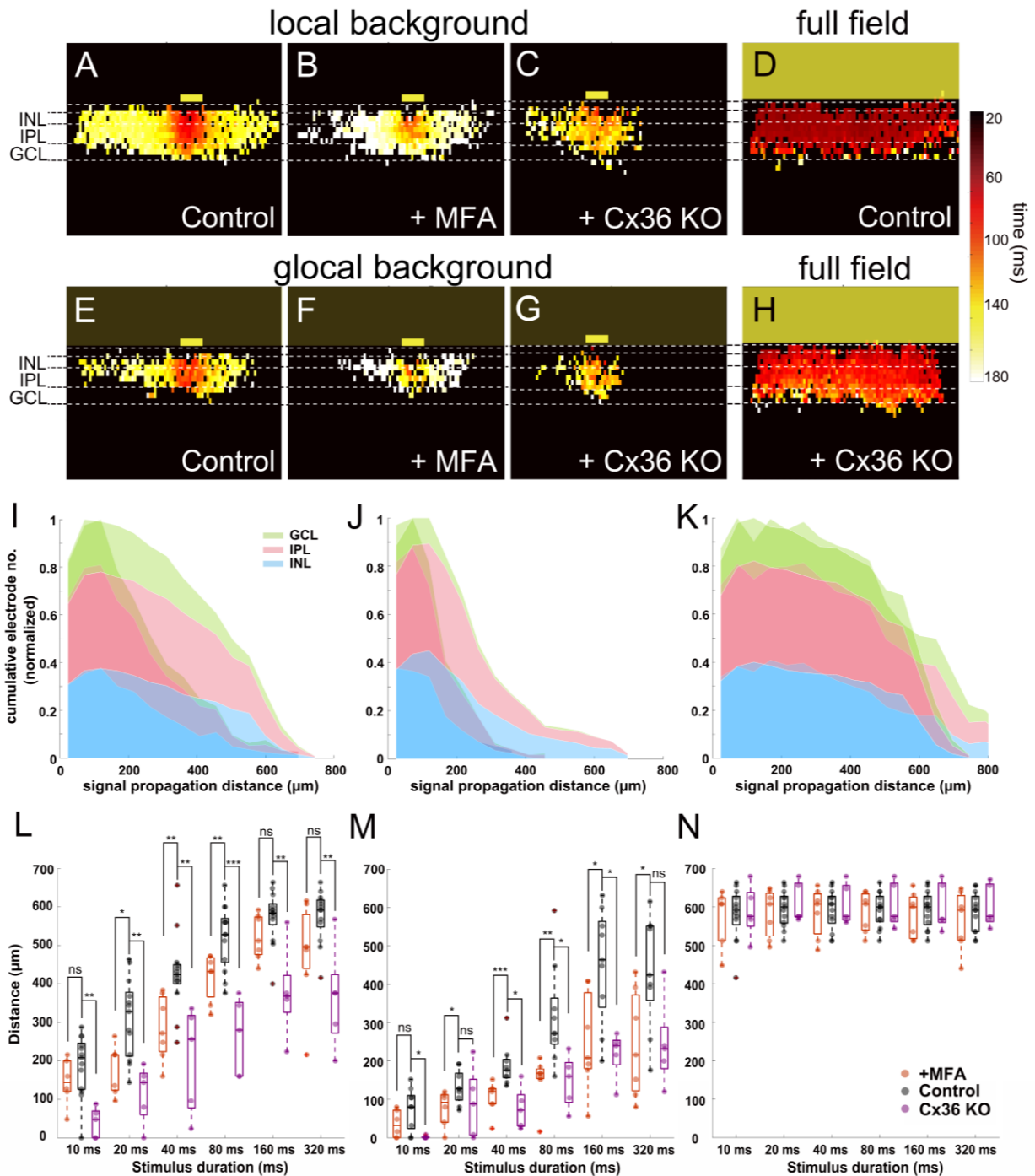
Figure 3.19: Blockage of gap junctions inhibits the lateral signal propagation. (A-H) Heatmaps of active electrodes color coded with peak latency in different retinal layers stimulated with 160 ms light pulse. A: local background stimulus B: local background stimulus + MFA (100μM) C: local background stimulus from Cx36 KO slice D: full field stimulus E: global background stimulus F: global background stimulus + MFA G: global background stimulus from Cx36 KO slice H: full field stimulus from Cx36 KO slice. Yellow boxes mark the stimulus positions. (I-K) Overlayed cumulative distribution diagrams from Cx36 KO slices (saturate color) with WT

control slices (transparent color) under three different stimuli. Diagrams present the normalized active electrodes number to distance from stimulus in different retinal layers with 160 ms of light stimulus. I: local background stimulus J: global background stimulus K: full field stimulus. (L) Boxplot of signal propagation distances under local background stimulus measured in INL with control (black), +MFA (red) and Cx36 KO (purple). The signal propagation distances after adding MFA or from Cx36 KO slice reduced significantly in most of the stimulus durations. Each symbol represents the result from one slice under the specified condition. (M) Same as (L) for global background stimulus. The signal propagation distances decreased after adding MFA or from Cx36 KO slice compare to the control group. (N) Same as (L) for full field stimulus, signal propagation distances were similar regardless of measuring from control, MFA or Cx36 KO slices. Significance test were performed with Wilcoxon rank-sum test. *: $P<0.05$; **: $P<0.01$; ***: $P<0.001$.

Chapter

4. Discussion

4.1.   **Long-range lateral signal transduction**

The first interesting result refers to the wide propagation of light-induced signals in vertical slices, which extended by far the classical receptive field center of BCs (Berntson and Taylor, 2000) or RGCs (Farrow and Masland, 2011; Baden et al., 2016).

For stimulation on local background or full field stimulation, the signals traveled to RGC layer, indicating that the signals recorded in INL were very likely the mixture of BCs and ACs, since BCs are the only cell type in INL that give excitatory input to RGCs. In the condition with local stimulus on a global background, the signals did not travel to RGC layer at the distal area, suggesting that the signal recorded at distal area was most likely attributed to ACs. Even there could be contribution from the excitatory postsynaptic potential from BCs, it would be minor because the amplitude was not even enough to evoke RGC spiking activity. The failure to evoke distal RGC spiking activity was most probably related to the low LFP peak amplitudes under this experimental condition (Figure 3.16).

Previous studies showed that the responses of BCs (Franke et al., 2017) and of RGCs (Sagdullaev and McCall, 2005) decrease when stimulated with large spots as compared to small spot stimulation (i.e. the size of central stimulation). The results from this study are in line with these reports that when an inhibitory background illumination was applied (the global background), the light response amplitude decreased (Figure 3.4F). One possible explanation could be that the lateral inhibition from the horizontal cells. In this preparation however, it was not possible to evaluate the contribution from horizontal cells because they

locate at the transition of the LFP polarity change (from hyperpolarization to depolarization) and therefore the positive and negative signals were easily cancelled out. With illumination on global background, signal propagation was restricted in the RGC layer to the proximal area (Figure 3.6 and 3.13). One recent study showed that central stimulation suppresses the distal ganglion cell population response as evaluated in flat-mounted retina (Deny et al., 2017). This explains why when there was a global background illumination, the RGCs at the distal area were unable to be activated. To the distal cells, their central receptive field was already activated by the background illumination. Therefore they were not able to respond to the small field stimulation, which would be the distal stimulation from the distal cells' perspective.

However, signal propagation in INL was always detected regardless of the background condition (Figure 3.13). After blocking gap junctions or by measuring Cx36 knock out mice significantly reduced the lateral propagation distance. This implies that Cx36 is involved in the mechanism and plays an important role in the lateral signal propagation (Figure 3.19).

Cx36 gap junction couplings are known to express between PRs in OPL and between AII-BC, AII-AII, GC-AC and GC-GC in the IPL (Bloomfield and Volgyi, 2009; Trenholm and Awatramani, 2017). The short-range gap junction couplings between cones have been found to improve the contrast sensitivity by increasing the signal to noise ratio at the cost of losing some visual acuity by 0.5 cone diameters (DeVries et al., 2002). However, 0.5 cone diameters would not explain the far distance of signal propagation observed from the experiments in this study.

The results of reduced signal propagation were restricted to the INL, therefore most likely to be mediated by Cx36 between AII-BC, AII-AII or GC-AC. In whole mount preparations, lateral signal propagation has been reported upon blocking inhibition to BCs (Toychiev et al., 2013), the propagation was also abolished by blocking gap junctions. The underlying mechanisms reported here and by Toychiev et al. appear similar: inhibition restricts the gap-junction mediated tangential signal propagation. The explanation of gap junctions in the INL being the main driver for the fast signal propagation phase implies that light-induced signals require to be processed by bipolar cells first. This leads to a constant time delay to the fast signal transduction phase (Figure 3.17C and 3.18C). Gap junctional couplings have been reported across species with different expression patterns (Kovacs-Oller et al., 2017). Further examination of this hypothesis may therefore involve interspecies comparison.

All ACs function over 6-7 log units of intensity (Xin and Bloomfield, 1999b), though the most well-known function of AII ACs is to convey the light-induced signal from rod pathway to cone BCs and RGCs under scotopic light intensity, evidences in mice (Pang et al., 2007), rabbit (Bloomfield et al., 1997) and primate (Strettoi et al., 2018) have shown that AII ACs also work at photopic range of light. Since signal propagation through gap junctions is bidirectional (Veruki et al., 2010), AII ACs could be activated with photopic stimulation via the activation of ON-cone BCs (Manookin et al., 2008; van Wyk et al., 2009; Hartveit and Veruki, 2012). The AII - ON CBC - AII network has been reported in the photoreceptor degenerated retina (Margolis et al., 2014; Trenholm and Awatramani, 2015), proving their strong connectivity. It would be reasonable to hypothesize that the long-range field potentials originate from the local stimulation of cones. These cones activate the ON-cone BCs in the central area, which further activate the connected AII ACs. Because these AII ACs are connected to further cone BCs, a network activation and thus longer distance of signal propagation is conceivable (Figure 4.1A).

4.2. Inhibitory network in the inner retina under different light conditions

The results obtained from stimulation on global background showed that though signals didn't propagate to RGC layer, depolarizing activity in the INL could still be recorded.

Previous studies have shown that the concept of receptive field may be much more complex than the classical center-surround concept. OFF RGCs respond to distal stimuli by the disinhibition of glycinergic ACs via GABAergic ACs (Deny et al., 2017). Large field light stimulation was found to suppress BC inhibition with serial connections between inhibitory ACs. More specifically, wide-field GABAergic ACs disinhibit BCs via inhibiting GABAergic ACs through $GABA_A$ receptors (Eggers and Lukasiewicz, 2010). On the other hand, disinhibition of the GABAergic network by glycinergic ACs was also reported (Franke et al., 2017). Crossover inhibition among ACs showed the complex modulation of inhibitory input to BCs (Molnar and Werblin, 2007; Hsueh et al., 2008).

The main difference between the two stimuli investigated here in depth (i.e. stimulus with local or global background) is that local stimulation would only stimulate small field ACs which are involve in local inhibitory circuitries. Global background includes the activation wide-field ACs that provide GABAergic input to BCs axon terminals (Franke and Baden,

2017) and inhibit BCs activity. When using full field strong stimulus instead of low intensity global background, the BCs depolarization overcame the inhibitory input and activated the downstream RGCs. The proposed signaling based on the results is summarized in Figure 4.1.

Even though wide-field stimulation was found to activate serial connections and further suppresses the inhibitory postsynaptic currents in BCs (Eggers and Lukasiewicz, 2010), results from this study (Figure 3.4) and previous reports (Franke et al., 2017) both showed that the inhibition is much stronger than the disinhibition effect, eventually causing the decrease of BCs response.
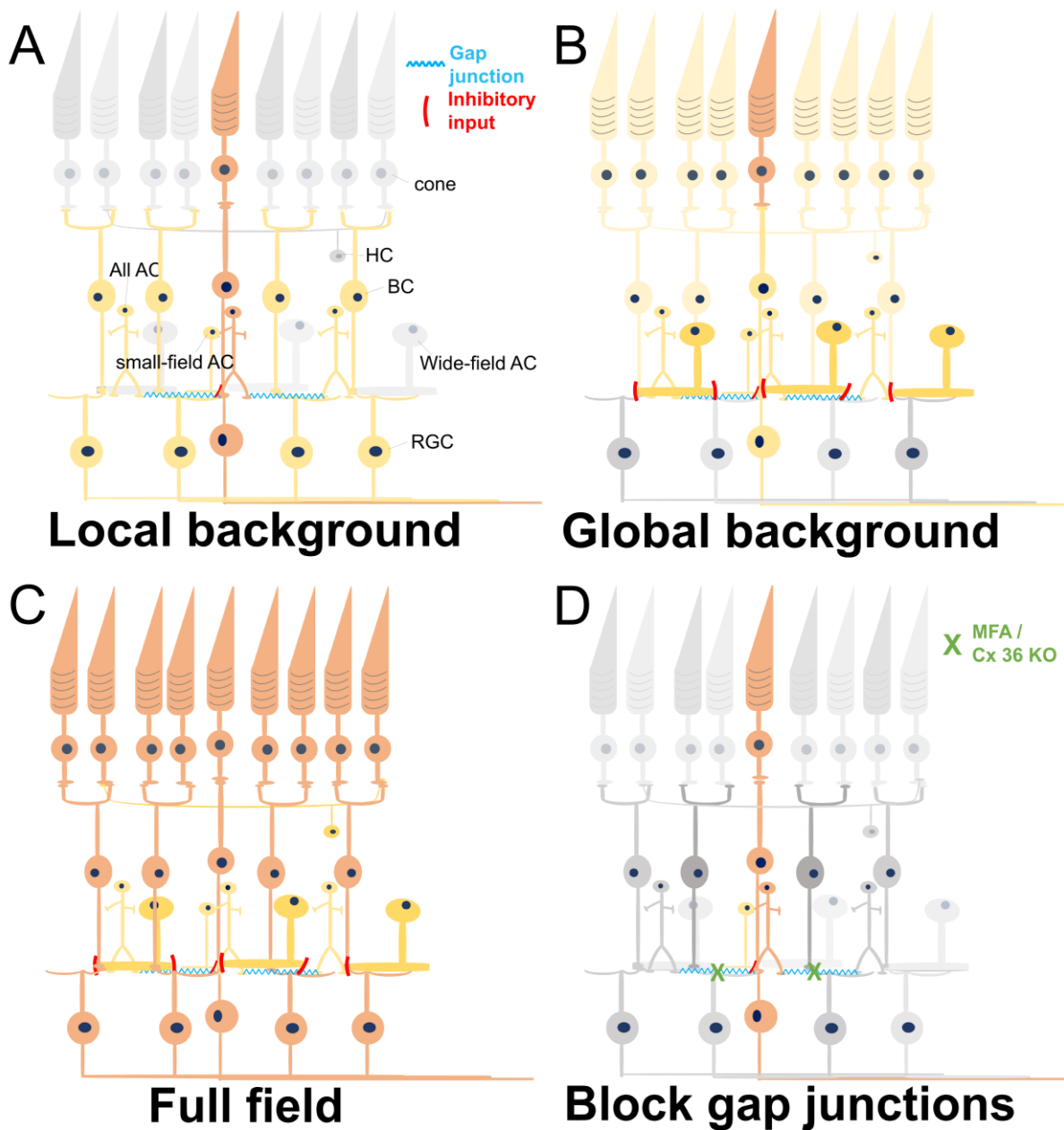
Figure 4.1: Summary of light-induced signal transduction pathways under different conditions.

Different colors represent for level of activity. Gray: no activation. Light yellow: weak activation. Dark yellow: medium activation. Orange-red: strong activation.

(A) A local stimulus strongly activates the central photoreceptors, which excite the synaptically connected BCs. The BCs activate AII amacrine cells via gap junctions, eventually forming a network activation. Small field ACs may also be activated by the local light stimulus and give a weak inhibitory input to the BCs. The network in the inner retina leads to a broad activation of remote RGCs.

(B) Weak activation of all photoreceptors by a weak global background in addition to the strong activation of central photoreceptors by a local stimulus. Except local circuitries, the wide-field inhibitory ACs are also recruited by the global background, weakening the responses of BCs and RGCs activated by the strong local stimulus.

(C) Full field stimulation activates all photoreceptors underneath the stimulus area and also their downstream BCs. In this case, all the excitatory and inhibitory retinal networks are activated, with excitation being stronger than inhibition.

(D) Reduction of gap junctional coupling leads to a local activation of PRs and BCs, but not to a wide network activation. Therefore, the activities only stay at very restricted area.

4.3.   **Stimulus-Duration dependent signal propagation**

In all of the results from slices, one phenomenon that was independent from background condition or drug application was the stimulus-dependent signal propagation. The longer the stimulation, the further the LFP propagated. Patch clamp recording from BCs showed that only the light intensity but not the duration changes the amplitude or latency of the transmembrane voltage (Euler and Masland, 2000). This is in line with the recordings in slice, where except for the very short stimuli (10 ms duration), all other stimuli evoked extracellular signals with very similar amplitude and latency (Figure 3.4E). Therefore, the duration dependent effect was not caused by the decay of the extracellular voltage from cells at the light stimulus.

Signals recorded by distal electrodes implies that more depolarizing cells were activated by longer stimuli. While very short light pulses could simply seem like noisy signals to the retina, longer stimulus not only could mean more important signal but also more chances for post synaptic cells to get enough input from their dendrites and send signals to their further downstream. Note that the longest duration used here was 320 ms, therefore it was not in the same range for adaptation (seconds to minutes).

Increasing the activated area and thereby the number of activated retinal cells could mean that the important input signal is amplified, but could also reduce the visual acuity and lead to inaccurate inference of the of the stimulus position. Though longer stimuli did activate more cells in the visual processing, it only turns into RGCs spiking output when the stimulus was on a local background (Figure 3.5). This interesting result could mean that when there is no other visual stimulation in the environment, RGCs choose to sense anything they can detect, even the stimulus locates far away from their own classical receptive field. Future research may evaluate this hypothesis.

4.4.   **Discrepancies between flat-mount and slice preparation**

There are some discrepancies between the results from flat-mount and slice preparation. For instance, the light response latency was shorter in flat-mount than in slice. In the flat-mount preparation, the averaged light response latency for ON RGCs was around 55- 65 ms (Figure 3.9). The latency was however dependent on the distance of the cell to the stimulus. The more distal the cell wss located, the longer the latency was (Figure 3.10). Most of the ON RGCs had the latency between 20-100 ms. The RGC first-spike latencies are in agreement with previous work (Stutzki et al., 2014; Tengolics et al., 2019). In the slice preparation, the light response peak latency increased by the distance as well (Figure 3.17 and 3.18), but it was much longer than the flat-mount preparation, starting from around 80 ms with the most proximal electrodes. This difference can be derived from the different ways to approach the data. As for the flat-mount preparation, the latency was considered as the time when the first spike appeared, in the slice preparation however, the peak latency was the latency when the LFP reaches 80% of the peak amplitude. Note that the spikes usually appear before the LFP reaches its maximum amplitude (Figure 4.2). Therefore, the latency can be overestimated in the slice preparation.

The difference could also come from the preparation itself. In the slice preparation, the retina was cut, therefore some interferences of the cell activity could be imagined. The discrepancy of the latency may originate from the interruption of the retinal network. This might also explain the differences of the distance the signal propagated in different preparation, especially under short stimulus duration. In the flat-mount preparation, some RGCs located at 400 or 600 μm showed light response with 10 ms stimulus (Figure 3.5B and 3.6B). In the slice preparation under the same stimulus condition, the signal propagation distance was only around 200-300 μm. The disruption of the connections at the surface of the cutting side was most likely the reason for the discrepancy.

In the slice preparation, damage to the cells located at the surface at the cutting side was unavoidable. However, it offered a great opportunity to study the mechanism of visual processing in the inner retina with MEA. From the point of well-intact circuitry, other methods like patch clamp or calcium imaging do have the strength. However, these methods are very limited to the recording area and always come with the trade-off between temporal and spatial resolution (Lillis et al., 2008; Zhao et al., 2020). This preparation offers a new option and perspective to study how vision works.
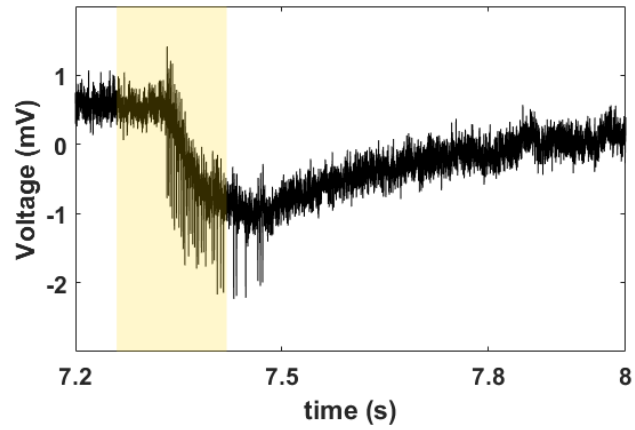
Figure 4.2: Raw trace of one electrode recording the RGC spiking activity on a flat-mount retina with 160 ms local background stimulus. Yellow box represents the light stimulus. The spiking occurs earlier than the peak of LFP.

4.5. **Electrical imaging signal propagation with high density CMOS-MEA**

In this study, I demonstrated how to analyze signal (LFP) propagation across and within different retinal layers in vertical slices using high-density CMOS-based MEAs.

Electrical imaging of LFPs using CMOS-based MEAs has been applied before to study other brain areas such as the well-known tri-synaptic hippocampal formation (Hutzler et al., 2006; Ferrea et al., 2012) or cortical structures (Viventi et al., 2012; Wickham et al., 2019) with the focus on epileptiform activities. Examples of propagating LFP were shown along the hippocampal CA region (Channappa et al., 2014) and in photoreceptor degenerated flat-mount mouse retina (Menzler and Zeck, 2011). Electrical imaging at a coarser spatial scale discussed the possibility of non-synaptic propagation of epileptiform activity in the unfolded hippocampus (Choi et al., 2014a).

In retina research, among the first results revealed by electrical imaging the developing retina of the RGC layer was the retinal waves (Meister et al., 1991). Recently, electrical imaging at high spatial-temporal resolution using CMOS-based MEAs revealed shrinkage of these waves during ontogeny down to the size of the spatial receptive fields of RGCs (Maccione et al., 2014b). Whereas in the healthy retina the synchronous retinal output largely disappears, it is consistently detected in photoreceptor degenerated retinas (Menzler and Zeck, 2011; Menzler et al., 2014). However, the RGC spiking alone does not provide a complete description of the functional changes occurring in these retinas. Strong sub-threshold oscillations of transmembrane potential (Choi et al., 2014a; Menzler et al., 2014) lead to LFPs, which emerge spontaneously and propagate at different speeds across the retinal layers.

Electrical imaging upon light stimulation may be affected by the CMOS MEAs sensitivity (Bertotti et al., 2017). Here any light artefact was avoided by using a 45° mirror next to the sensor array and projected the light as shown in Figure 2.9. I further demonstrated that there were no light artefacts (i.e. Fig.3.2A, trace iii), which may interfere with our results.

One limitation of the current study was the failure to detect both, LFPs and single-cell activity of RGCs and potentially of spiking BCs in the vertical slice. This may be overcome by adding three-dimensional electrodes (Jones et al., 2020) to the sensor area and thereby enabling a tight contact to the slice. A second caveat is the mixture of signals from ON and OFF bipolar cells. Future work may combine two-photon imaging of the two major inner retinal layers (Zhao et al., 2020) with CMOS-MEA recording (Ackert et al., 2006).

Alternatively, calcium imaging within restricted layers (INL, GCL) of the retinal slices may investigate to what degree the observed effect of remote activation (Figure 3.5) is cell class specific.

Chapter

5. Conclusion

Electrical imaging light-induced signal propagation in different retinal layers visualizes how signals propagate within and across the distinct retinal layers. This method was applied for one simple, pulsatile and localized stimulus. Light stimulus conditions for remote activation were analyzed. By applying pharmacological treatments and using transgenic mice, the results strongly supported the possibilities and potentials of using electrical imaging to reveal neural circuits and the underlying mechanisms. Future work may extend the approach to more elaborate stimuli to reveal the full potential of the intriguing signal processor implemented by the mammalian retina.

Chapter

6. Future Perspective

This study showed the potential of using electrical imaging to reveal the mechanism of vertical and lateral circuits at the same time in a relatively large scale (mm^2). The approach overcame the disadvantage of the fluorescence-based methods with the trade-off between temporal and spatial resolution and therefore offers great opportunities for studies that require monitoring neural activities involve large area or different regions. More importantly, this method showed the possibility to use MEA to record beyond RGCs.

The dynamics, interaction and interference of signals from more complex stimuli (for example: multiple stimuli at different locations) within different retinal layers will be interesting topics for this approach.

This method is also suitable for the study of spontaneous activities. For instance, MEA have been widely used to study the developmental spontaneous activity retinal waves (Stacy et al., 2005; Kirkby and Feller, 2013). While CMOS MEA has allowed to study retinal waves in at near cellular resolution at the RGC layer (Maccione et al., 2014a), the vertical slice approach would give a better understanding to the retinal wave or wave-like activities (Toychiev et al., 2013) across different retinal layers. Similar concept can be applied to the understandings of spontaneous oscillatory rhythms in the degenerating retina (Euler and Schubert, 2015; Trenholm and Awatramani, 2015).

Chapter

7. References

Ackert JM, Wu SH, Lee JC, Abrams J, Hu EH, Perlman I, Bloomfield SA (2006) Light-induced changes in spike synchronization between coupled ON direction selective ganglion cells in the mammalian retina. J Neurosci 26:4206-4215.

Anishchenko A, Greschner M, Elstrott J, Sher A, Litke AM, Feller MB, Chichilnisky EJ (2010) Receptive field mosaics of retinal ganglion cells are established without visual experience. J Neurophysiol 103:1856-1864.

Baden T, Berens P, Franke K, Roman Roson M, Bethge M, Euler T (2016) The functional diversity of retinal ganglion cells in the mouse. Nature 529:345-350.

Baker A (2016) Lateral Inhibition and Protons: The First Level of Contrast in Stimulation of the Retina? In.

Behrens C, Schubert T, Haverkamp S, Euler T, Berens P (2016) Connectivity map of bipolar cells and photoreceptors in the mouse retina. Elife 5.

Berntson A, Taylor WR (2000) Response characteristics and receptive field widths of on-bipolar cells in the mouse retina. J Physiol 524 Pt 3:879-889.

Bertotti G, Velychko D, Dodel N, Keil S, Wolansky D, Tillak B, Schreiter M, Röhler S, Zeck G, Thewes R (2014) A CMOS-based sensor array for in-vitro neural tissue interfacing with 4225 recording sites and 1024 stimulation sites. In: Biomedical Circuits and Systems Conference (BioCAS), 2014 IEEE, pp 304-307: IEEE.

References

Bertotti G, Jetter F, Keil S, Dodel N, Schreiter M, Wolansky D, Boucsein C, Boven K-H, Zeck G, Thewes R (2017) Optical stimulation effects on TiO 2 sensor dielectric used in capacitively-coupled high-density CMOS microelectrode array. IEEE Electron Device Letters 38:967-970.

Bloomfield SA, Volgyi B (2004) Function and plasticity of homologous coupling between AII amacrine cells. Vision Res 44:3297-3306.

Bloomfield SA, Volgyi B (2009) The diverse functional roles and regulation of neuronal gap junctions in the retina. Nat Rev Neurosci 10:495-506.

Bloomfield SA, Xin D, Osborne T (1997) Light-induced modulation of coupling between AII amacrine cells in the rabbit retina. Vis Neurosci 14:565-576.

Channappa L, Helmhold F, Zeck G (2014) Electrical Imaging of Local Field Potentials in Organotypic and Acute Hippocampal Slices Using CMOS MEAs. In: Proc. 9th Int. Meeting on Substrate-Integrated Microelectrodes (Stett A, ed). Reutlingen.

Chapot CA, Euler T, Schubert T (2017) How do horizontal cells 'talk' to cone photoreceptors? Different levels of complexity at the cone-horizontal cell synapse. J Physiol 595:5495-5506.

Chiao CC, Masland RH (2003) Contextual tuning of direction-selective retinal ganglion cells. Nat Neurosci 6:1251-1252.

Chiao CC, Lin CI, Lee MJ (2020) Multiple Approaches for Enhancing Neural Activity to Promote Neurite Outgrowth of Retinal Explants. Methods Mol Biol 2092:65-75.

Choi H, Zhang L, Butts D, Singer JH, Riecke H (2014a) Intrinsic bursting of AII amacrine cells underlies oscillations in the rd1 mouse retina. JNeurophysiol 112.

Choi H, Zhang L, Cembrowski MS, Sabottke CF, Markowitz AL, Butts DA, Kath WL, Singer JH, Riecke H (2014b) Intrinsic bursting of AII amacrine cells underlies oscillations in the rd1 mouse retina. J Neurophysiol 112:1491-1504.

Deny S, Ferrari U, Mace E, Yger P, Caplette R, Picaud S, Tkacik G, Marre O (2017) Multiplexed computations in retinal ganglion cells of a single type. Nat Commun 8:1964.

DeVries SH, Qi X, Smith R, Makous W, Sterling P (2002) Electrical coupling between mammalian cones. Curr Biol 12:1900-1907.

Diamond JS (2017) Inhibitory Interneurons in the Retina: Types, Circuitry, and Function. Annu Rev Vis Sci 3:1-24.

Dorgau B, Herrling R, Schultz K, Greb H, Segelken J, Stroh S, Bolte P, Weiler R, Dedek K, Janssen-Bienhold U (2015) Connexin50 couples axon terminals of mouse horizontal cells by homotypic gap junctions. J Comp Neurol 523:2062-2081.

Eggers ED, Lukasiewicz PD (2010) Interneuron circuits tune inhibition in retinal bipolar cells. J Neurophysiol 103:25-37.

References

Euler T, Masland RH (2000) Light-evoked responses of bipolar cells in a mammalian retina. J Neurophysiol 83:1817-1829.

Euler T, Schubert T (2015) Multiple Independent Oscillatory Networks in the Degenerating Retina. Front Cell Neurosci 9:444.

Farrow K, Masland RH (2011) Physiological clustering of visual channels in the mouse retina. J Neurophysiol 105:1516-1530.

Ferguson LR, Dominguez JM, 2nd, Balaiya S, Grover S, Chalam KV (2013) Retinal Thickness Normative Data in Wild-Type Mice Using Customized Miniature SD-OCT. PLoS One 8:e67265.

Ferrea E, Maccione A, Medrihan L, Nieus T, Ghezzi D, Baldelli P, Benfenati F, Berdondini L (2012) Large-scale, high-resolution electrophysiological imaging of field potentials in brain slices with microelectronic multielectrode arrays. Front Neural Circuits 6:80.

Field GD, Sher A, Gauthier JL, Greschner M, Shlens J, Litke AM, Chichilnisky EJ (2007) Spatial properties and functional organization of small bistratified ganglion cells in primate retina. J Neurosci 27:13261-13272.

Franke K, Baden T (2017) General features of inhibition in the inner retina. J Physiol 595:5507-5515.

Franke K, Berens P, Schubert T, Bethge M, Euler T, Baden T (2017) Inhibition decorrelates visual feature representations in the inner retina. Nature 542:439-444.

Hagins WA, Penn RD, Yoshikami S (1970) Dark current and photocurrent in retinal rods. Biophys J 10:380-412.

Hartveit E, Veruki ML (2012) Electrical synapses between AII amacrine cells in the retina: Function and modulation. Brain Res 1487:160-172.

Hombach S, Janssen-Bienhold U, Sohl G, Schubert T, Bussow H, Ott T, Weiler R, Willecke K (2004) Functional expression of connexin57 in horizontal cells of the mouse retina. Eur J Neurosci 19:2633-2640.

Hsueh HA, Molnar A, Werblin FS (2008) Amacrine-to-amacrine cell inhibition in the rabbit retina. J Neurophysiol 100:2077-2088.

Hutzler M, Lambacher A, Eversmann B, Jenkner M, Thewes R, Fromherz P (2006) High-resolution multitransistor array recording of electrical field potentials in cultured brain slices. J Neurophysiol 96:1638-1645.

Jin NG, Chuang AZ, Masson PJ, Ribelayga CP (2015) Rod electrical coupling is controlled by a circadian clock and dopamine in mouse retina. J Physiol 593:1597-1631.

Jones PD, Moskalyuk A, Barthold C, Gutöhrlein K, Heusel G, Schröppel B, Samba R, Giugliano M (2020) Low-impedance 3D PEDOT: PSS ultramicroelectrodes. Frontiers in Neuroscience 14:405.

Kandel ER, Schwartz JH, Jessell TM (2000) Principles of neural science, 4th Edition. New York: McGraw-Hill, Health Professions Division.

Kim IJ, Zhang Y, Yamagata M, Meister M, Sanes JR (2008) Molecular identification of a retinal cell type that responds to upward motion. Nature 452:478-482.

Kirkby LA, Feller MB (2013) Intrinsically photosensitive ganglion cells contribute to plasticity in retinal wave circuits. Proc Natl Acad Sci U S A 110:12090-12095.

Klapper SD, Swiersy A, Bamberg E, Busskamp V (2016) Biophysical Properties of Optogenetic Tools and Their Application for Vision Restoration Approaches. Front Syst Neurosci 10:74.

Kothmann WW, Massey SC, O'Brien J (2009) Dopamine-stimulated dephosphorylation of connexin 36 mediates AII amacrine cell uncoupling. J Neurosci 29:14903-14911.

Kovacs-Oller T, Debertin G, Balogh M, Ganczer A, Orban J, Nyitrai M, Balogh L, Kantor O, Volgyi B (2017) Connexin36 Expression in the Mammalian Retina: A Multiple-Species Comparison. Front Cell Neurosci 11:65.

Lasater EM (1987) Retinal horizontal cell gap junctional conductance is modulated by dopamine through a cyclic AMP-dependent protein kinase. Proc Natl Acad Sci U S A 84:7319-7323.

Leibig C, Wachtler T, Zeck G (2016) Unsupervised neural spike sorting for high-density microelectrode arrays with convolutive independent component analysis. J Neurosci Methods 271:1-13.

Lillis KP, Eng A, White JA, Mertz J (2008) Two-photon imaging of spatially extended neuronal network dynamics with high temporal resolution. J Neurosci Methods 172:178-184.

Maccione A, Hennig MH, Gandolfo M, Muthmann O, van Coppenhagen J, Eglen SJ, Berdondini L, Sernagor E (2014a) Following the ontogeny of retinal waves: pan-retinal recordings of population dynamics in the neonatal mouse. J Physiol 592:1545-1563.

Maccione A, Hennig MH, Gandolfo M, Muthmann O, van Coppenhagen J, Eglen SJ, Berdondini L, Sernagor E (2014b) Following the ontogeny of retinal waves: pan-retinal recordings of population dynamics in the neonatal mouse. J Physiol 592:1545-1563.

Mani A, Schwartz GW (2017) Circuit Mechanisms of a Retinal Ganglion Cell with Stimulus-Dependent Response Latency and Activation Beyond Its Dendrites. Curr Biol 27:471-482.

Manookin MB, Beaudoin DL, Ernst ZR, Flagel LJ, Demb JB (2008) Disinhibition combines with excitation to extend the operating range of the OFF visual pathway in daylight. J Neurosci 28:4136-4150.

Margolis DJ, Gartland AJ, Singer JH, Detwiler PB (2014) Network oscillations drive correlated spiking of ON and OFF ganglion cells in the rd1 mouse model of retinal degeneration. PLoS One 9:e86253.

Meister M, Wong RO, Baylor DA, Shatz CJ (1991) Synchronous bursts of action potentials in ganglion cells of the developing mammalian retina. Science 252:939-943.

Menzler J, Zeck G (2011) Network oscillations in rod-degenerated mouse retinas. J Neurosci 31:2280-2291.

Menzler J, Channappa L, Zeck G (2014) Rhythmic ganglion cell activity in bleached and blind adult mouse retinas. PLoS One 9:e106047.

Meyer A, Hilgen G, Dorgau B, Sammler EM, Weiler R, Monyer H, Dedek K, Hormuzdi SG (2014) AII amacrine cells discriminate between heterocellular and homocellular locations when assembling connexin36-containing gap junctions. J Cell Sci 127:1190-1202.

Molnar A, Werblin F (2007) Inhibitory feedback shapes bipolar cell responses in the rabbit retina. J Neurophysiol 98:3423-3435.

Olveczky BP, Baccus SA, Meister M (2003) Segregation of object and background motion in the retina. Nature 423:401-408.

Pang JJ, Abd-El-Barr MM, Gao F, Bramblett DE, Paul DL, Wu SM (2007) Relative contributions of rod and cone bipolar cell inputs to AII amacrine cell light responses in the mouse retina. J Physiol 580:397-410.

Passaglia CL, Enroth-Cugell C, Troy JB (2001) Effects of remote stimulation on the mean firing rate of cat retinal ganglion cells. J Neurosci 21:5794-5803.

Passaglia CL, Freeman DK, Troy JB (2009) Effects of remote stimulation on the modulated activity of cat retinal ganglion cells. J Neurosci 29:2467-2476.

Patel LS, Mitchell CK, Dubinsky WP, O'Brien J (2006) Regulation of gap junction coupling through the neuronal connexin Cx35 by nitric oxide and cGMP. Cell Commun Adhes 13:41-54.

Pearson JT, Kerschensteiner D (2015) Ambient illumination switches contrast preference of specific retinal processing streams. J Neurophysiol 114:540-550.

Perez De Sevilla Muller L, Shelley J, Weiler R (2007) Displaced amacrine cells of the mouse retina. J Comp Neurol 505:177-189.

Protti DA, Flores-Herr N, Li W, Massey SC, Wassle H (2005) Light signaling in scotopic conditions in the rabbit, mouse and rat retina: a physiological and anatomical study. J Neurophysiol 93:3479-3488.

Puller C, Manookin MB, Neitz J, Rieke F, Neitz M (2015) Broad thorny ganglion cells: a candidate for visual pursuit error signaling in the primate retina. J Neurosci 35:5397-5408.

Raven MA, Oh EC, Swaroop A, Reese BE (2007) Afferent control of horizontal cell morphology revealed by genetic respecification of rods and cones. J Neurosci 27:3540-3547.

Sagdullaev BT, McCall MA (2005) Stimulus size and intensity alter fundamental receptive-field properties of mouse retinal ganglion cells in vivo. Vis Neurosci 22:649-659.

Shelley J, Dedek K, Schubert T, Feigenspan A, Schultz K, Hombach S, Willecke K, Weiler R (2006) Horizontal cell receptive fields are reduced in connexin57-deficient mice. Eur J Neurosci 23:3176-3186.

Stacy RC, Demas J, Burgess RW, Sanes JR, Wong RO (2005) Disruption and recovery of patterned retinal activity in the absence of acetylcholine. J Neurosci 25:9347-9357.

Strettoi E, Masri RA, Grunert U (2018) AII amacrine cells in the primate fovea contribute to photopic vision. Scientific reports 8:16429.

Stutzki H, Leibig C, Andreadaki A, Fischer D, Zeck G (2014) Inflammatory stimulation preserves physiological properties of retinal ganglion cells after optic nerve injury. Front Cell Neurosci 8:38.

Tengolics AJ, Szarka G, Ganczer A, Szabo-Meleg E, Nyitrai M, Kovacs-Oller T, Volgyi B (2019) Response Latency Tuning by Retinal Circuits Modulates Signal Efficiency. Scientific reports 9:15110.

Tetenborg S, Yadav SC, Bruggen B, Zoidl GR, Hormuzdi SG, Monyer H, van Woerden GM, Janssen-Bienhold U, Dedek K (2019) Localization of Retinal Ca(2+)/Calmodulin-Dependent Kinase II-beta (CaMKII-beta) at Bipolar Cell Gap Junctions and Cross-Reactivity of a Monoclonal Anti-CaMKII-beta Antibody With Connexin36. Front Mol Neurosci 12:206.

Toychiev AH, Yee CW, Sagdullaev BT (2013) Correlated spontaneous activity persists in adult retina and is suppressed by inhibitory inputs. PLoS One 8:e77658.

Trenholm S, Awatramani GB (2015) Origins of spontaneous activity in the degenerating retina. Front Cell Neurosci 9:277.

Trenholm S, Awatramani GB (2017) Dynamic Properties of Electrically Coupled Retinal Networks.183-208.

Tsukamoto Y, Omi N (2017) Classification of Mouse Retinal Bipolar Cells: Type-Specific Connectivity with Special Reference to Rod-Driven AII Amacrine Pathways. Front Neuroanat 11:92.

van Wyk M, Wassle H, Taylor WR (2009) Receptive field properties of ON- and OFF-ganglion cells in the mouse retina. Vis Neurosci 26:297-308.

Veleri S, Lazar CH, Chang B, Sieving PA, Banin E, Swaroop A (2015) Biology and therapy of inherited retinal degenerative disease: insights from mouse models. Dis Model Mech 8:109-129.

Veruki ML, Oltedal L, Hartveit E (2010) Electrical coupling and passive membrane properties of AII amacrine cells. J Neurophysiol 103:1456-1466.

Viventi J et al. (2012) Flexible, foldable, actively multiplexed, high-density electrode array for mapping brain activity in vivo. Nat Neurosci 14:1599-1605.

Wassle H (2004) Parallel processing in the mammalian retina. Nat Rev Neurosci 5:747-757.

Weng S, Sun W, He S (2005) Identification of ON-OFF direction-selective ganglion cells in the mouse retina. J Physiol 562:915-923.

Wickham J, Corna A, Schwarz N, Uysal B, Layer N, Wuttke TV, Koch H, Zeck G (2019) Human cerebrospinal fluid induces neuronal excitability changes in resected human neocortical and hippocampal brain slices. bioRxiv:730036.

Wienbar S, Schwartz GW (2018) The dynamic receptive fields of retinal ganglion cells. Prog Retin Eye Res 67:102-117.

Xin D, Bloomfield SA (1999a) Dark- and light-induced changes in coupling between horizontal cells in mammalian retina. J Comp Neurol 405:75-87.

Xin D, Bloomfield SA (1999b) Comparison of the responses of AII amacrine cells in the dark- and light-adapted rabbit retina. Vis Neurosci 16:653-665.

Zeck G (2016) Aberrant Activity in Degenerated Retinas Revealed by Electrical Imaging. Front Cell Neurosci 10:25.

Zeck G, Jetter F, Channappa L, Bertotti G, Thewes R (2017) Electrical imaging: investigating cellular function at high resolution. Advanced Biosystems 1:1700107.

Zhao Z, Klindt DA, Maia Chagas A, Szatko KP, Rogerson L, Protti DA, Behrens C, Dalkara D, Schubert T, Bethge M, Franke K, Berens P, Ecker AS, Euler T (2020) The temporal structure of the inner retina at a single glance. Scientific reports 10:4399.

8. Acknowledgement

I want to thank all the committees of the examination board to this thesis.

Dr. Günther Zeck for supervising my PhD study and offered all the resources that were needed for this study. All the discussion and meetings and the opportunity for me to participate in this and other projects.

Prof. Dr. Thomas Euler for always offering great advices, making the Switchboard project possible and hosting me during my secondment in the lab.

Prof. Dr. Alexandra Koschak for offered me a small project during the secondment and all the suggestions to this work.

Prof. Dr. Frank Schäffel for agreeing on being one of the committee to my defense, also the vary nice vision lecture at the graduate school.

Many thanks to Prof. Dr. Karin Dedek for kindly providing Cx36 KO mice for this study.

I would like to thank all the members in the Euler's group, especially Dr. Timm Schubert and Gordon Eske for showing me different techniques in the lab. Helping me with experiments and imaging.

Special thanks to Prerna Srivastava for your patience for me. Those time we spent together were precious.

Thank you Dr. Peter Jones for your help and knowledge with the mirror assembly on the CMOS-MEA, along with your coat and sofa. It was nice to have you as a nice colleague and neighbor.

Thank you all the members in the Switchboard project. I am happy to meet you all and I will remember everything we experienced together, all those meetings, workshops and adventures.

I would like to give my most sincere appreciation to all my colleagues at NMI. Miriam, Pauline, Julia, Pranoti, Lena, Jenny, Michael, Thoralf, Andreas and Florian. Thank you all, without your help and support, I would not be able to finish my PhD training.

Thank you Shang-Chun, I've learned great lessons in life from you. Thank you for the good and bad times, you made me a better person.

Thank you Hüseyin, I am so greatful for your company, support and understanding.

Finally, I would like to thank my family. To my grandpa and grandma, I hope you could have participated this part of my life, I hope I made you proud. To my aunt, for always being there for me no matter what. To my parents, thank you for the good education you've gave me and for being so supportive at the most difficult times.